Effectiveness of Urban Partnership Agreement Traffic Operations Measures in the I-35W Corridor

Final Report

Prepared by:

John Hourdos
Stephen Zitzow

Minnesota Traffic Observatory
Department of Civil Engineering
University of Minnesota

Seraphin Chally Abou

Department of Mechanical and Industrial Engineering
Northland Advanced Transportation Systems Research Laboratories
University of Minnesota Duluth

CTS 13-22

Technical Report Documentation Page

1. Report No.	2.	3. Recipients Accession No.
CTS 13-22		

4. Title and Subtitle	5. Report Date
Effectiveness of Urban Partnership Agreement Traffic Operations Measures in the I-35W Corridor	August 2013
	6.

7. Author(s)	8. Performing Organization Report No.
John Hourdos, Seraphin Chally Abou, and Stephen Zitzow	

9. Performing Organization Name and Address		10. Project/Task/Work Unit No.
Minnesota Traffic Observatory Department of Civil Engineering University of Minnesota 500 Pillsbury Drive, SE Minneapolis, MN 55455	Department of Mechanical and Industrial Engineering University of Minnesota Duluth 1305 Ordean Court Duluth, MN 55812	CTS Project #2010104
		11. Contract (C) or Grant (G) No.

12. Sponsoring Organization Name and Address	13. Type of Report and Period Covered
Intelligent Transportation Systems Institute Center for Transportation Studies University of Minnesota 200 Transportation and Safety Building 511 Washington Ave. SE Minneapolis, Minnesota 55455	Final Report
	14. Sponsoring Agency Code

15. Supplementary Notes

http://www.its.umn.edu/Publications/ResearchReports/

16. Abstract (Limit: 250 words)

One of the leading transportation project initiatives of the Minnesota Department of Transportation (MnDOT) is to reduce transportation system congestion. The Minneapolis Urban Partnership Agreement (UPA) project is one of the five major projects funded by the U.S. DOT's Strategy to Reduce Congestion on America's Transportation Network. Minnesota's UPA is concerned with Active Traffic Management (ATM) systems along I-35W from the southern junction with I-35 to downtown Minneapolis (which will be referred to as the UPA corridor). Three separate but related evaluations are included in this UPA related project: the effects of the variable speed limit (VSL) system on congestion and driver behavior, the impact of severe weather conditions on road safety, and the behavior of bus rapid transit (BRT) vehicles and their impacts on traffic conditions between 46th Street and Lake Street.

17. Document Analysis/Descriptors	18. Availability Statement
Active Traffic Management, Highway traffic control, Speed harmonization, Hydroplaning, Bus rapid transit	No restrictions. Document available from: National Technical Information Services, Alexandria, Virginia 22312

19. Security Class (this report)	20. Security Class (this page)	21. No. of Pages	22. Price
Unclassified	Unclassified	142	

Effectiveness of Urban Partnership Agreement Traffic Operations Measures in the I-35W Corridor

Final Report

Prepared by:

John Hourdos
Stephen Zitzow

Minnesota Traffic Observatory
Department of Civil Engineering
University of Minnesota

Seraphin Chally Abou

Department of Mechanical and Industrial Engineering
Northland Advanced Transportation Systems Research Laboratories
University of Minnesota Duluth

August 2013

Published by:

Intelligent Transportation Systems Institute
Center for Transportation Studies
University of Minnesota
200 Transportation and Safety Building
511 Washington Ave. S.E.
Minneapolis, Minnesota 55455

Acknowledgements

We would like to thank the Intelligent Transportation Systems (ITS) Institute, a program of the University of Minnesota's Center for Transportation Studies (CTS), for supporting this project. The ITS Institute is a federally funded program administrated through the Research and Innovative Technology Administration (RITA). We would like to acknowledge the help, support and, cooperation of Mr. Brian Kary and others at the MnDOT Regional Traffic Management Center. We would also like to thank the Minnesota Traffic Observatory for hosting this research project, providing material and software support.

Table of Contents

List of Figures

List of Tables

Executive Summary

One of the leading transportation project initiatives of the Minnesota Department of Transportation (MnDOT) is to reduce transportation system congestion. The Minneapolis Urban Partnership Agreement (UPA) project is one of the five major projects funded by the U.S. DOT's Strategy to Reduce Congestion on America's Transportation Network. Minnesota's UPA is concerned with Active Traffic Management (ATM) systems along I-35W from the southern junction with I-35 to downtown Minneapolis (which will be referred to as the UPA corridor). Three separate but related evaluations are included in this UPA related project: the effects of the variable speed limit (VSL) system on congestion and driver behavior, the impact of severe weather conditions on road safety, and the behavior of bus rapid transit (BRT) vehicles and their impacts on traffic conditions between 46th Street and Lake Street.

Variable Speed Limits

In July 2010, individual lane variable message signs were activated along the UPA corridor to display advisory speed limits during periods of congestion. This VSL system (Kwon 2001 and Kwon et al, 2011) is designed to prevent the rapid propagation of the shockwaves caused by fixed or moving bottlenecks by gradually reducing the speed levels of the incoming flows. Vehicle behavior before and after VSL implementation was examined to (1) determine if and how the congestion throughout the corridor is impacted by the system and (2) determine if the driver behavior is changed and, if it is, how this affects the traffic flow characteristics of the instrumented freeway segments. This study did not evaluate the compliance and behavior of individual drivers but focused only on the aggregate effect such behaviors have on traffic flow.

The study utilized loop detector measurements combined with speed sign activation records available from MnDOT. Through this information, the impact of the variable speed limits was explored through (1) examination of the actuations of each station as compared to the estimated speeds throughout the corridor based on 30-second loop detector data, (2) generation of fundamental diagram curves for specific detectors, and (3) tabulation of speed-based congestion for each region of the UPA corridor. The first two analysis techniques focused on well-correlated days based on 15-minute aggregated volumes along the boundary of each corridor (upstream station and entrance ramps)

In general, from the available data a very small compliance to the advisory speed limits is observed. Additionally, for the days were data were collected it seems that the speed of the congestion wave is too fast for the VSL signs to give timely warning to oncoming traffic. Regardless, looking at the general congestion patterns, the VSL system does appear to positively impact the most severe congestion (speeds below 10-15 mph). Specifically, the instances and spread of extreme congestion waves (speeds bellow 10 mph) has been reduced after the VSL system activation. Severe shockwaves propagating upstream are a serious danger of rear-end collisions therefore their reduction is a valuable effect of the VSL. Although it is not possible to make definitive observations of this effect through loop detector data, the analysis of the fundamental diagram curves for specific detectors shows that although drivers do not comply with the advisory speed limit, they do take it into consideration. One can hypothesize that the

drivers use the advisory speed limit as a gage of downstream congestion and prepare themselves for encountering the upcoming shockwaves. The effect is observable albeit weak.

Finally, in order to evaluate the system-wide effect the VSL system has on speeds and in extend congestion, a statistical analysis of all before and after speeds was conducted. Although perforce varies from bottleneck to bottleneck, on average, the morning peak experienced over 17% less congestion with the VSL system in place, although for those same days the lower speeds were largely unchanged (25 mph or less). The entire VSL active region had 7.6 minutes less congestion during the average AM peak.

Evaluation of UPA Corridor Operations during Inclement Weather Conditions

The objective of this part of the project was to evaluate to what extent inclement weather conditions may affect road safety and formulate recommendations that can help improve traffic operations and the safety of the traveling public. The method used in this analysis considered visual and technical design data of the highway, rainfall frequency and duration relationships throughout Minnesota areas, and a modified Gallaway's hydroplaning equation, [22], [10], [8], [9]. Continuity equation and control volume principle [7], is used to develop storm rain accumulation model and predict the depth of standing water on the roadway.

Both the rainfall water accumulation rate and the hydroplaning models describe the ways that aggregate inherent risk factors which are calculated can be used to implement a weather-responsive algorithm that can help make informed decisions: (1) Determine under what rainy conditions the PDSL should be closed; and (2) Provide a set of performance measures for the monitoring of the operation of the speed harmonization system on the highway section between Blackdog Road and 90th Street based on the prediction of rainfall accumulation.

The most important conclusion of this research is that weather matters—weather conditions have an important impact on traffic safety, traffic demand, and traffic flow. Such a systematic framework of quantitative risk analysis procedure can facilitate efficient risk management. Moreover, the proposed risk assessment tool can be combined with ITS, and risk communication and operation control in order to predict relative crash susceptibility in various segments of the corridor based on knowledge of local geography, topography, storm rain intensity, and other risk factors.

Evaluation of Bus Operations on the MnPASS PDSL

One of the biggest advantages of the 35W BRT corridor is the fact that the busses are traveling on the MnPASS lane therefore guaranteeing travel under uncongested traffic conditions. To facilitate quick boardings and alightings of transit passengers as well as to reduce the delay involved in entering and exiting the freeway, the 46th St. BRT station is located in the median of I-35W. The BRT operation would have been straightforward if the old right side station on Lake St. was not there or was transferred in the median. Since this is not the case today, some of the MTA transit lines are required to traverse several freeway lanes to in order to reach both stations. This part of the project was tasked in evaluating the effect of these lane changes on the traffic flow, the behavior of the drivers in terms of utilizing the MNPASS lane, and estimated the delay accumulated as compared to having a Lake St. median station.

From the observations and data collected it is suggested that the bus drivers underutilize the MNPASS lane. They tend to perform the left to right lane changes as soon as possible after leaving the 46th St median station. In addition, the bus lane changes as it traverses the freeway do generate a visible disturbance under moderate and heavy congestion but such disturbances do not amplify and therefore do not seem to be the cause of flow breakdown in this freeway section. Finally, there is an accumulated delay of 12 to 19 minutes daily due to the present bus driver behavior and the fact that several lane changes are need to move from the median station to the right side on Lake street. This eliminating this delay would be a benefit if the Lake St station is transferred to the median.

1. Introduction

One of the leading transportation project initiatives of the Minnesota Department of Transportation (MnDOT) is to reduce transportation system congestion. The Minneapolis Urban Partnership Agreement (UPA) project is one of the five major projects funded by the U.S. DOT's Strategy to Reduce Congestion on America's Transportation Network. Minnesota's UPA is concerned with Active Traffic Management (ATM) systems along I-35W from the southern junction with I-35 to downtown Minneapolis (which will be referred to as the UPA corridor). Three separate but related evaluations are included in this UPA related project: the effects of the variable speed limit (VSL) system on congestion and driver behavior, the impact of severe weather conditions on road safety, and the behavior of bus rapid transit (BRT) vehicles and their impacts on traffic conditions between 46th Street and Lake Street.

1.1 Project Objectives

The project covered three independent but related research objectives.

1.1.1 Variable Speed Limits

In July 2010, individual lane variable message signs were activated along the UPA corridor to display advisory speed limits during periods of congestion. This VSL system (Kwon 2001 and Kwon et al, 2011) is designed to prevent the rapid propagation of the shockwaves caused by fixed or moving bottlenecks by gradually reducing the speed levels of the incoming flows. Vehicle behavior before and after VSL implementation was examined to (1) determine if and how the congestion throughout the corridor is impacted by the system and (2) determine if the driver behavior is changed and, if it is, how this affects the traffic flow characteristics of the instrumented freeway segments. The study utilized loop detector data available from MnDOT and employed several analysis methodologies to expose aspects of the effect the VSL system has in the traffic. This study did not evaluate the compliance and behavior of individual drivers but focused only on the aggregate effect such behaviors have on traffic flow.

In November 2009, reconstruction on the corridor was completed from I-35 to north of I-494. Construction continued on the northern portions of the corridor until completion in 2010. The variable message signs, when activated, show the same speed for all lanes at a particular location, referred to as a station.

The northbound morning peak period (5 am to 10 am) and the southbound evening peak period (2 pm to 7 pm) were considered. Mid-week days (Tuesdays, Wednesdays, and Thursdays) were selected from November 2009 through December 2011. These days represent 'normal' behavior of traffic and are consistent with the analysis practices of MnDOT.

As noted in Figures 1.1 and 1.2, there are four sections of I-35W that behave as semi-autonomous pieces during northbound morning peak: I-35 to T.H. 13/Cliff Road (the Cliff Road bottleneck), Cliff Road to slightly north of I-494 (the I-494 bottleneck), the region surrounding MN-62, and MN-62 to I-94. For the southbound evening peak, similar regions are of note: I-94 to MN-62, the region surrounding MN-62, MN-62 to 106th Street (98th Street and I-494 bottlenecks), and 106th Street to I-35 (T.H. 13 bottleneck)

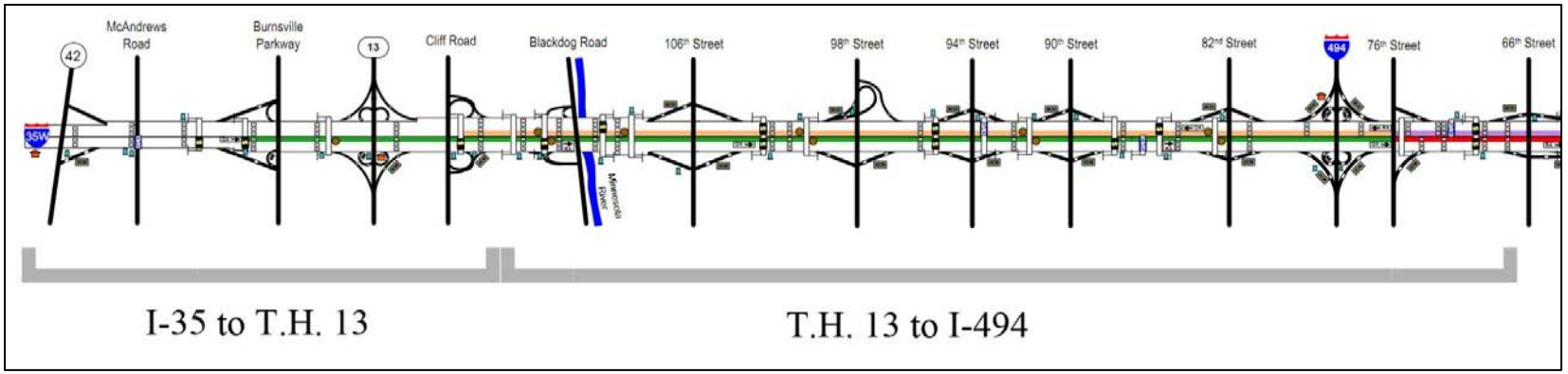

Figure 1.1: I-35W corridor diagram of the southern two sections of interest for northbound (north is to the right); connects to Figure 1.2 on the right.

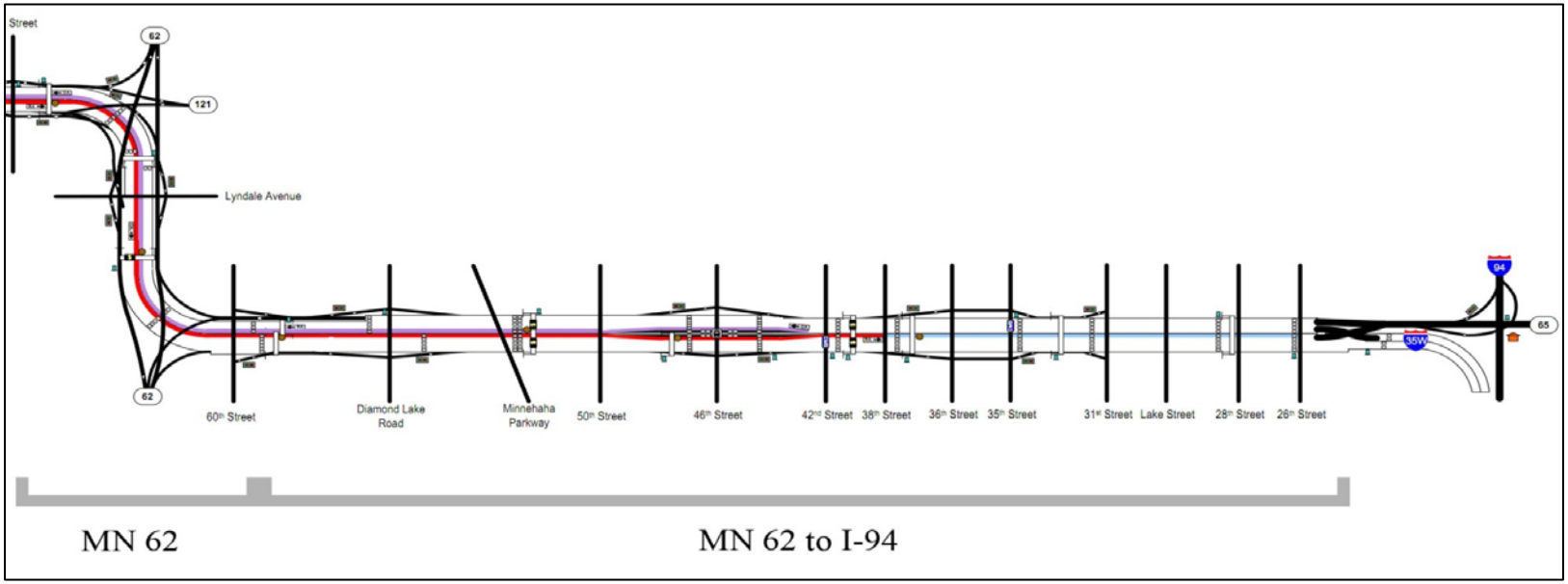

Figure 1.2: I-35W corridor diagram of the northern two sections of interest for northbound (north is to the right); connects to Figure 1.1 on the left.

The impact of the variable speed limits was explored through (1) examination of the actuations of each station as compared to the estimated speeds throughout the corridor based on 30-second loop detector data, (2) generation of fundamental diagram curves for specific detectors, and (3) tabulation of speed-based congestion for each region of the UPA corridor. The first two analysis techniques focused on well-correlated days based on 15-minute aggregated volumes along the boundary of each corridor (upstream station and entrance ramps).

1.1.2 Severe Weather Impacts

From the roadway safety perspective, this evaluation focuses on the analysis of severe weather condition effects on the safety of the traveling public and the effectiveness achieved by the design-build process of the UPA corridor. Often, roadway geometric design practice applies a uniform nationwide standard in terms of assumed weather impacts on geometric design. The Minneapolis UPA project is not an exception to this rule. Presumably, much could be gained by adjusting this standard to account for weather conditions that may deviate greatly from the norm. Adverse weather is often considered as an external factor that can affect freeway traffic operations. Moreover, standing/moving water can unexpectedly hydroplane light to medium size vehicles moving at speeds of 50 MPH or higher and lead to loss of control of the vehicle resulting in catastrophic events. It is known that adverse weather is the second largest cause of non-recurring congestion, accounting for about 25% of freeway delays. From a safety perspective, the Federal Highway Administration (FHWA) is advancing advisory, control, and management strategies that include information dissemination and methods to regulate or optimize the traffic stream and ensure that roads are clear of obstructions. In addition, the Highway Capacity Manual (HCM) considers that adverse weather can reduce free-flow speeds and uses evidence that different weather conditions can impact the form of speed-flow relationships, [24]. Along the UPA corridor, there are a number of sag points. However, at this time, the focus was put on the evaluation of probable major flooding risks around 42nd Street as shown in Figure 1.3.

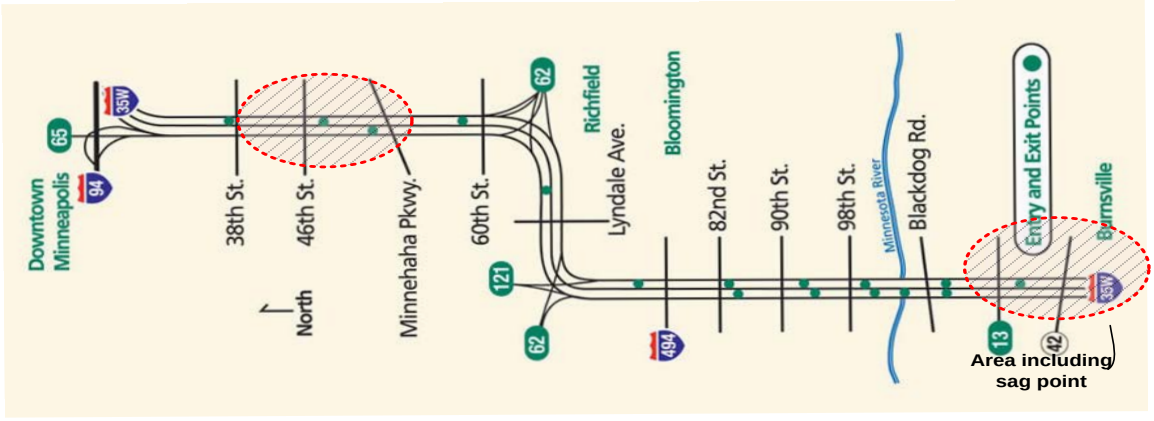

Figure 1.3: Area of concerns around the sag point.

The objective of this portion of the project is to evaluate to what extent inclement weather conditions may affect road safety and formulate recommendations that can help improve traffic operations and the safety of the traveling public. Heavy rain conditions may also have great effect on traffic flow and road safety as congestion worsens, resulting in vehicles crashes. Most

of the literature describes the impacts of snowy conditions on highway transportation, while only a few references were found to estimate the impacts of rain, standing water, and reduced visibility, [19], [23], [12]. This evaluation process is based on the worst-case scenario where the existing storm drain systems design data is considered as initial conditions for the prediction model of the storm rain accumulation. The method used in this analysis considered visual and technical design data of the highway, rainfall frequency and duration relationships throughout Minnesota areas, and a modified Gallaway's hydroplaning equation, [22], [10], [8], [9]. Continuity equation and control volume principle [7], is used to develop storm rain accumulation model and predict the depth of standing water on the roadway.

Both the rainfall water accumulation rate and the hydroplaning models describe the ways that aggregate inherent risk factors which are calculated can be used to implement a weather-responsive algorithm that can help make informed decisions: (1) Determine under what rainy conditions the PDSL should be closed; (2) Provide a set of performance measures for the monitoring of the operation of the speed harmonization system on the highway section between Blackdog Road and 90th Street based on the prediction of rainfall accumulation; and (3) Improve mobility and roadway safety.

1.1.3 Bus Rapid Transit Operations

One of the biggest advantages of the 35W BRT corridor is the fact that the buses are traveling on the MnPASS lane therefore guaranteeing travel under uncongested traffic conditions. To facilitate quick boarding and alighting of transit passengers as well as to reduce the delay involved in entering and exiting the freeway, the 46th St. BRT station is located in the median of I-35W. Although such design is common in freeway BRT corridors, its interaction with the existing right hand side station on Lake St. could be an issue.

According to Metro Transit plans, routes 152,535, and 578 utilize the 46th St. station with a peak frequency between 5 and 7.5 minutes. Additional routes may exist like the 467 and 477V of MVTA. Not all of these routes utilize the Lake St. station. This research focuses on route 535 which has both high frequency and utilizes both stations. These buses have to traverse four lanes between the MnPASS lane on the left and transfer to the Lake St. station. There is a proposal and discussion of constructing a new median placed Lake St. station, a multi-million dollar project. This research may assist policy makers in their deliberations.

The 46th St. Transit station as planned came online in late fall 2010. After this period, the research focused on two perspectives of the bus lane changes, the impact these lane changes have on the freeway mainline flow and the safety implications for the buses making these lane changes. The latter also includes a performance evaluation of the BRT corridor operations. Two types of information were involved in this analysis.

a) Buses require larger gaps and have reduced acceleration capabilities. Depending on the state of the traffic flow such lane changes take place, the bus may cause shockwaves and possibly initiate a traffic flow breakdown. We propose to primarily try to utilize information from the bus AVL system to locate when/where these maneuvers take place and correlate that with volume/occupancy information. Additional MTO owned GPS

recorders, can be used as in the BRT research project on Cedar Ave (El-Geneidy, et. al 2009).

b) The amount of difficulty in performing the required lane changes will determine the location where the drivers will select to enter/exit the MnPASS lane. Metro transit drivers will adapt to road reality as they did with driving on the shoulder. A survey of bus drivers along with measurement data analysis will detect and quantify any loss of safety and performance from using less of the MnPASS lane.

Either based on instrumented buses or estimated based on traffic flow theory, the amount and frequency of available gaps correlated with measurements of traffic density will allow, if so desired, the development of a predictive model relating mainline demand with BRT performance and bus service frequency with congestion.

1.2 Report Organization

The report is organized into four major chapters. The present chapter is an overall introduction, chapter 2 presents the evaluation of the before and after condition on 35W due to the implementation of the Variable Speed Limit system, chapter 3 explores the impact of severe weather and especially rainfall on the safety and operations of the MNPASS lane, chapter 4 contains the evaluation of the bus operations between the 46th St median station and the Lake St right side stop. Finally chapter 5 contains a summary of the overall findings and some recommendations.

2. Evaluation of Speed Harmonization System

2.1 Introduction

In July 2010, individual lane variable message signs were activated along I-35W to display advisory speed limits during periods of congestion. This Variable Speed Limit (VSL) system (Kwon 2001 and Kwon et al, 2011) is designed to prevent the rapid propagation of the shockwaves caused by fixed or moving bottlenecks by gradually reducing the speed levels of the incoming flows with VSLs. This report summarizes the results of an independent study on the impacts of the VSL system on the roadway by comparing vehicle behavior before and after to (1) determine if and how the congestion throughout the corridor is impacted by the system and (2) determine if the driver behavior is changed and if it is how this affects the traffic flow characteristics of the instrumented freeway segments. The study utilized loop detector data available from MnDOT and employed different analysis methodologies in an effort of uncovering all the aspects of the effect the VSL system has in the traffic. This study did not evaluate the compliance and behavior of individual drivers but focused only on the aggregate effect such behaviors have on traffic flow.

The corridor of interest begins at I-35 at the south end of the Twin Cities metro area and ends near downtown Minneapolis and the junction with I-94 (see Figure 2.1 and Figure 2.2). In November 2009, reconstruction on the corridor was completed from I-35 to north of I-494. Construction continued on the northern portions of the corridor until completion in 2010.

The northbound morning peak period (5 am to 10 am) and the southbound evening peak period (2 pm to 7 pm) were considered. Mid-week days (Tuesdays, Wednesdays, and Thursdays) were selected from November 2009 through December 2011. These days represent ‘normal’ behavior of traffic and are consistent with the analysis practices of MnDOT.

As noted in Figures 1.1 and 1.2, there are four sections of I-35W that behave as semi-autonomous pieces during northbound morning peak: I-35 to T.H. 13/Cliff Road (the Cliff Road bottleneck), Cliff Road to slightly north of I-494 (the I-494 bottleneck), the region surrounding MN-62, and MN-62 to I-94. For the southbound evening peak, similar regions are of note: I-94 to MN-62, the region surrounding MN-62, MN-62 to 106th Street (98th Street and I-494 bottlenecks), and 106th Street to I-35 (T.H. 13 bottleneck).

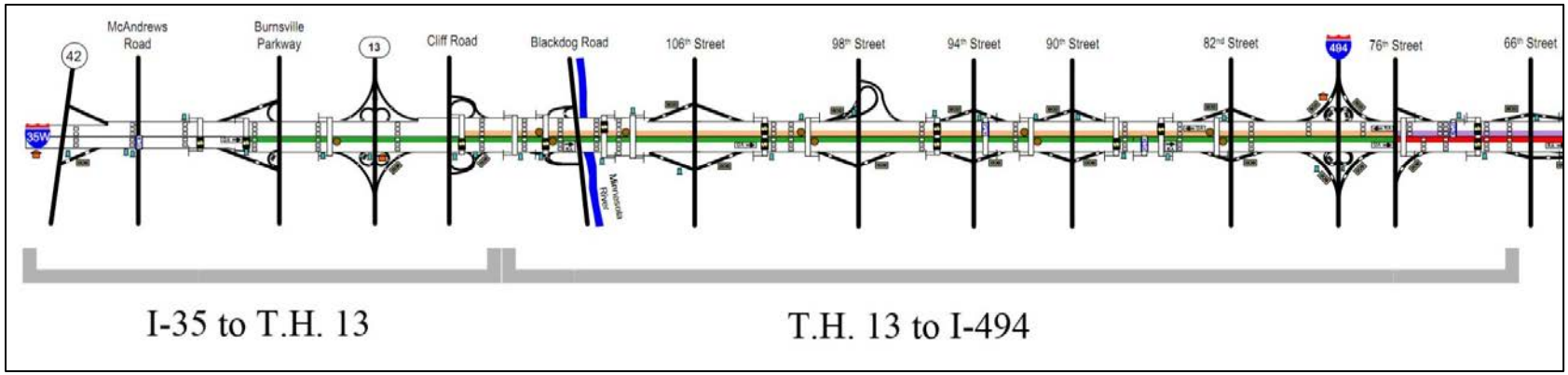

Figure 2.1: I-35W corridor diagram of the southern two sections of interest for northbound (north is to the right); connects to Figure 2.2 on the right.

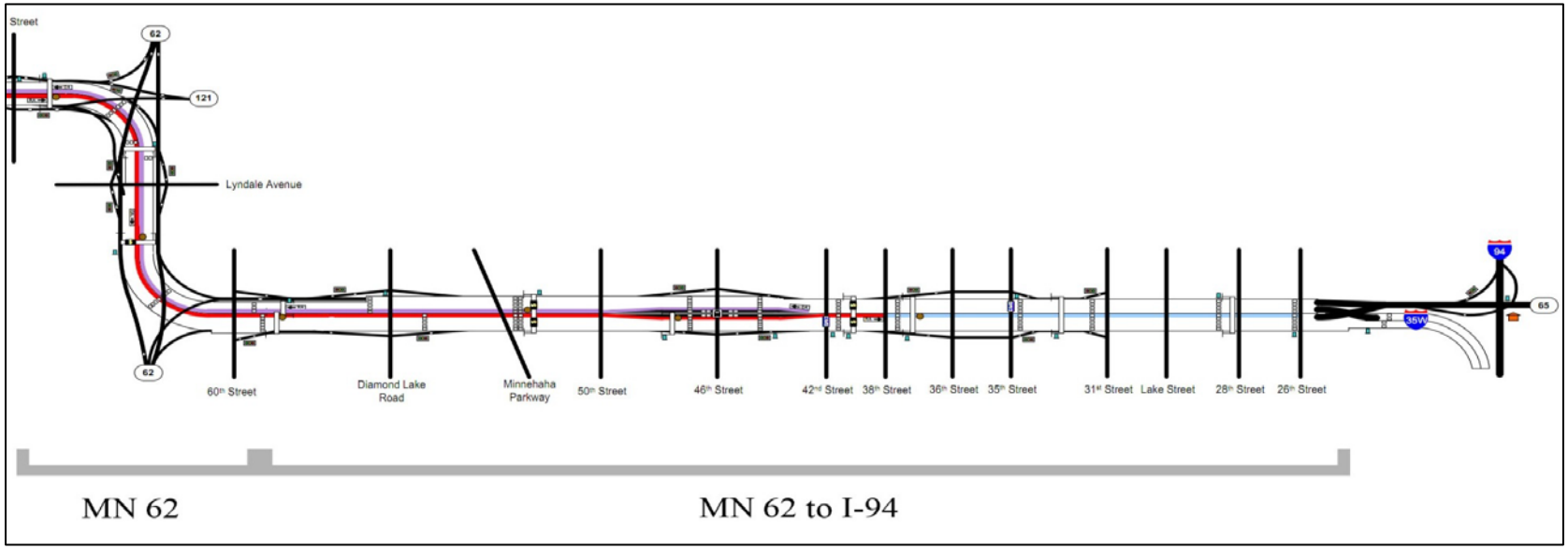

Figure 2.2: I-35W corridor diagram of the northern two sections of interest for northbound (north is to the right); connects to Figure 2.1 on the left.

2.2 Data Collection and Preparation Methodology

To examine the behavior of traffic within the corridor, two sources of data were collected and analyzed: 30-second loop detector data (volume and occupancy) and all actuations of all VSL signs in the corridor. The loop detector data is automatically collected and stored at the Regional Traffic Management Center (RTMC) in Roseville, MN. A program was created to query the database at the RTMC and download the appropriate data for every detector along I-35W during the periods of interest. The VSL actuations were provided by the RTMC in an offline database containing the sign identification string, event date, and actuation string.

Prior to performing any analysis, the data for the corridor required preliminary preparation and cleaning. The detectors along the I-35W corridor are single-loop detectors. This means that they are capable of determining the volume and occupancy of traffic at a given location, but cannot directly measure vehicle speed. Using calibrated field lengths for each detector, extracted from an XML configuration file describing the entire freeway network of the Twin Cities and available from the RTMC, the speeds for each 30-second volume and occupancy pair were estimated. The field lengths were extracted from a December 2010 version of the XML configuration file and assumed to be accurate across the analysis period (November 2009 to December 2011). Unfortunately, although the loop detector field lengths are calibrated often, the historical values of these field lengths are not retained and only the latest numbers are available.

The VSL sign data were retrieved as a database of individual actuations. Each actuation was described by the sign identification number, date and time of actuation, and the command string sent to the sign (containing the speed to be displayed). A query was constructed to extract the speed from the command string and store it alongside the other data in a separate table. With the data prepared for use, a series of programs were written to manipulate and tabulate the data.

Three general approaches were taken to examining the data: the estimated speeds and VSL actuations for the corridor were plotted to qualitatively analyze the behavior of the VSL signs, the flow-density relationship (fundamental diagram) was generated for detectors along the roadway to look for changes in driver behavior at specific locations, and speeds were examined across the network to measure aggregated changes in congestion patterns for the corridor.

2.2.1 Correlation

To carefully select days for analysis, a correlation program was created to examine the boundary conditions along the roadway. This correlation process was used in both the flow-density and speed-based congestion analyses to focus each analysis method on the impacts of the VSL system while minimizing variations from other sources.

The boundary conditions for each segment of the I-35W corridor were defined at one mainline station immediately upstream of the region and all entrance ramps into the corridor segment. Using these detectors, all vehicles entering each segment of the roadway were captured for correlation. For the ramps, the queue detectors were used to capture the arrival behavior of traffic from the arterials. In a few cases, the queue detectors malfunctioned for significant portions of the analysis period, so they were replaced, where possible, by the passage detector from the ramp meters. The boundary detectors were aggregated to 15-minute volumes for the

AM peak (northbound segments) or PM peak (southbound segments). A matrix for each day in the analysis period was constructed with each row representing one of the detectors along the segment boundary and each column representing a 15-minute segment.

To compare these matrices of entrance volumes, a program was developed to calculate the GEH statistic for each day prior to VSL implementation against each day following VSL implementation. Although the GEH statistic is not a strict statistical test, the values were used as a relative indicator of goodness-of-fit between days. The GEH statistics were used to select a set of well-correlated days for closer examination. These well-correlated day sets were used for the speed-based congestion analyses.

Finally, the well-correlated days were further reduced and also examined using historical weather data to determine which had similar prevailing conditions during the period of interest (5-10 AM for northbound, and 2-7 PM peak for southbound). This produced sets of highly-correlated days suitable for the Flow-Density analysis.

2.2.2 Speed Contours with VSL Actuations

Prior to creating the speed contours for each day in the analysis period, all mainline detectors were grouped into their respective stations. (The detectors in the network are aligned in sets which span the width of the road, one detector per lane, and are given a station identification number.) To match the logic used with the VSL signs, the speed for each station was calculated as the average for the non-HOV/HOT detectors for the station.

Since these stations are not evenly spaced along the roadway, the coordinates for each station (taken from the XML configuration file) were used along with a model of the I-35W corridor to 'snap' the stations to the roadway using ArcGIS. This produced a list of distances which related each station to the south-most point of I-35W (where it joins with I-35E).

By combining these distances with the speed values, the contours could be constructed. Figure 2.3 is an example of one such plot without any VSL actuations. The contour shows the corridor from upstream to downstream (bottom to top) and time from left to right. The stations used to create the contour are labeled at the left side with some major interchanges indicated on the right for reference. The speeds were filled using a color map with cool colors indicating regions of high-speed traffic and warm colors indicating regions of low-speed, congested traffic.

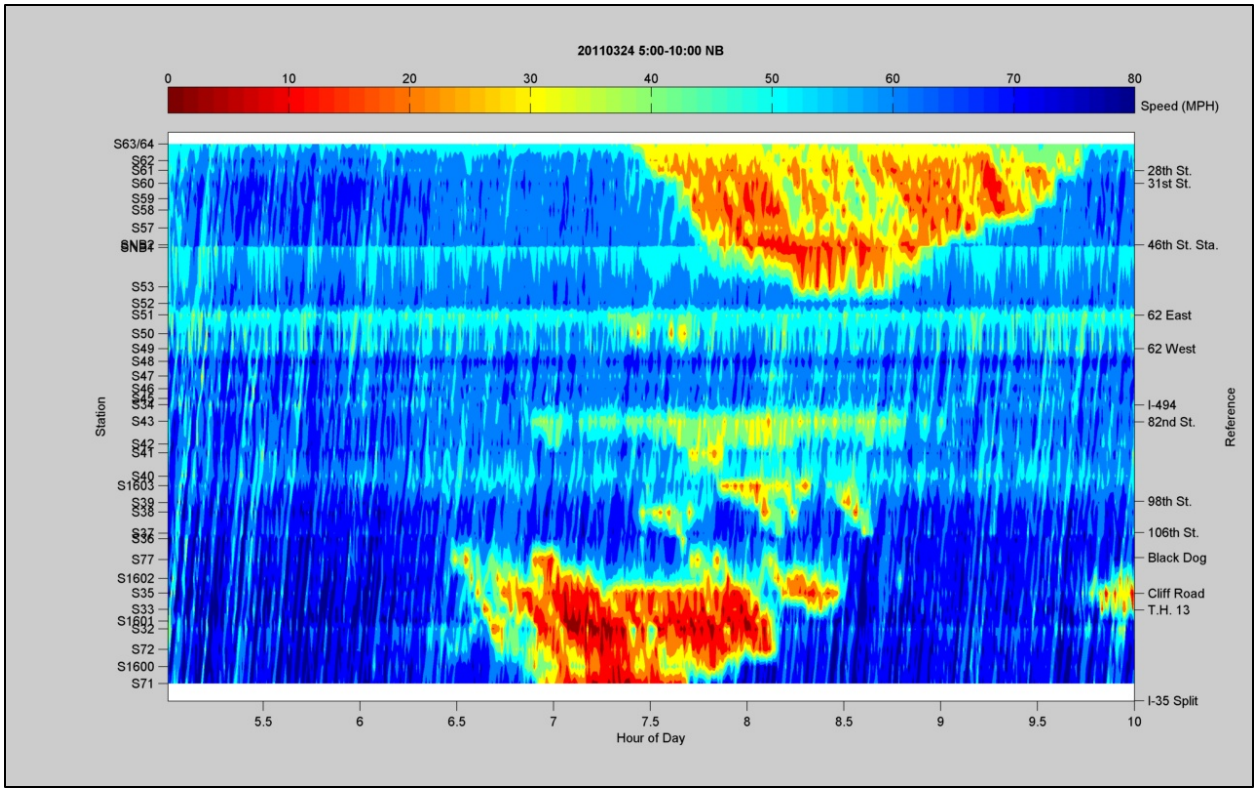

Figure 2.3: Speed contour for I-35W northbound during morning peak for March 24th, 2011.

A similar method of aggregation was used to capture the VSL sign actuations. The signs are mounted in groups on gantries above the roadway, with one sign per lane. All signs were queried for any actuations during a period of interest (AM or PM peak on a particular day) and matching entries were grouped based on their location (i.e. which gantry they belong to). Unlike the detectors, which do not necessarily measure the same speed for each lane at a station, the VSL system is currently designed to always display the same advisory speed across all lanes at a given location. As such, each query of the database returned many duplicate entries (same gantry, same speed). These duplicate entries were eliminated to form a single time series of actuations for each gantry.

To plot these actuations, the speeds shown were related to the same color map as the speed contours for the stations. Using this relation, the VSL sign activations were plotted as horizontal color bars on top of the speed contours. Figure 2.4 shows a sample date with the speed contour and the VSL actuations overlaid.

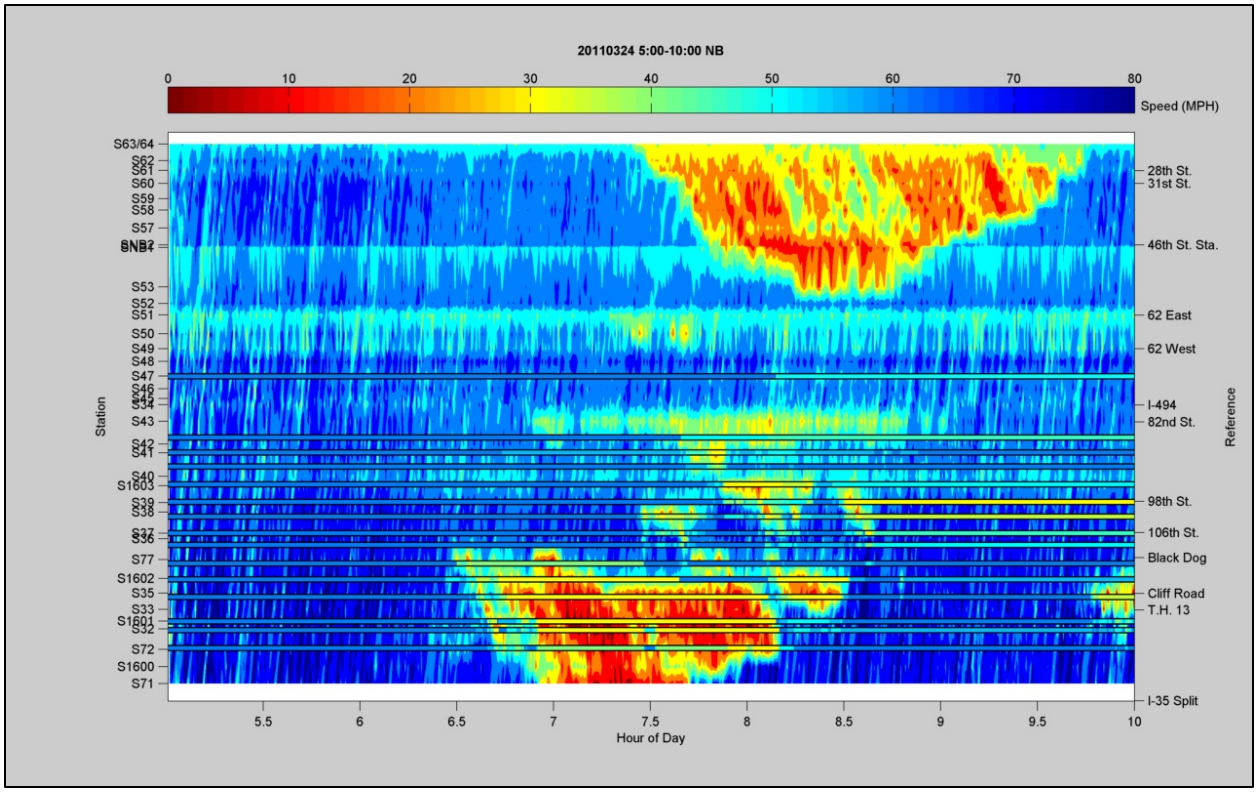

Figure 2.4: Speed contours with VSL actuations for I-35W northbound during morning peak for March 24th, 2011.

2.2.3 The Flow-Density Relationship

To examine the effect of the VSL system on vehicle behavior at a localized level, the fundamental relationship between flow and density was explored. The volume (flow per 30-seconds) and occupancy (a corollary of density) for each detector were isolated for plotting. Due to the size of the potential data sets and the noise introduced by the loop detectors, a 5-point moving average smoothing was applied (i.e. each point was averaged with the two from each side).

Using the highly-correlated set of sample dates found using the correlation regime from Section 0, the volume and smoothed occupancy values were plotted to form the fundamental diagram for each detector in the corridor, as in Figure 2.5.

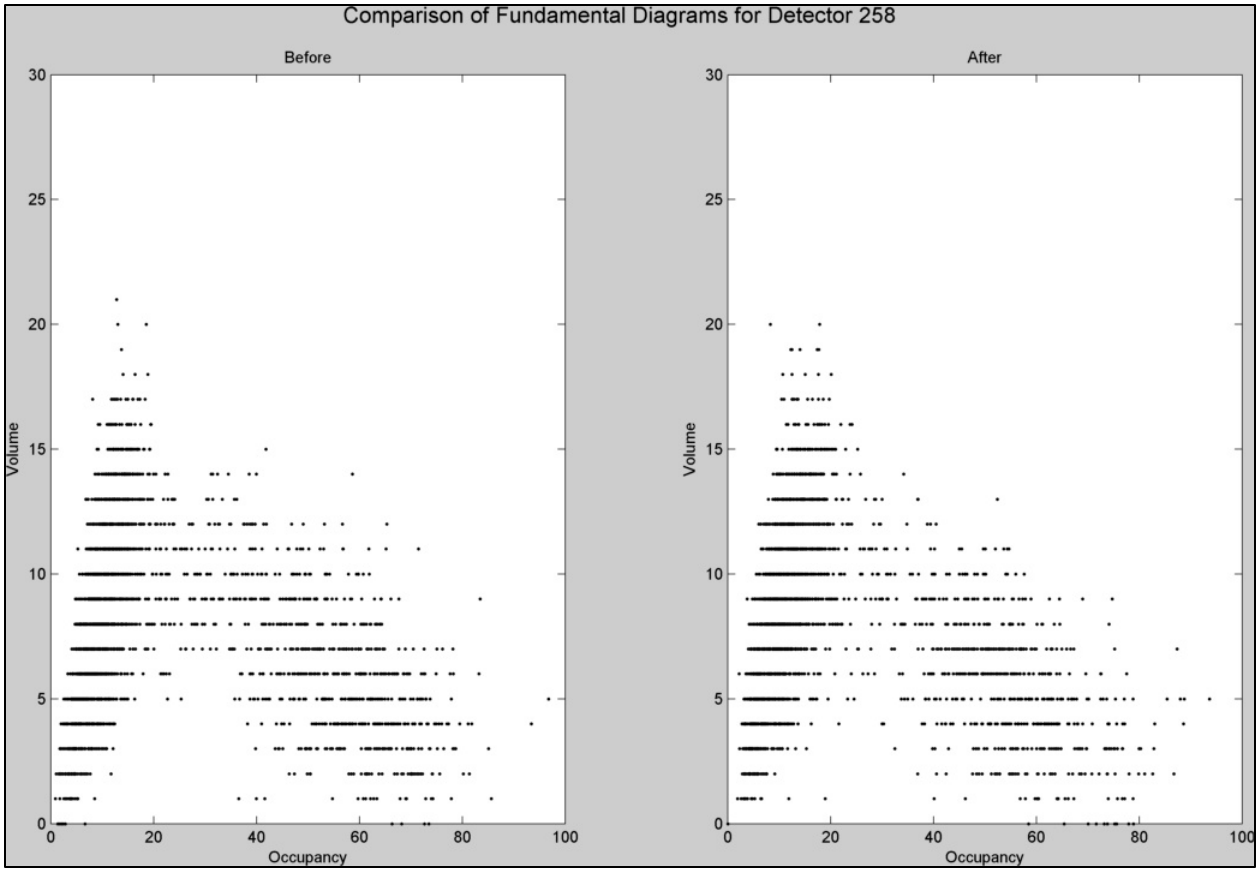

Figure 2.5: Volume v. Occupancy diagrams for select dates before and after VSL implementation for Detector 258 (northbound AM peak).

Since the VSL system is active only when congestion is occurring, the 'clouds' of points on the right side of the fundamental diagram figures are of particular interest. To further quantify the congestion behavior, the clouds were broken into vertical slices with widths of 5% occupancy. All points falling within these slices were then used to determine the median and quartiles for the slice. The medians and quartiles were collected and used to create two plots: one with the medians plotted as solid lines and the quartiles as dashed lines (Figure 2.6), and one with only the median lines (Figure 2.7).

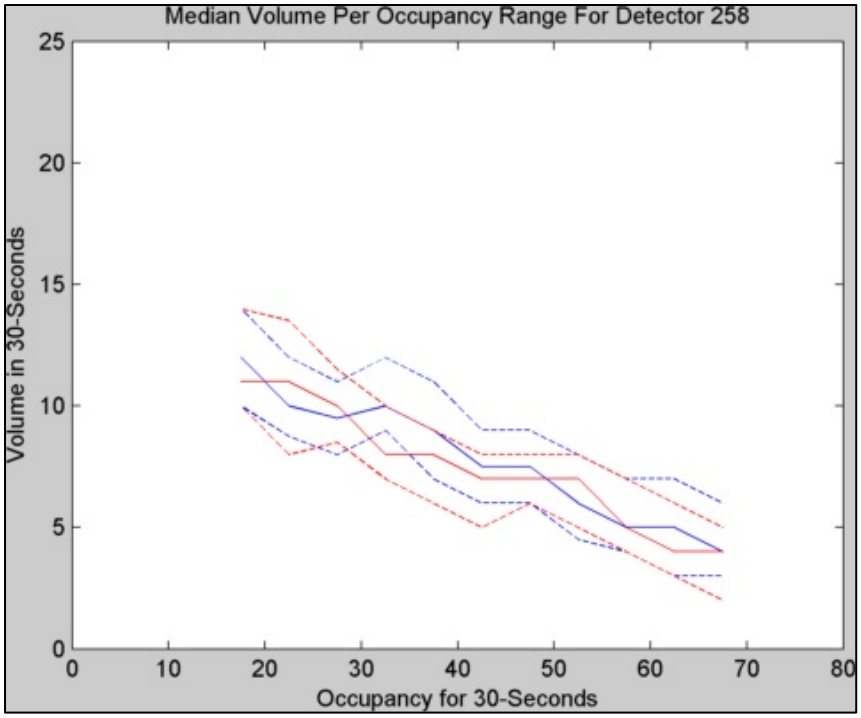

Figure 2.6: Medians and quartiles for congestion region of Detector 258 before (blue) and after (red) VSL implementation.

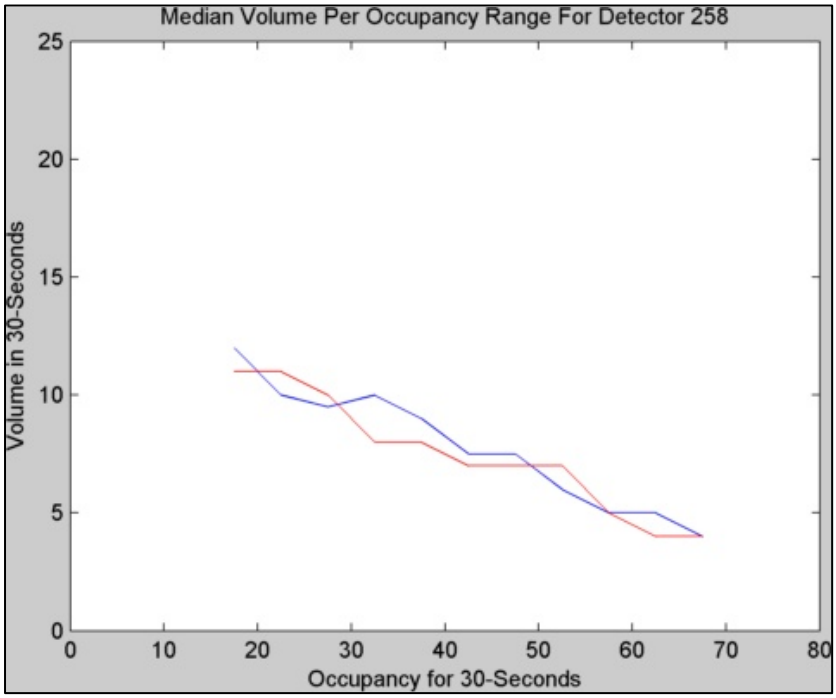

Figure 2.7: Medians only for congestion region of Detector 258 before (blue) and after (red) VSL implementation.

For a select number of detectors, the medians were used to find a least squares linear model of the congestion cloud before and after VSL implementation.

2.2.4 Speed-Based Congestion

The previous methods of plotting and analyzing the data for the I-35W corridor have focused on localized impacts of the VSL. This final method examines the aggregate behavior of traffic throughout the corridor and in large segments of the corridor (relating to the corridor's several bottlenecks). Mn/DOT defines congestion as any speed lower than 45 mph along the mainline of a freeway corridor. To get a more granular picture of congestion within the corridor, speeds were tabulated according to multiple thresholds: speeds below 10 mph, speeds below 15 mph, and so forth, up to speeds below 45 mph. In this way, the contribution of various speed ranges could be examined.

The data for each day in the analysis period were tabulated into these groups. One additional group was added to find any 30-second data points which had no data or reported an error message. Days with significant quantities of missing data were discarded from examination.

These congestion counts were then divided by the total number of possible points during a peak period (600 * N, where 600 is the number of 30-second segments in 5 hours and N is the number of stations in a given segment of the roadway) to determine the 'congestion rate' for each speed. In other words, the congestion rate is the portion of points which make up the speed contour plot which are under a given speed threshold.

To examine the changes in these congestion rates, the values were averaged across each week (Tuesday to Thursday) to find a weekly congestion rate for the time period of interest (AM or PM peak). These weekly rates were then plotted, as in Figure 2.8. A vertical bar was added to each plot to indicate the time of activation of the VSL system. Also, the entrance volumes for the entire day for the corridor (expanding on the data taken to determine the correlation matrices) were summed to find the total volume for the corridor during each day. These values were also averaged across each week and plotted to show the trend in overall traffic volumes for the roadway.

A number of different filters were applied to the dates for these plots to eliminate irregularities, such as weather, crash events, holidays, etc. First, days with abnormal (high or low) overall volume were eliminated, along with dates with unusual congestion patterns (such as those found during severe snow events, etc.). A second pass of filtering was done by plotting all days individually and removing any outlier congestion days. Figure 2.9 shows the same region as Figure 2.8 with the filters applied.

Finally, the correlation matrices were used to find blocks of days which were strongly correlated and had similar overall traffic volumes. These well correlated days were used to create daily and weekly plots to show the variation in congestion over time.

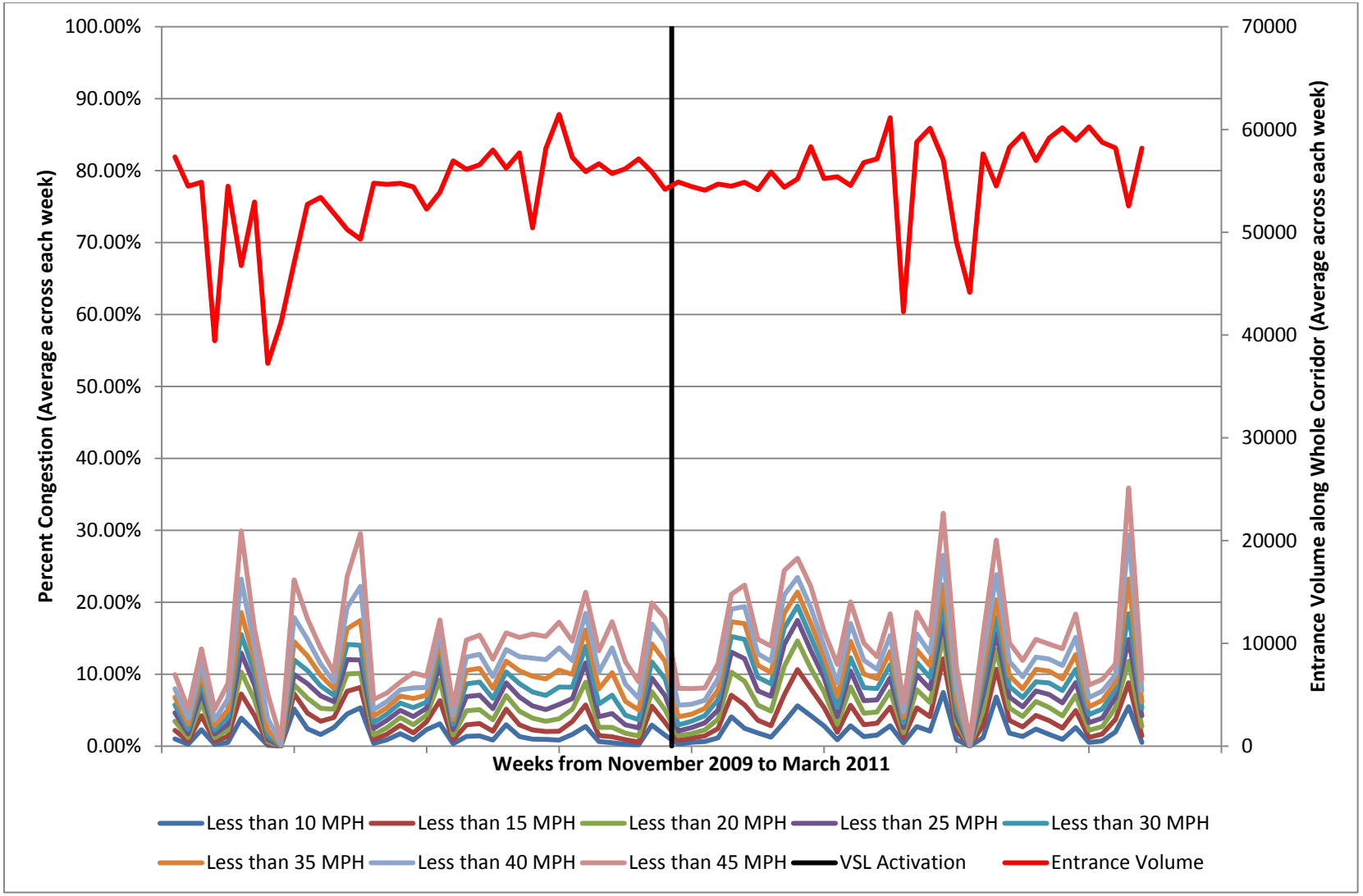

Figure 2.8: Speed-based congestion rates for I-35W northbound during AM peak for the region from I-35 to north of I-494 for dates from November 2009 through March 2011. Each point represents the average across Tuesday, Wednesday, and Thursday for single week, with no filter applied.

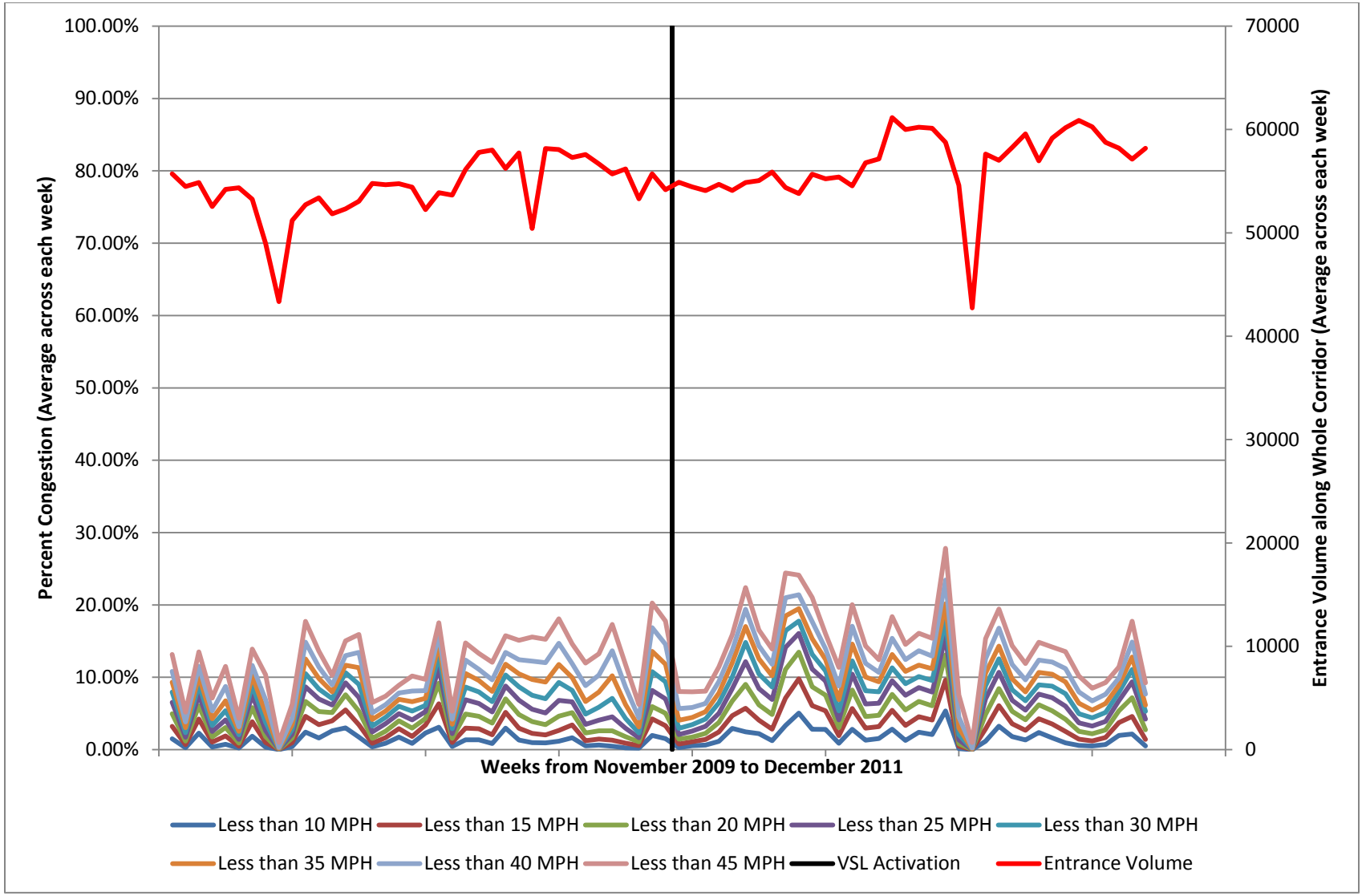

Figure 2.9: Speed-based congestion rates for I-35W northbound during AM peak for the region from I-35 to north of I-494 for dates from November 2009 through December 2011. Two rounds of filters have been applied to remove the most irregular dates from consideration.

2.3 Results

2.3.1 VSL Actuations

By examining the VSL actuations against the speed contours for the corridor, several categories of VSL actuation behavior were observed. Two categories were commonly noted: VSL signs responding to congestion as the congestion shockwave reached the gantry (type I), and VSL signs responding to congestion after the congestion shockwave reached the gantry (type II). A third, less common category was also noted: VSL signs responding to congestion well before the congestion shockwave reached the gantry (type III).

To illustrate type I behavior, Figure 2.10 shows the actuations for a portion of the southbound corridor for January 12, 2011. In the major section of congestion, the VSL signs around stations S27 through S25 all begin showing slower speeds as congestion begins. For a short period of time, the speed displayed is in the 45-50 mph range, but almost immediately drops to 30 mph (the minimum for the system) and stays there throughout the block of congestion.

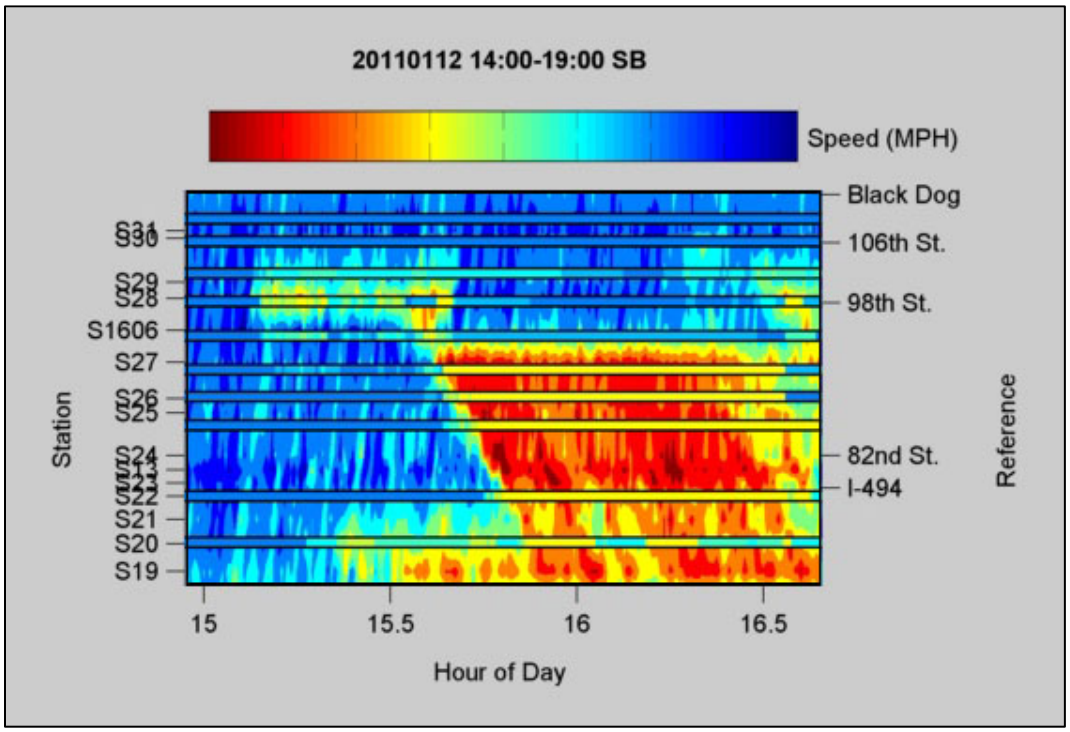

Figure 2.10: Portion of I-35W southbound during evening peak showing VSL actuations of behavior type I.

Note that each gantry along the segment only begins displaying an advisory speed shortly before the onset of congestion. The building congestion wave moves upstream activating gantries just before passing each location.

Northbound showed the same behavior as southbound, as shown in Figure 2.11. Near letter C, the signs encounter congestion and respond as the congestion wave reaches the sign (type I), but not significantly before the congestion. They then get to 30 mph after a short period of time and

remain there for the duration of congestion. (Note that several detectors were not reporting correctly, but the signs near stations S1602, 35, and 1601 were only dependent upon correctly reporting detectors.)

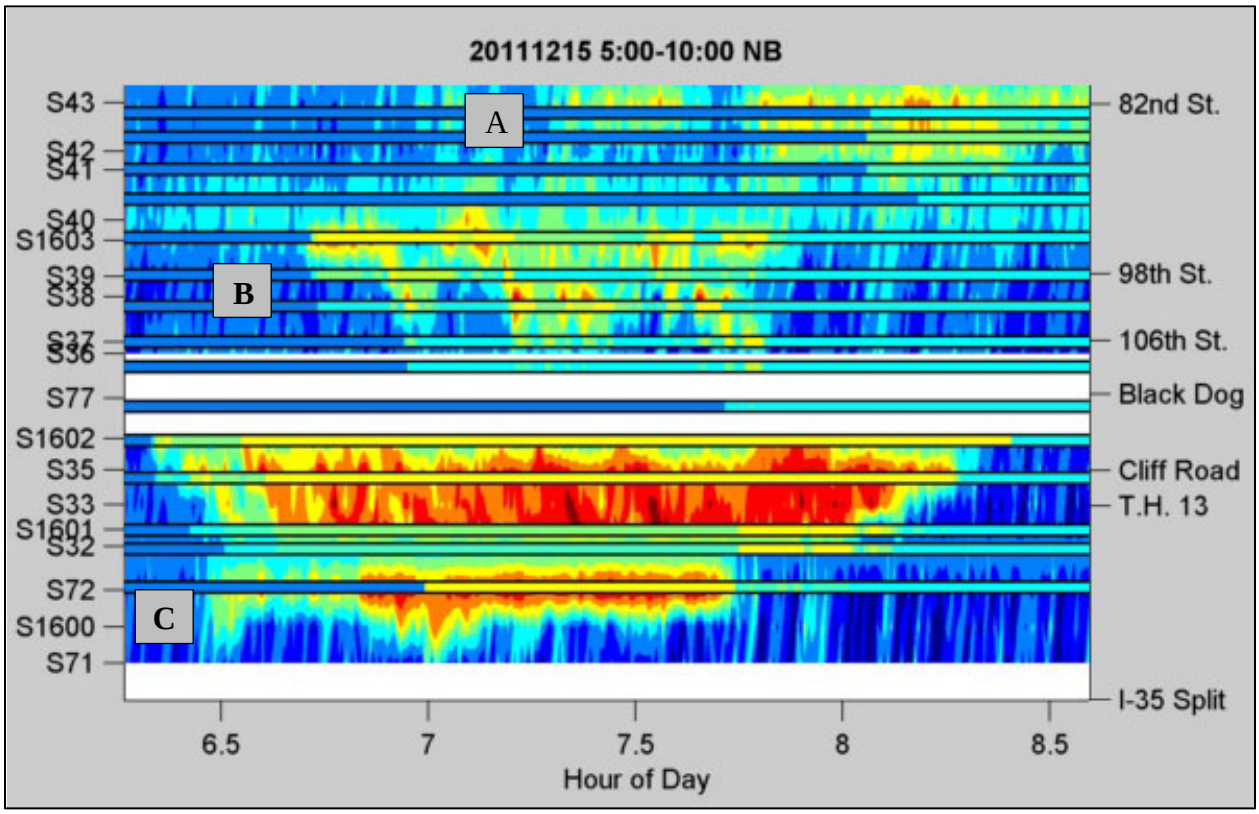

Figure 2.11: Sample of December 15, 2011 speed contour showing VSL actuations.

Letter A shows the VSL signs responding late to congestion near 82nd Street (type II). Congestion activity is ongoing in the region of the gantries, but no actuations are made for approximately one hour. When the gantries do activate, they immediately jump to between 40 and 50 mph and remain at the same actuation level until the end of congestion.

However, near Letter B, the VSL signs show a strong response to the building congestion wave near station S1603 (type III). The two signs upstream of congestion activate at approximately the same time to slow oncoming traffic. As the congestion builds upstream just before 7:00 AM, the next two signs activate at approximately the same time to slow the next block of roadway. These activations come significantly before congestion reaches the signs (the sign upstream of S38 in the first activation set, the sign upstream of S36 in the second activation set). This behavior gives drivers a significant window in which to note the VSL advisory and respond while still being relevant to an active congestion region downstream.

In general, the signs respond individually or with one immediate neighbor, and only rarely in groups of three. Since they only activate along short lengths of the network as congestion begins, the congestion wave travels back past the influence of the activated signs. The next set of signs then catch the wave, but again only activate along a short region of the roadway. The

speed of the congestion wave is too fast for the VSL signs to give significant warning to oncoming traffic.

However, despite the issue of late onset, the VSL system does appear to positively impact the most severe congestion (speeds below 10-15 mph). Figure 2.12 and Figure 2.13 show the speed contours for two dates approximately one year apart. The first date (April 27th, 2010 - prior to the activation of the VSL system) shows significant severe congestion at the Cliff Road bottleneck. Of particular note are the darkest red bands that propagate upstream extremely quickly (appearing at nearly the same time in several locations). The sudden appearance of these stopped or idling queues represents a significant safety issue within the congested region of traffic.

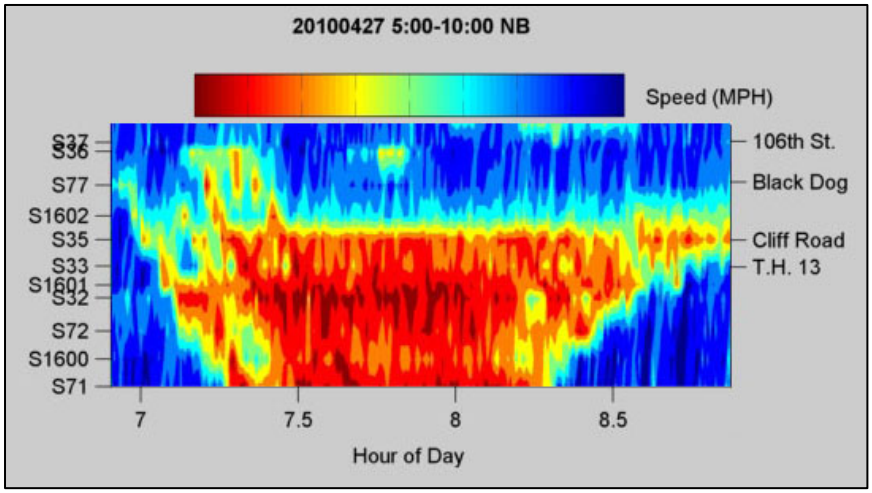

Figure 2.12: Major congestion surrounding Cliff Road for April 27th, 2010 (Before VSL Activation).

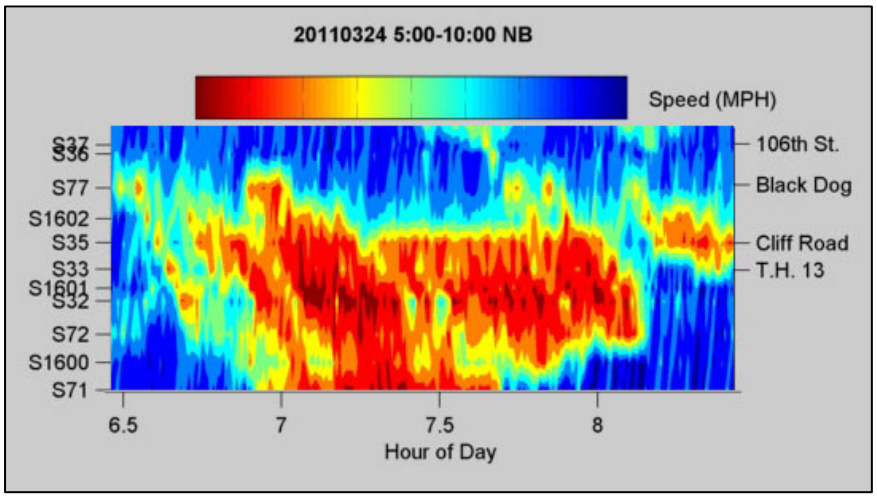

Figure 2.13: Major congestion surrounding Cliff Road for March 24th, 2011 (After VSL Activation).

By comparison, the most severe congestion on March 24th, 2011 has less stopped/idling congestion and very little upstream propagation. (The VSL system actuated to show 30 mph as the advisory speed from prior to 7 AM in the particular portion of the corridor of interest. The VSL actuations are not shown as they obscure the speed contours.) The presence of smaller stopped-traffic queues indicates that the behavior of drivers after congestion has begun is different with the VSL system in place.

2.3.2 Effect on Traffic Flow Characteristics

As noted above, the VSL system appears to alter the behavior of drivers during congestion. To explore this further, a small sample of dates were selected. These dates were among the highest correlated and had similar weather conditions with each other. The detector data for those days were used to create fundamental diagrams for detectors along the corridor. These fundamental diagrams, such as Figure 2.14, relate volume and occupancy.

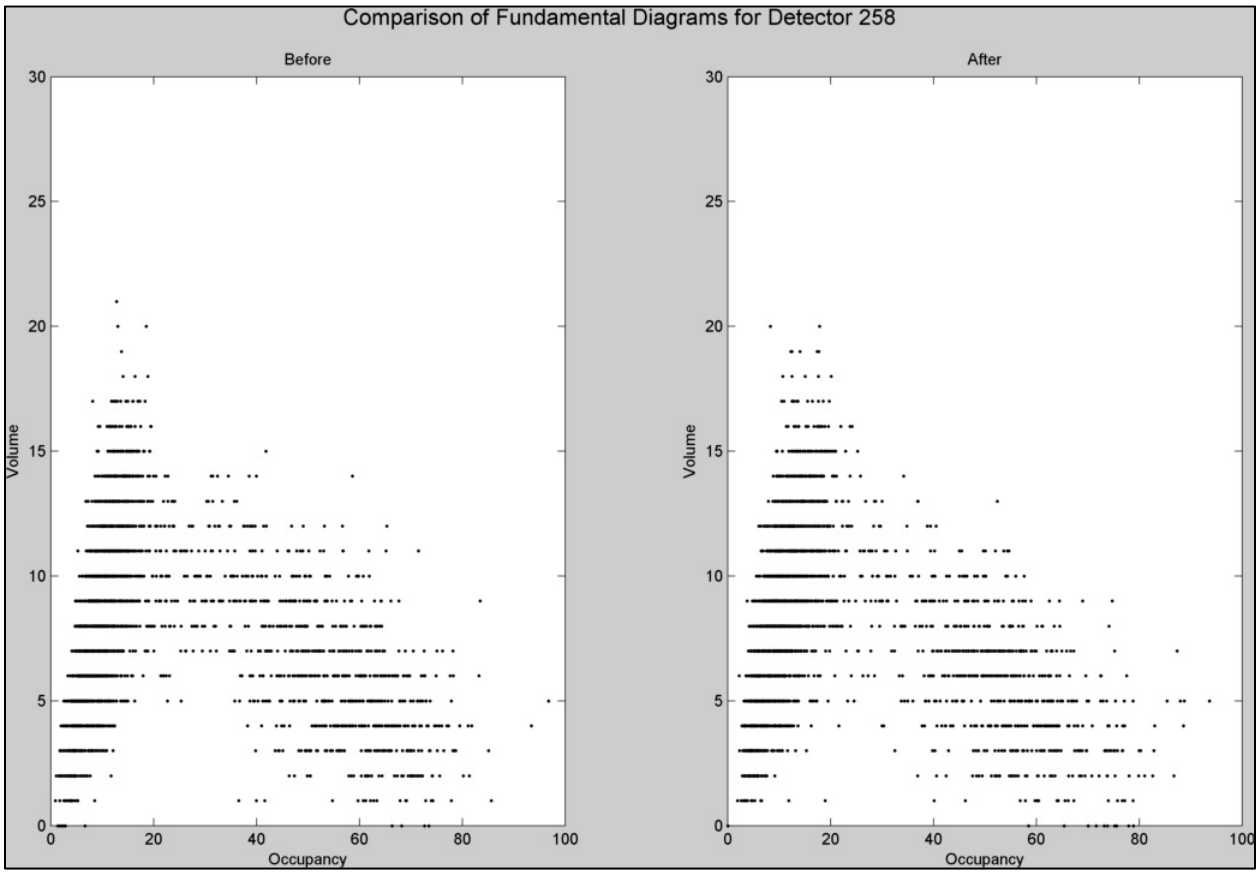

Figure 2.14: Fundamental diagrams for Detector 258 for highly correlated dates before and after VSL activation.

From the speed contour plots, it was observed that the VSL system generally acts only during congestion. Thus, any impacts to drivers, and any changes to the fundamental diagram, would be located in the congested region only. As can be noted from Figure 2.14, the congested region is difficult to visually inspect due to the size of the 'cloud' of points. To quantify the congested behavior for each detector in a way more easily interpreted, the median and quartiles were

extracted for each 5% segment of occupancy between 15% and 70% (i.e. points with 15-20% occupancy were grouped, etc.). These medians and quartiles were then plotted for each detector, such as in Figure 2.15 (note that the 15-20% occupancy values are plotted at 17.5% occupancy, etc.).

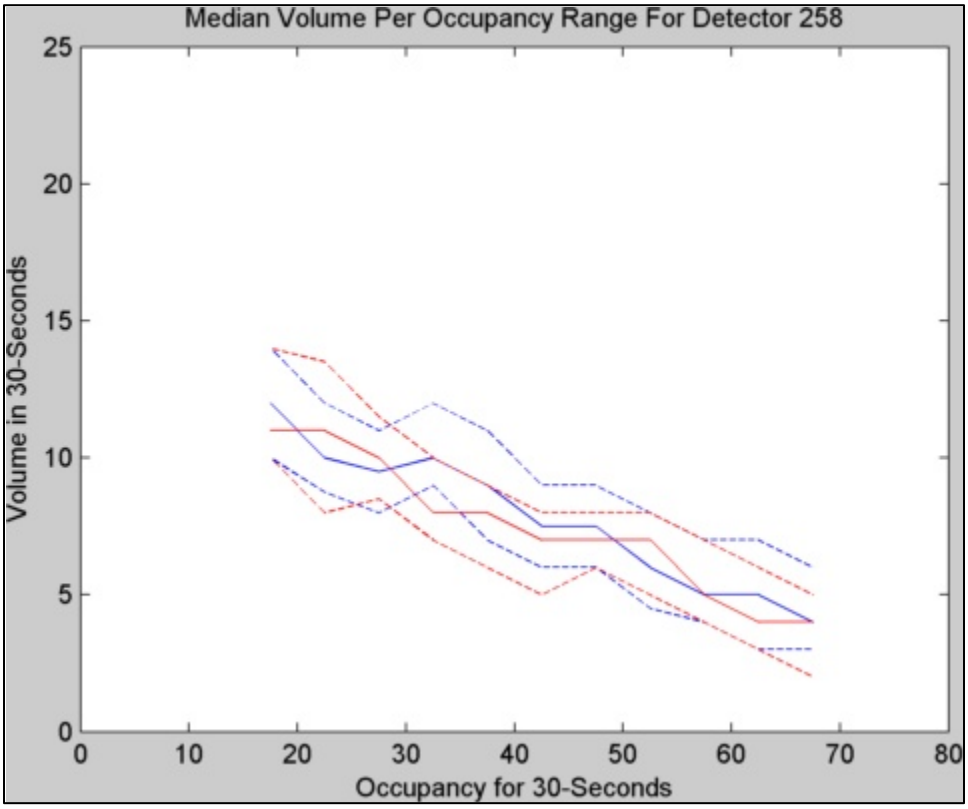

Figure 2.15: Medians and quartiles for the congested region of the fundamental diagrams for detector 258 before (blue) and after (red) VSL actuation.

Detector 258 belongs to station 32 and is at the heart of much of the worst congestion from the Cliff Road bottleneck. For occupancies between roughly 30 and 50 percent, the volume in 30 seconds is seen in Figure 2.15 to be slightly less after VSL implementation. Alternately, for a given volume level the occupancy observed decreases which means speed increases. This suggests that drivers are able to drive faster but with larger gaps during congestion.

For detector 258, these median values were used to find linear fit lines for both before and after VSL implementation. Figure 2.16 shows the fit lines with their equations; the post-VSL fit is nearer to the origin across the entire congested region. The slopes of the two lines are similar, although the post-VSL fit is nearer to the pre-VSL fit at higher occupancy values. This suggests that in the congestion region shockwaves are slightly slower with the VSL system in place.

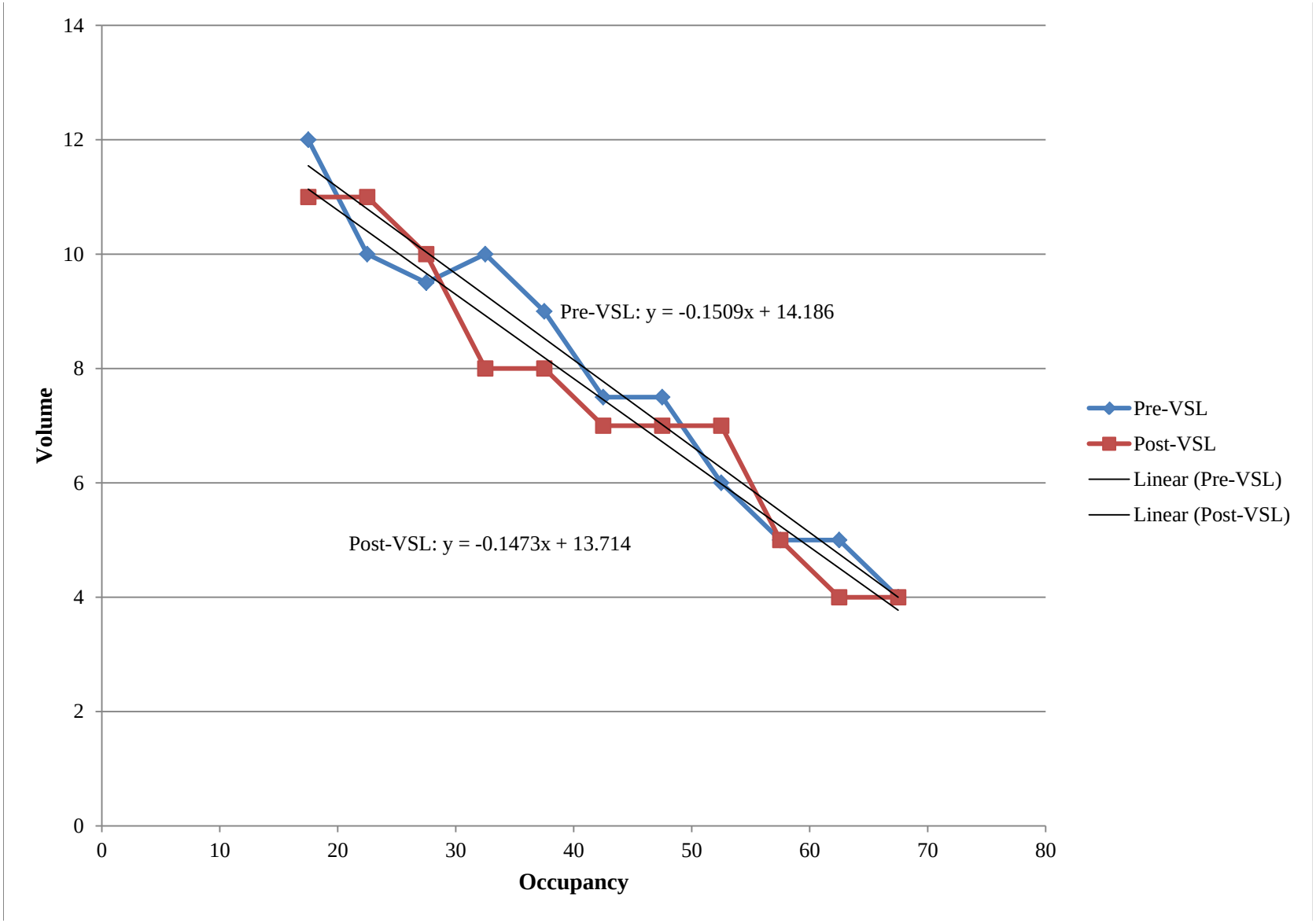

Figure 2.16: Linear fits (with equations) of congestion region of fundamental diagrams for detector 258.

To ensure that the variations seen above were not the result of grouping 5% segments of occupancy, the same analysis was done with 2% segments and the entire fundamental diagram instead of just the congested region. The detectors for the Cliff Road bottleneck were arranged according to lane and position along the roadway to create Figure 2.17. From this figure, we can see a pattern in the behavior of drivers during congestion.

County Road 42 is furthest upstream and does not interact sufficiently with the system to experience a change (it is marked with a gray bar to indicate this no-change condition). Progressing downstream, the right-lane detectors from McAndrews Road to upstream of Highway 13 show a lower curve in the congestion region between 30 and 50% occupancy (as illustrated above with detector 258). The detectors immediately upstream of Highway 13 and at McAndrews Road do not show the behavior as clearly as the middle two locations (all four are marked with a blue bar to indicate this condition).

The two stations at the bottleneck, those at Highway 13 and Cliff Road, again show no change due to the VSL system. Downstream of the bottleneck, an effect is once again present in the fundamental diagram. For the stations around Blackdog Road (the top three in the figure), the maximum occupancy values increased after the VSL system was implemented. The left-lane detector at Blackdog Road is the best example of this behavior: the post-VSL curve extends to much higher occupancies than the pre-VSL curve. Vehicles leaving the bottleneck do so with slightly lower speed than before.

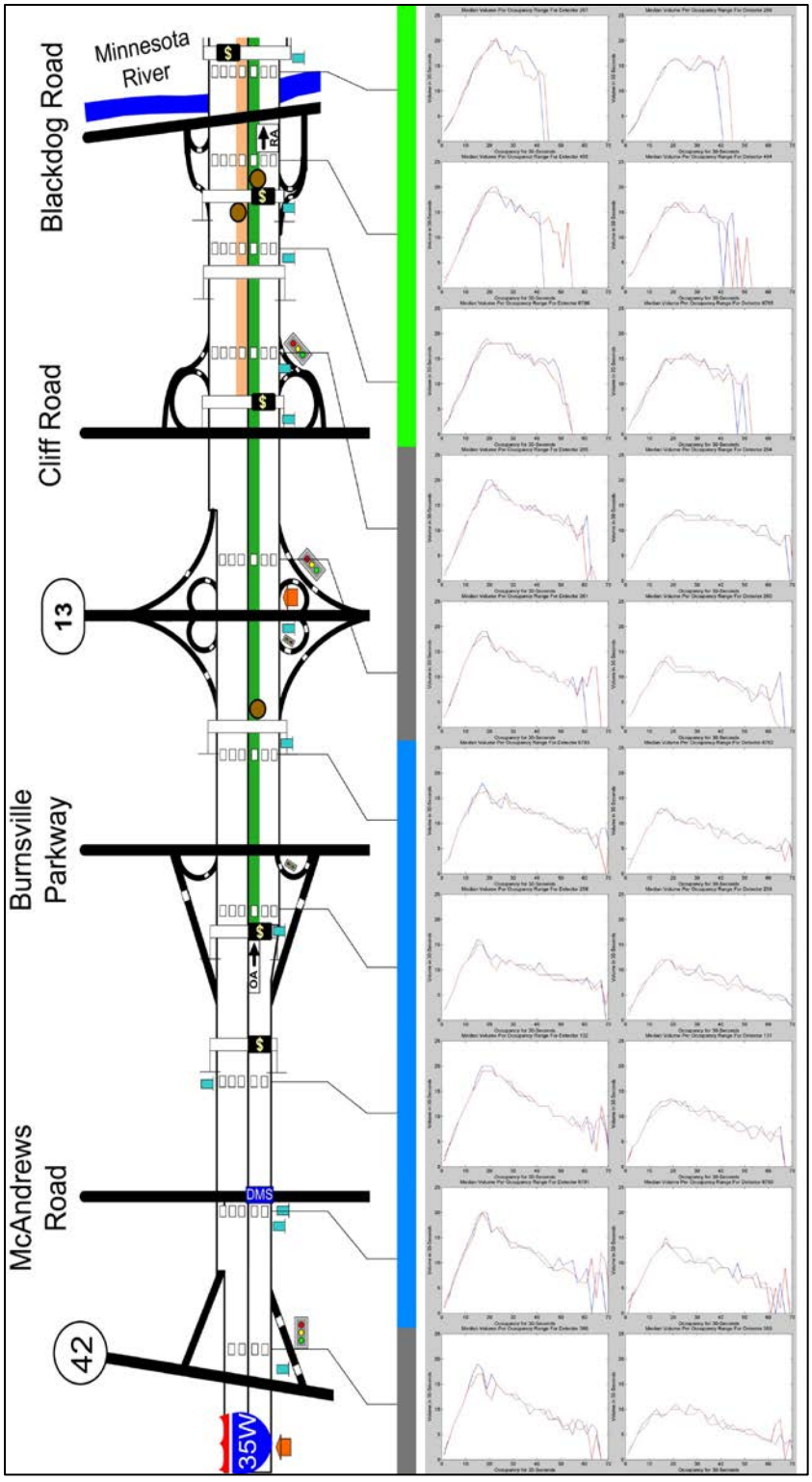

Figure 2.17: Medians of for the entire fundamental diagram for mainline detectors from County Road 42 to Blackdog Road; Right side fundamental diagrams are for the right-most lane, left side fundamental diagram medians are for the left or middle lanes (depending on location).

Further evidence of smoother shockwaves during congestion was found by examining before and after data for individual detectors using DataPlot. Two of the highly correlated days for AM peak – one before VSL implementation and one after – were plotted together showing flow, occupancy, and speed. Figure 2.18 and Figure 2.19 show detectors 258 and 259 (the same location as discussed above). At the onset of congestion, the speed at each detector drops significantly in a short period of time. However, the post-VSL cases show a more gradual decrease in speed.

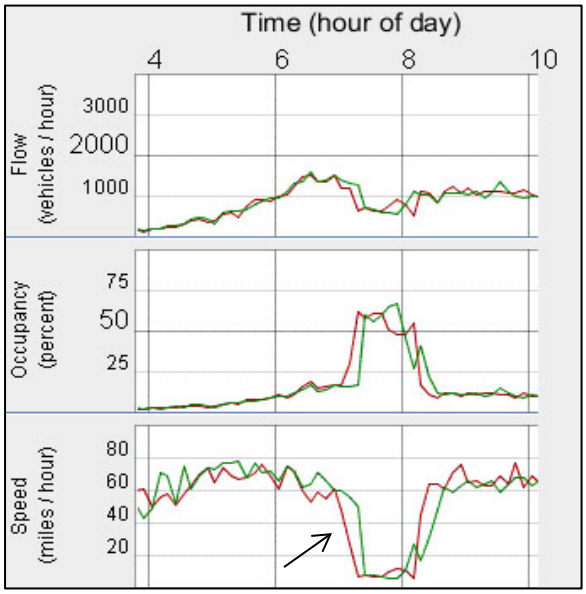

Figure 2.18: Flow, Occupancy, and Speed for Detector 258 between two of the most highly correlated dates; green is before VSL, red is after VSL.

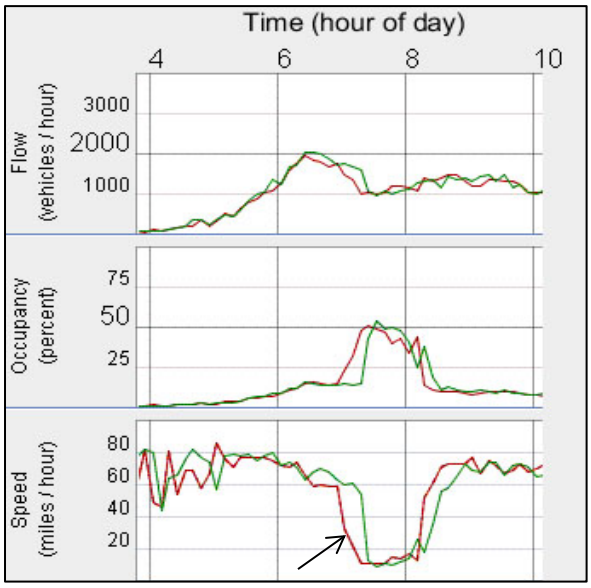

Figure 2.19: Flow, Occupancy, and Speed for Detector 259 between two of the most highly correlated dates; green is before VSL, red is after VSL.

In a few cases, the speed during pre-VSL dates showed a spike during the transition to congested conditions. This indicates that the traffic conditions near the detector were unstable, causing more than one major congestion shockwave to occur. After the VSL was implemented, these cases of double shockwaves were reduced as in Figure 2.20.

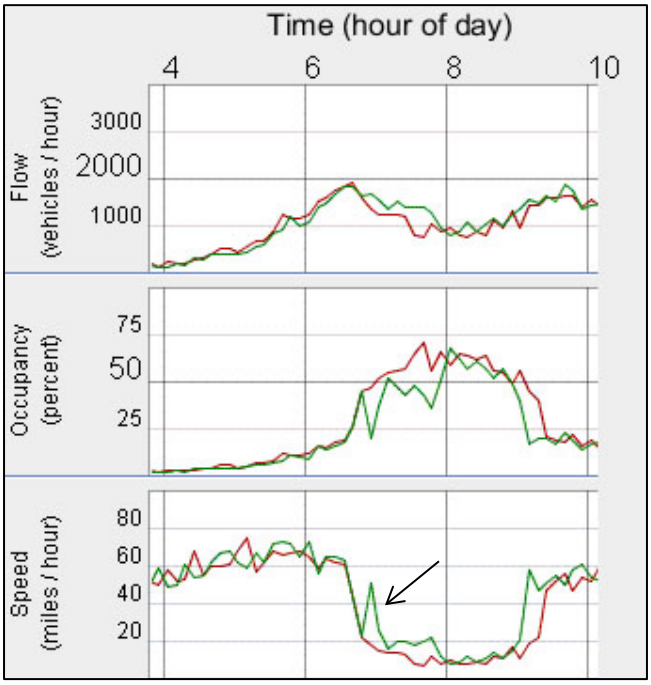

Figure 2.20: Flow, Occupancy, and Speed for Detector 6818 between two of the most highly correlated dates; green is before VSL, red is after VSL.

The detectors that exhibited behavior as in these figures were all in locations that observed significant congestion and were influenced by the VSL signs. Those detectors that were outside of the congestion block were not affected.

Similar conditions were found for the PM peak. However, the southbound side of the corridor was notably different from the northbound side in two ways: the boundary condition correlations were overall much worse (less correlated) than the northbound side, and fewer detectors experienced significant congestion among the best correlated days. The detectors experiencing major congestion still showed signs of smoother transitions and less evidence of double shockwaves. The detectors at stations 26, 27, and 1606 all showed smoother congestion periods with less evidence of double shockwaves and fewer large changes in speeds. Figure 2.21, Figure 2.22, and Figure 2.23 show the DataPlot information for each pair of detectors.

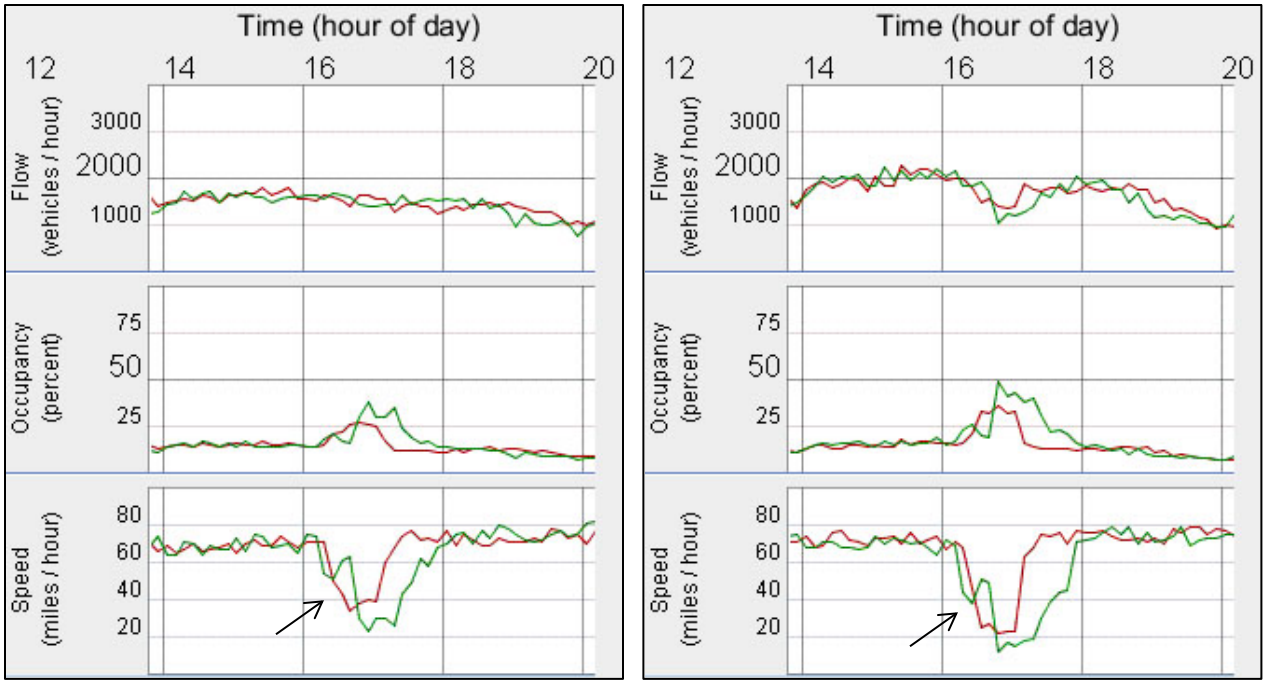

Figure 2.21: Flow, Occupancy, and Speed for Detectors 246 (left) and 247 (right) between two of the most highly correlated dates; green is before VSL, red is after VSL.

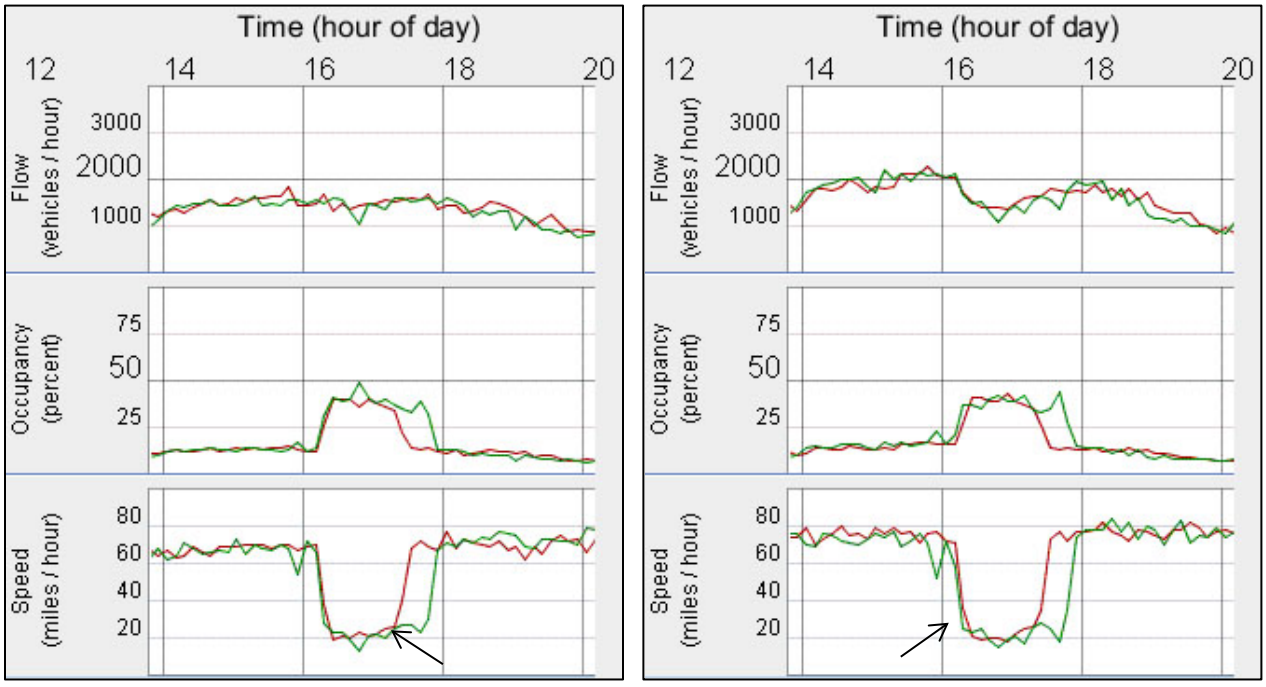

Figure 2.22: Flow, Occupancy, and Speed for Detectors 248 (left) and 249 (right) between two of the most highly correlated dates; green is before VSL, red is after VSL.

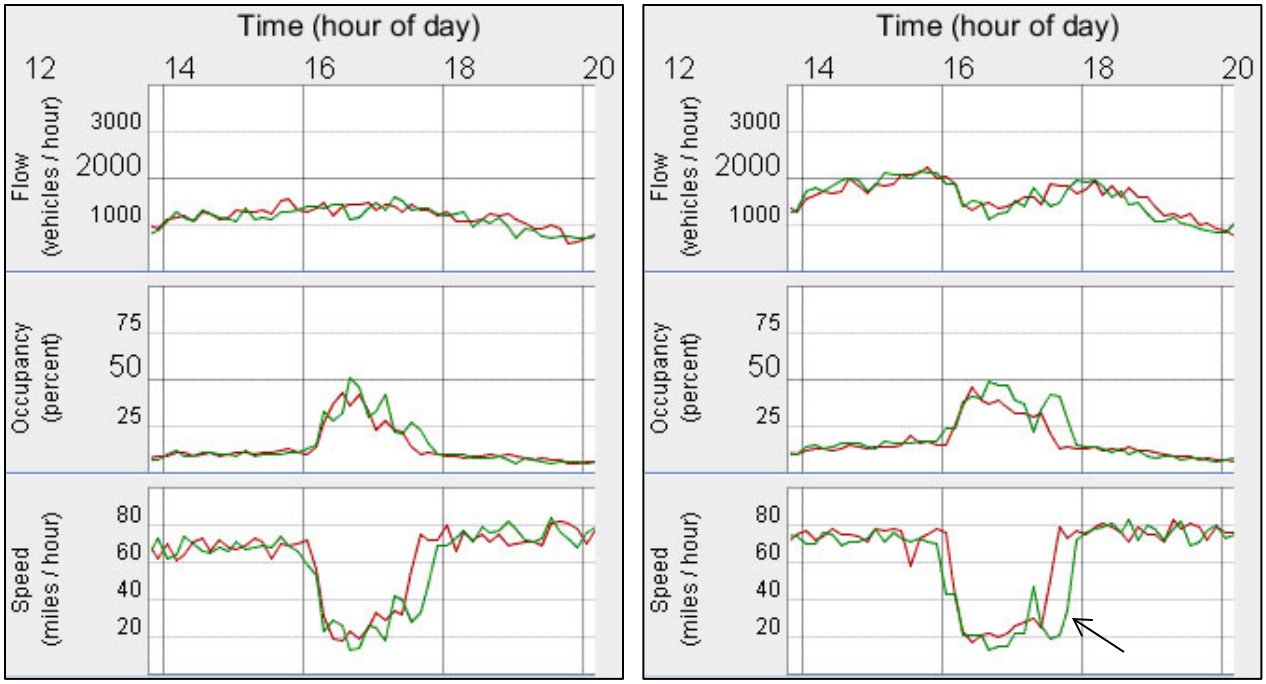

Figure 2.23: Flow, Occupancy, and Speed for Detectors 6799 (left) and 6800 (right) between two of the most highly correlated dates; green is before VSL, red is after VSL.

2.3.3 Speed-Based Congestion

The previous methods of analysis have focused on localized impacts of the VSL system: the VSL actuations only apply at specific segments of roadway, and the fundamental diagram only applies to individual detectors. To get a larger view of the impact of the VSL system, the speed contours from Section 2.4 were numerically analyzed.

By looking at the speed contours for the entire corridor, several segments of the roadway were identified for analysis. In the morning peak, two major bottlenecks were noted: Cliff Road and Highway 13 together form a bottleneck, and I-494. In the afternoon peak, only one major bottleneck was identified at 98th Street. In both directions, the detectors north of highway 62 were disregarded due to a combination of construction issues and lack of VSL activity.

2.3.3.1 Cliff Road Bottleneck (AM Northbound)

After tabulating the detector measurements for each speed threshold for the Cliff Road bottleneck segment, the percentages (as described in Section 2.4) were averaged for each week in the applicable analysis period and are shown in Figure 2.24. Weeks from November 2009 through May 2011 were averaged, while weeks from June 2011 to December 2011 were disregarded due to significant detector issues. Figure 2.24 shows the weekly averages without any filter applied to remove holidays, days with severe weather, and other irregular events affecting traffic.

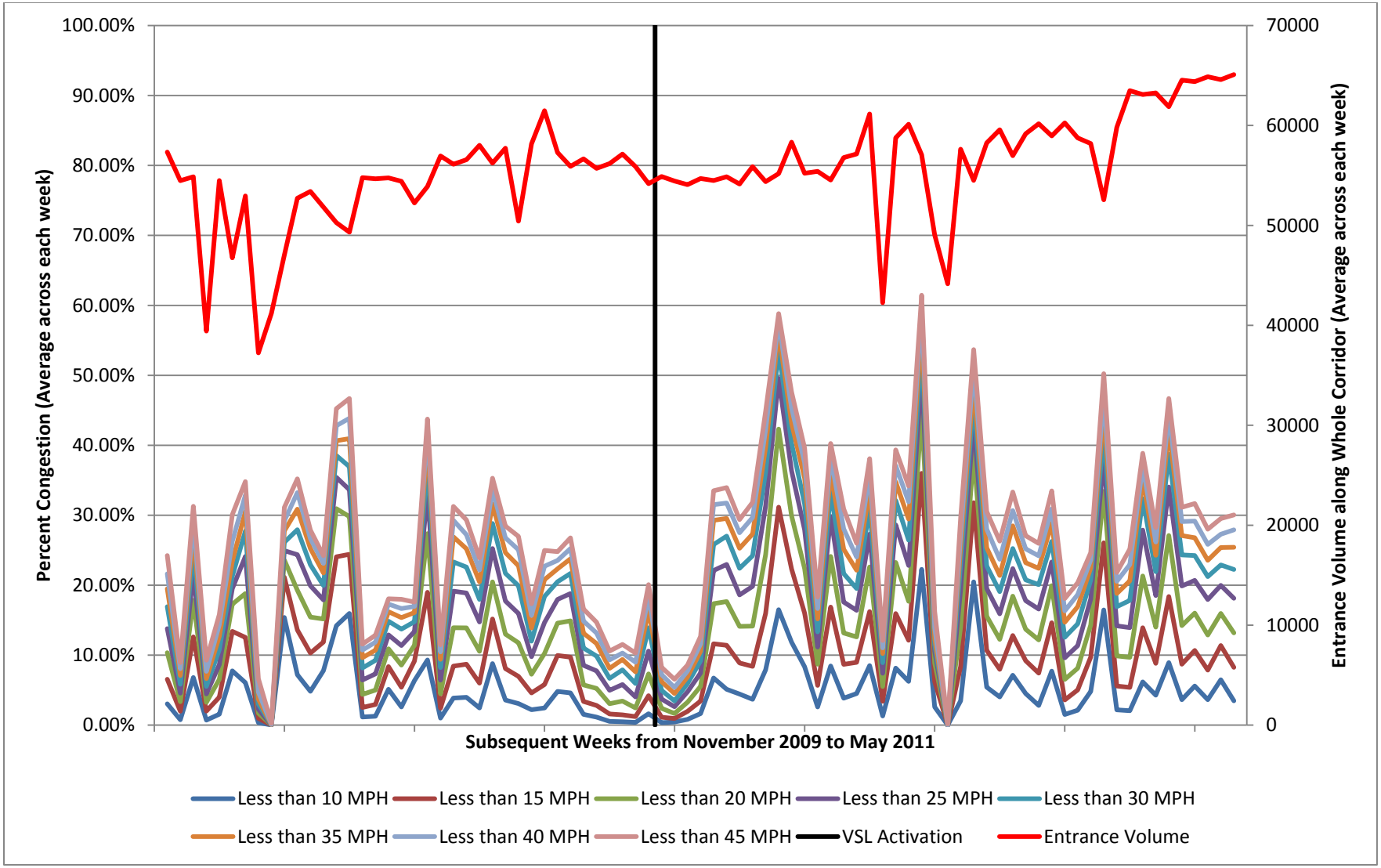

Figure 2.24: Average weekly speed-based congestion for all days between November 2009 and May 2011 for the Cliff Road bottleneck segment.

As can be seen in Figure 2.24, the weekly averages show significant fluctuations in congestion rates during AM peak. To further condense the values, all days before VSL implementation and all days after VSL implementation were averaged (see Table 2.1). As can be seen, with all days included, the total congestion levels for the Cliff Road bottleneck during AM peak increased at all speed thresholds.

Table 2.1: Average percent of AM peak below speed thresholds from 10 mph to 45 mph for the Cliff Road bottleneck region based on all Tuesdays, Wednesdays, and Thursdays between November 2009 and May 2011.

	Speed Threshold (mph)							
	10	**15**	**20**	**25**	**30**	**35**	**40**	**45**
Before VSL Implementation	4.34%	8.09%	11.67%	14.77%	17.30%	19.33%	20.95%	22.58%
After VSL Implementation	5.85%	11.33%	16.40%	20.68%	23.84%	26.28%	28.20%	30.16%

However, this includes the impacts of weather, holidays, etc. To reduce the impacts of factors unrelated to the VSL system, the well correlated days identified using the GEH statistic were used to generate the same type of figure and table as above. Table 2.2 shows the average percentages for each speed threshold and Figure 2.25 shows the averages for the weeks containing well correlated days.

Table 2.2: Average percent of AM peak under speed thresholds from 10 mph to 45 mph for the Cliff Road bottleneck region based on well correlated days before and after VSL implementation.

	Speed Threshold (mph)							
	10	**15**	**20**	**25**	**30**	**35**	**40**	**45**
Before VSL Implementation	2.83%	6.02%	9.45%	12.61%	15.28%	17.38%	19.01%	20.55%
After VSL Implementation	2.42%	5.45%	8.58%	11.52%	13.84%	15.82%	17.44%	19.16%

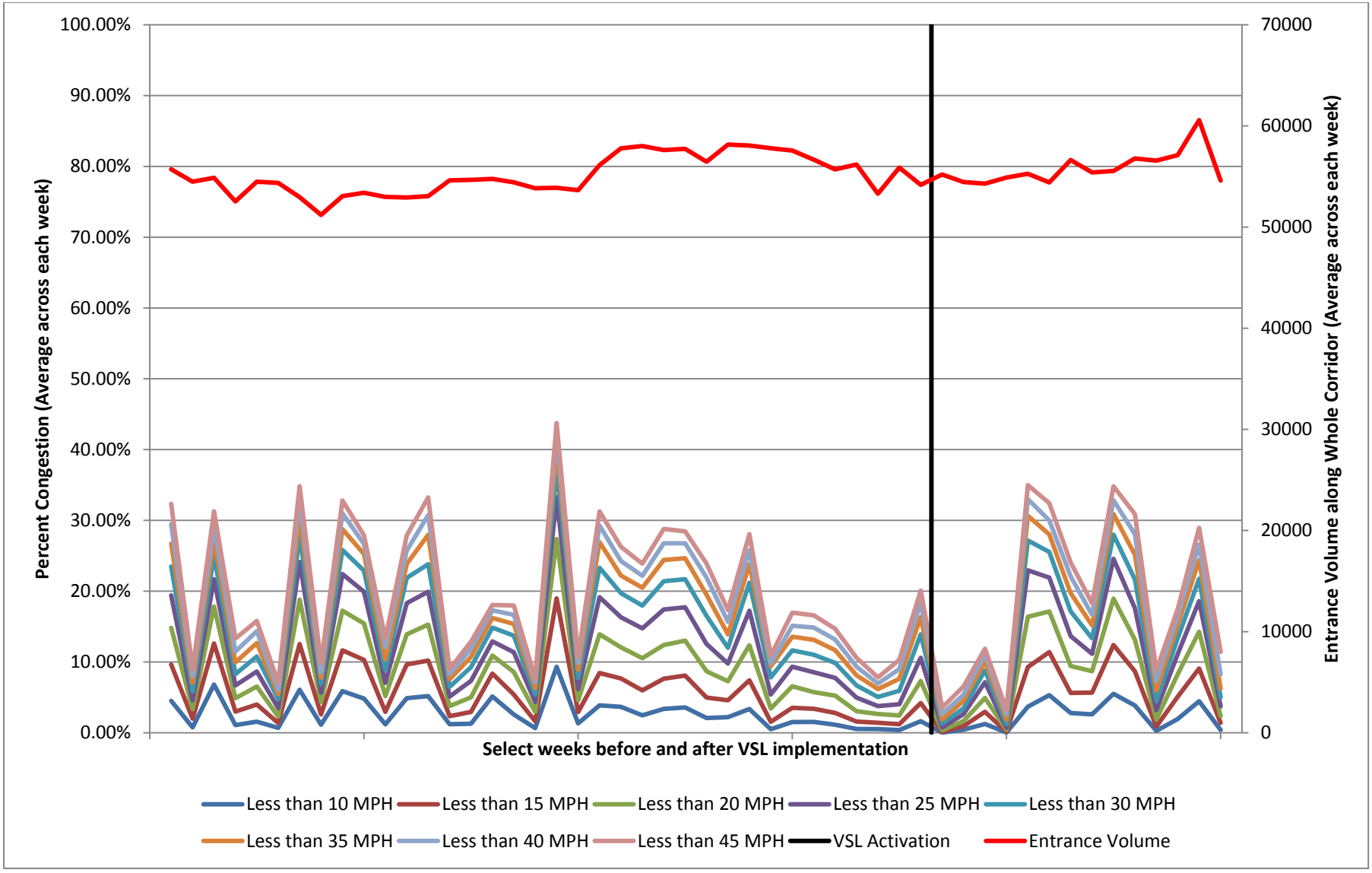

Figure 2.25: Average weekly speed-based congestion for well correlated days for the Cliff Road bottleneck.

Among well correlated days, after the VSL system was implemented, the Cliff Road bottleneck showed a slight decrease in congestion at each speed threshold. To put these values into perspective in terms of time, Table 2.3 shows these percentages as minutes per AM peak. Two additional rows were added to show the absolute difference for each speed threshold and the percentage change from before VSL to after VSL implementation.

Table 2.3: Minutes per AM peak for each speed threshold for the Cliff Road bottleneck region based on well correlated days before and after VSL implementation.

	Speed Threshold (mph)							
	10	**15**	**20**	**25**	**30**	**35**	**40**	**45**
Before VSL Implementation	8.5	18.1	28.4	37.8	45.8	52.1	57.0	61.6
After VSL Implementation	7.2	16.4	25.7	34.6	41.5	47.5	52.3	57.5
Absolute Improvement	1.3	1.7	2.7	3.2	4.3	4.6	4.7	4.1
Percent Improvement	15.3%	9.4%	9.5%	8.5%	9.4%	8.8%	8.2%	6.7%

After VSL implementation, overall congestion (speeds under 45 mph) were decreased by nearly 7% for well correlated days. Speeds below 40 mph were cut by slightly more than 8% and extremely low speeds were reduced by about 15%. For well correlated days, the average AM peak between 4 and 5 minutes less congestion along the entire segment than before the VSL system was implemented.

To look closer at the change in congestion percentages, the contribution of each speed range was calculated by taking the difference of subsequent columns in Table 2.2. These differences are found in Table 2.4. As can be seen, the lower speed segments tend to contribute more congestion (i.e. percent of AM peak) than the higher speed segments. After the VSL system was implemented, the lower speeds (0 mph to 30 mph) saw decreases in frequency, while the higher speeds (30 mph to 45 mph) stayed roughly the same or increased slightly.

Table 2.4: Average percent of AM peak in speed ranges for the Cliff Road bottleneck region based on well correlated days before and after VSL implementation.

	Speed Range (mph)							
	0-10	**10-15**	**15-20**	**20-25**	**25-30**	**30-35**	**35-40**	**40-45**
Before VSL Implementation	2.83%	3.19%	3.43%	3.16%	2.66%	2.10%	1.64%	1.53%
After VSL Implementation	2.42%	3.04%	3.13%	2.94%	2.33%	1.98%	1.62%	1.71%

2.3.3.2 I-494 Bottleneck (AM Northbound)

Using the same analysis method as for the Cliff Road bottleneck, the speed contours for the I-494 bottleneck segment were analyzed and tabulated. Weeks from November 2009 to March 2011 were used (April 2011 to December 2011 had significant detector issues). Again, the unfiltered weekly averages show significant variation in congestion rates through the bottleneck segment as shown in Figure 2.26.

Condensing the values, all days before VSL implementation and all days after VSL implementation were averaged in Table 2.5. Even with the irregular dates included, the overall congestion for the I-494 bottleneck decreased at each speed threshold.

Table 2.5: Average percent of AM peak below speed thresholds from 10 mph to 45 mph for the I-494 bottleneck region based on all Tuesdays, Wednesdays, and Thursdays between November 2009 and March 2011.

	Speed Threshold (mph)							
	10	**15**	**20**	**25**	**30**	**35**	**40**	**45**
Before VSL Implementation	0.31%	0.66%	1.09%	1.74%	2.72%	4.19%	6.29%	9.50%
After VSL Implementation	0.25%	0.55%	0.95%	1.54%	2.42%	3.73%	5.71%	8.65%

Using the well correlated days based on the GEH statistic, the impacts from non-VSL sources were minimized and the impact of the VSL system was isolated. Table 2.6 shows the percent of AM peak for each speed threshold based on only the well correlated days, and the weekly averages are shown in Figure 2.27.

Table 2.6: Average percent of AM peak under speed thresholds from 10 mph to 45 mph for the I-494 bottleneck region based on well correlated days before and after VSL implementation.

	Speed Threshold (mph)							
	10	**15**	**20**	**25**	**30**	**35**	**40**	**45**
Before VSL Implementation	0.55%	1.16%	1.78%	2.65%	3.99%	5.99%	8.64%	12.25%
After VSL Implementation	0.32%	0.75%	1.24%	1.86%	2.72%	3.84%	5.47%	8.01%

For well correlated days, the I-494 bottleneck showed a decrease in overall congestion of approximately one-third, with similar decreases for each speed threshold. Again, to put these values in terms of time, Table 2.7 shows the percentages as minutes per AM peak.

Table 2.7: Minutes per AM peak for each speed threshold for the I-494 bottleneck region based on well correlated days before and after VSL implementation.

	Speed Threshold (mph)							
	10	**15**	**20**	**25**	**30**	**35**	**40**	**45**
Before VSL Implementation	1.7	3.5	5.3	7.9	12.0	18.0	25.9	36.8
After VSL Implementation	1.0	2.2	3.7	5.6	8.2	11.5	16.4	24.0
Absolute Improvement	0.7	1.2	1.6	2.3	3.8	6.4	9.5	12.7
Percent Improvement	42.3%	35.5%	30.2%	29.6%	31.9%	35.9%	36.7%	34.6%

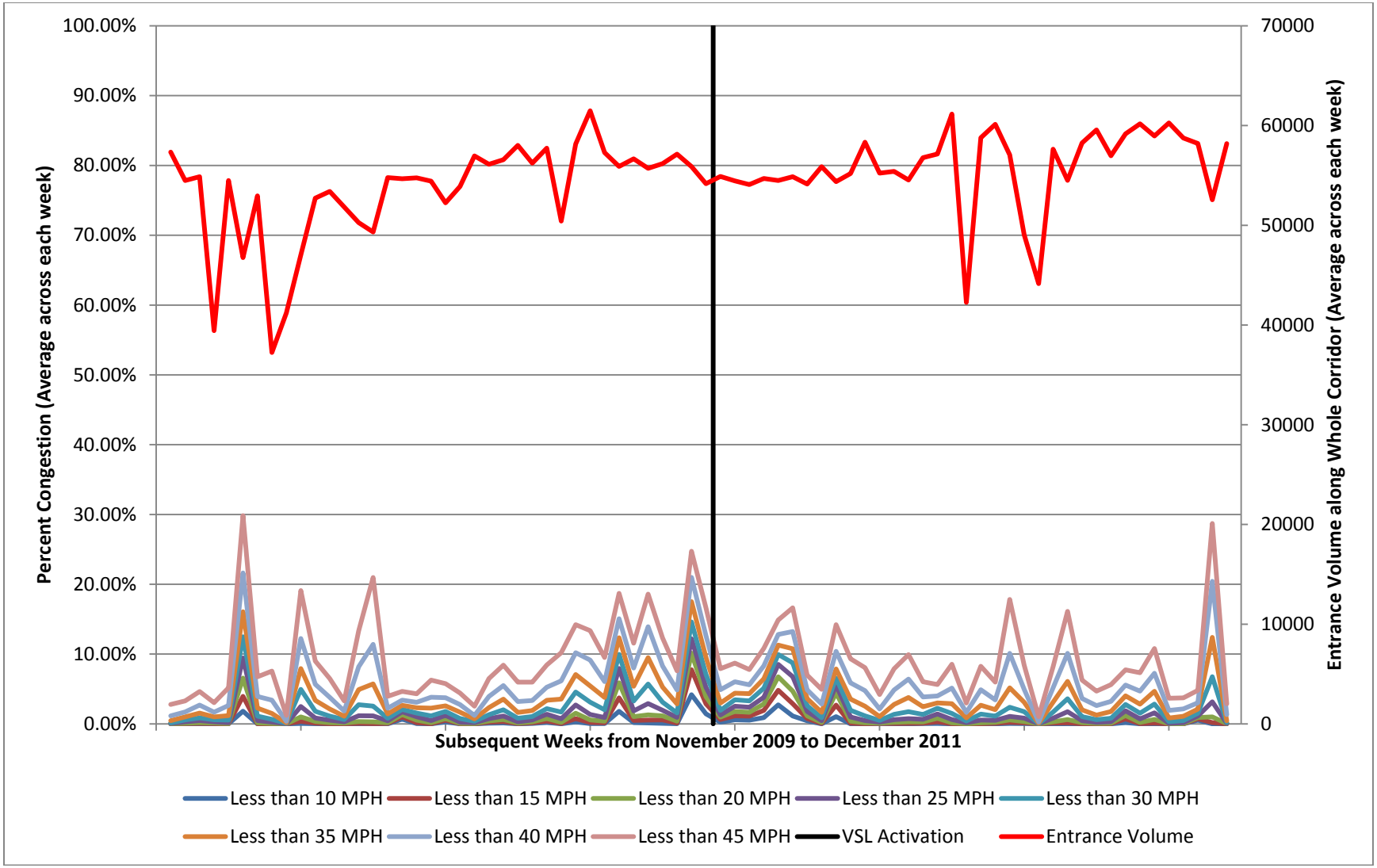

Figure 2.26: Average weekly speed-based congestion for all days between November 2009 and December 2011 for the I-494 bottleneck.

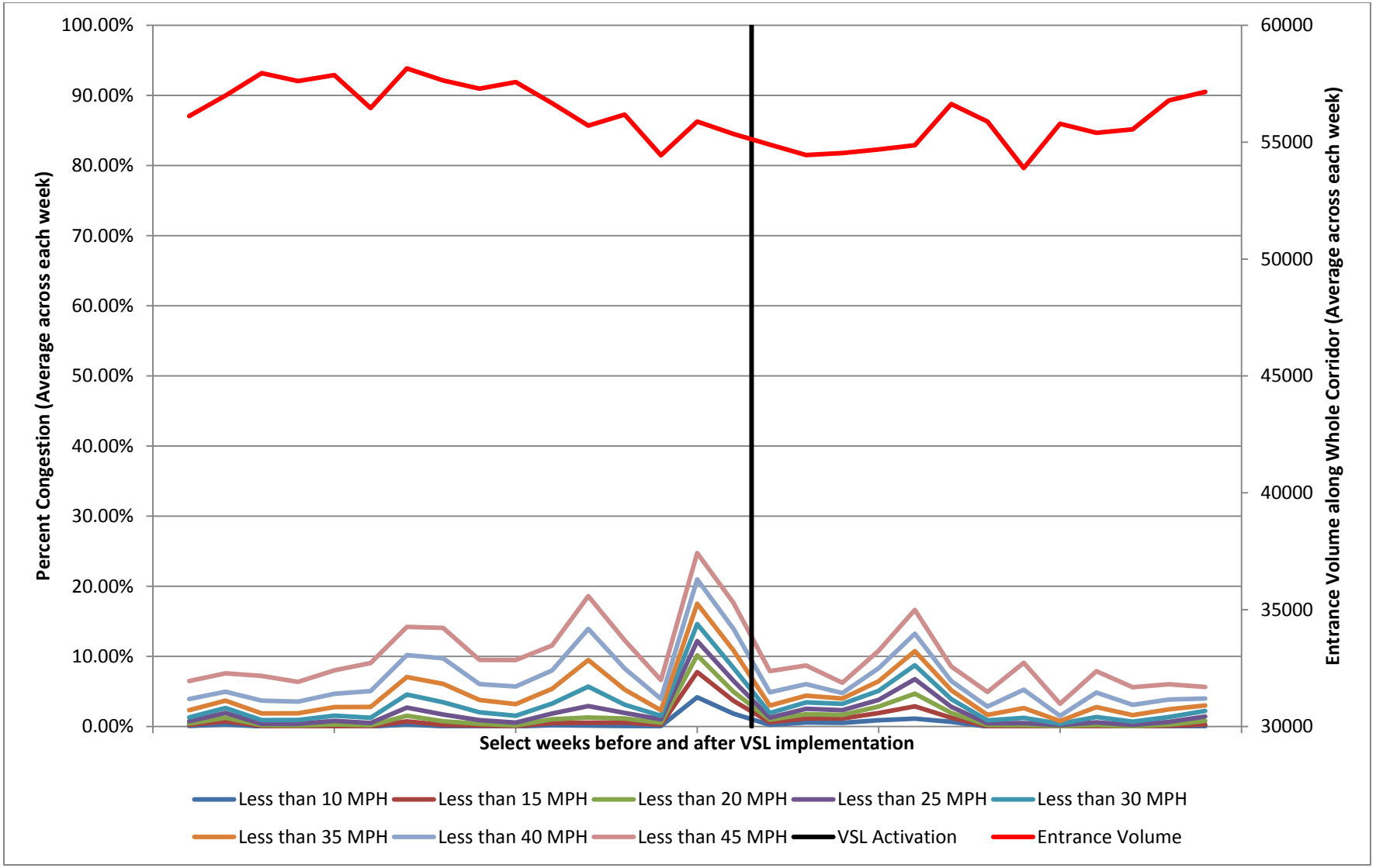

Figure 2.27: Average weekly speed-based congestion for well correlated days for the Cliff Road bottleneck.

The amount of time spent under 45 mph for the I-494 bottleneck region fell by nearly 13 minutes per morning among the well correlated days. The contribution of the slowest speeds (under 10 mph), while relatively small even before the VSL implementation, were reduced by approximately 40%.

Table 2.8 shows the contribution of each speed range (found by taking the difference of subsequent columns in Table 2.6). For the I-494 bottleneck, the major contributions to congestion are in the upper speed ranges (30 to 45 mph) but all speed segments showed a decrease in congestion after the VSL system was implemented.

Table 2.8: Average percent of AM peak in speed ranges for the I-494 bottleneck region based on well correlated days before and after VSL implementation.

	Speed Range (mph)							
	0-10	**10-15**	**15-20**	**20-25**	**25-30**	**30-35**	**35-40**	**40-45**
Before VSL Implementation	0.55%	0.61%	0.62%	0.87%	1.35%	1.99%	2.65%	3.61%
After VSL Implementation	0.32%	0.43%	0.49%	0.62%	0.85%	1.12%	1.63%	2.54%

2.3.3.3 Cliff Road and I-494 Combined (AM Northbound)

Taking the Cliff Road and I-494 bottleneck segments together gives an aggregate picture of the change in speed-based congestion activity for the VSL-active portion of I-35W during AM peak. The days with detector issues for the I-494 and Cliff Road bottlenecks were removed from consideration, leaving the weeks between November 2009 and March 2011. Figure 2.28 shows the unfiltered weekly averages for the combined region.

Taking the before and after VSL implementation days and finding the averages for each speed threshold (see Table 2.9), it can be seen that the overall congestion rate rose by just under 2% of AM peak. Each speed threshold showed a similar increase, with slightly smaller absolute increases for the lower speed thresholds.

Table 2.9: Average percent of AM peak below speed thresholds from 10 mph to 45 mph for the Cliff Road and I-494 bottleneck regions combined based on all Tuesdays, Wednesdays, and Thursdays between November 2009 and May 2011.

	Speed Threshold (mph)							
	10	**15**	**20**	**25**	**30**	**35**	**40**	**45**
Before VSL Implementation	1.65%	3.13%	4.61%	6.07%	7.57%	9.23%	11.18%	13.85%
After VSL Implementation	2.23%	4.28%	6.20%	7.95%	9.54%	11.21%	13.15%	15.75%

Again, the congestion rates fluctuate due to a variety of causal factors. To isolate the impact of the VSL system, the well correlated days for the entire segment were selected. Table 2.10 shows

the tabulated results and Figure 2.29 shows the weekly averages for those weeks with well correlated days.

Table 2.10: Average percent of AM peak under speed thresholds from 10 mph to 45 mph for the Cliff Road and I-494 bottleneck regions combined based on well correlated days before and after VSL implementation.

	Speed Threshold (mph)							
	10	**15**	**20**	**25**	**30**	**35**	**40**	**45**
Before VSL Implementation	1.03%	2.30%	3.77%	5.40%	7.21%	9.22%	11.51%	14.40%
After VSL Implementation	1.06%	2.39%	3.83%	5.32%	6.72%	8.11%	9.71%	11.87%

Among well correlated days for the segment, after the VSL system was implemented, the combined Cliff Road bottleneck and I-494 bottleneck region of I-35W showed a decrease in overall congestion with little change in 25 mph and lower thresholds. Once again, Table 2.11 shows these percentages in terms of minutes per AM peak for perspective.

Table 2.11: Minutes per AM peak for each speed threshold for the Cliff Road bottleneck and I-494 bottleneck regions combined based on well correlated days before and after VSL implementation.

	Speed Threshold (mph)							
	10	**15**	**20**	**25**	**30**	**35**	**40**	**45**
Before VSL Implementation	3.1	6.9	11.3	16.2	21.6	27.7	34.5	43.2
After VSL Implementation	3.2	7.2	11.5	15.9	20.1	24.3	29.1	35.6
Absolute Improvement	-0.1	-0.3	-0.2	0.2	1.5	3.3	5.4	7.6
Percent Improvement	-2.8%	-4.2%	-1.7%	1.5%	6.9%	12.0%	15.6%	17.6%

On average, the morning peak experienced over 17% less congestion with the VSL system in place, although for those same days the lower speeds were largely unchanged (25 mph or less). The entire VSL active region had 7.6 minutes less congestion during AM peak.

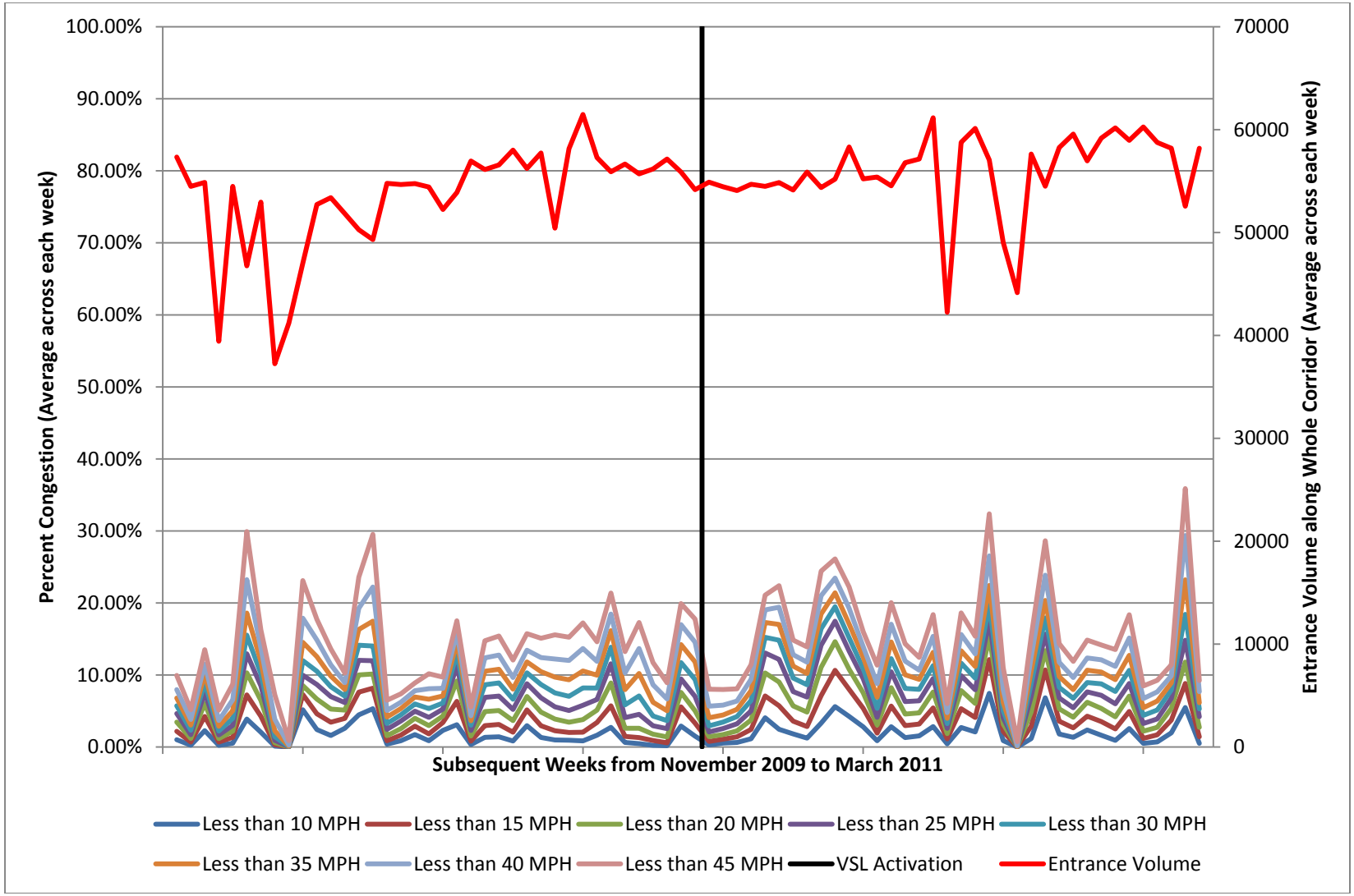

Figure 2.28: Average weekly speed-based congestion for all days between November 2009 and March 2011 for the Cliff Road and I-494 bottleneck regions combined.

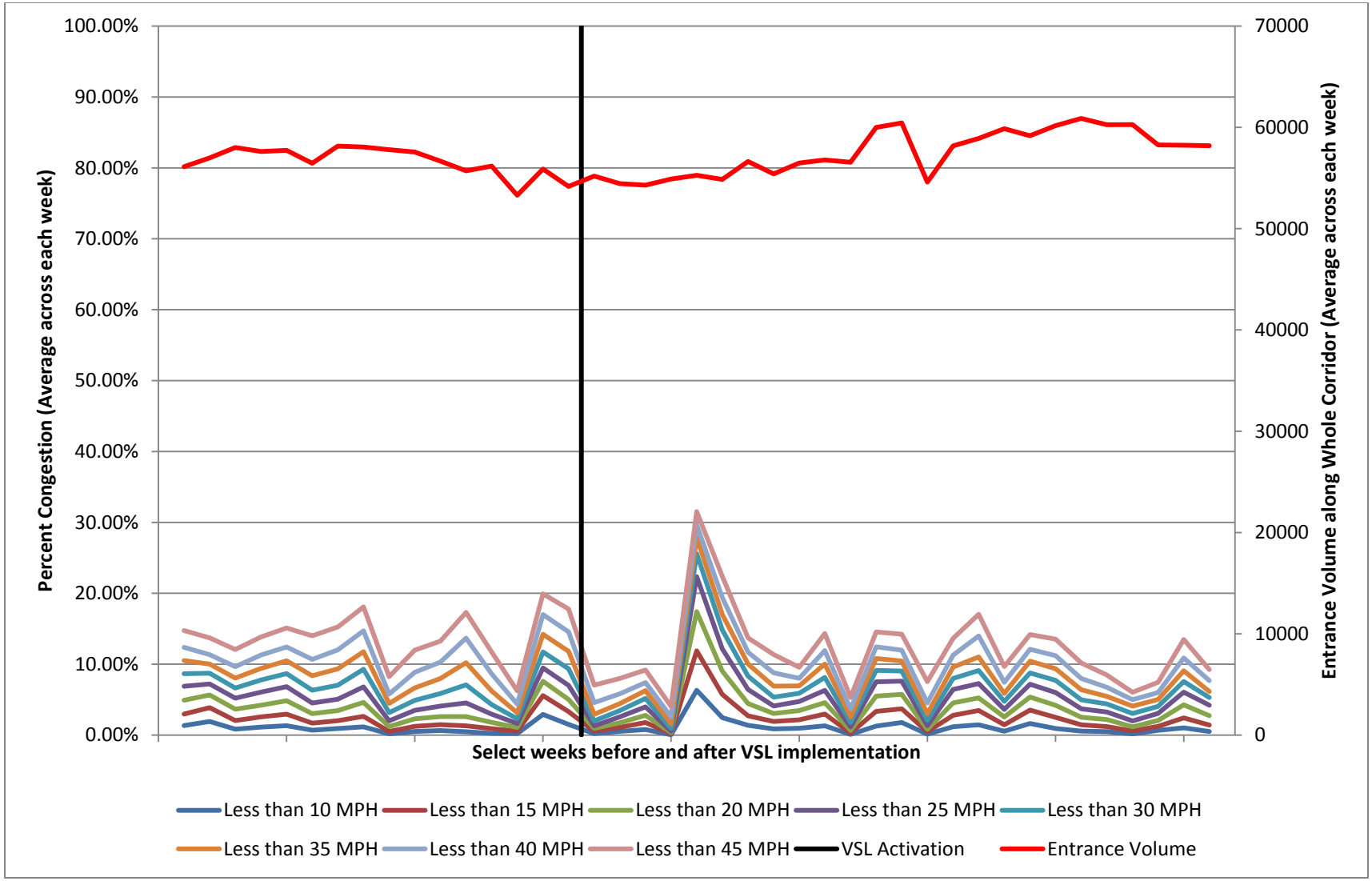

Figure 2.29: Average weekly speed-based congestion for well correlated days for the Cliff Road bottleneck and I-494 bottleneck regions combined.

Table 2.12: Average percent of AM peak in speed ranges for the Cliff Road bottleneck and I-494 bottleneck regions combined based on well correlated days before and after VSL implementation.

	Speed Range (mph)							
	0-10	**10-15**	**15-20**	**20-25**	**25-30**	**30-35**	**35-40**	**40-45**
Before VSL Implementation	1.03%	1.26%	1.47%	1.63%	1.81%	2.01%	2.29%	2.89%
After VSL Implementation	1.06%	1.33%	1.44%	1.49%	1.40%	1.40%	1.60%	2.16%

2.3.3.4 Southbound PM Peak

The bottlenecks on the southbound side of I-35W within the VSL active area are not as distinct as the bottlenecks on the northbound side. Two major bottlenecks were noted: one at 98th Street which showed major congestion during a significant portion of the analysis period, and a less active bottleneck at T.H. 13. On the occasions when the T.H. 13 bottleneck was active, the congestion was sufficiently severe that the shockwaves propagated upstream to the 98th Street bottleneck. As a result, the entire segment from highway 62 south to I-35 was analyzed as one piece.

As with the northbound segments, the week-to-week averages were calculated for every speed threshold as in Figure 2.30. Similar to the segments for the northbound AM peak, several detector issues arose in the spring of 2011 that persisted until the end of the analysis period. Dates from March 29th, 2011 to December 2011 were discarded.

Taking the before and after VSL implementation days and finding the averages for each speed threshold (see Table 2.13), it can be seen that the overall congestion rate rose by about 2.4% of PM peak. Each speed threshold showed a similar increase, with slightly smaller absolute increases for the lower speed thresholds.

Table 2.13: Average percent of PM peak below speed thresholds from 10 mph to 45 mph for the Cliff Road and 98th Street bottleneck regions combined based on all Tuesdays, Wednesdays, and Thursdays between November 2009 and March 2011.

	Speed Threshold (mph)							
	10	**15**	**20**	**25**	**30**	**35**	**40**	**45**
Before VSL Implementation	0.13 %	0.36 %	0.71 %	1.16 %	1.67 %	2.14 %	2.65 %	3.35 %
After VSL Implementation	0.25 %	0.63 %	1.23 %	2.08 %	3.05 %	3.92 %	4.75 %	5.72 %

To isolate the impact of the VSL system, the well correlated days for the entire segment were selected. In general, the correlation values for the southbound side were higher than those for the AM peak (i.e. the PM peak traffic entrance patterns are more variable). As such the VSL system impacts are not as effectively isolated as for the AM peak. Table 2.14 shows the tabulated results using the best correlated of the days and Figure 2.31 shows the weekly averages based on the same set of days.

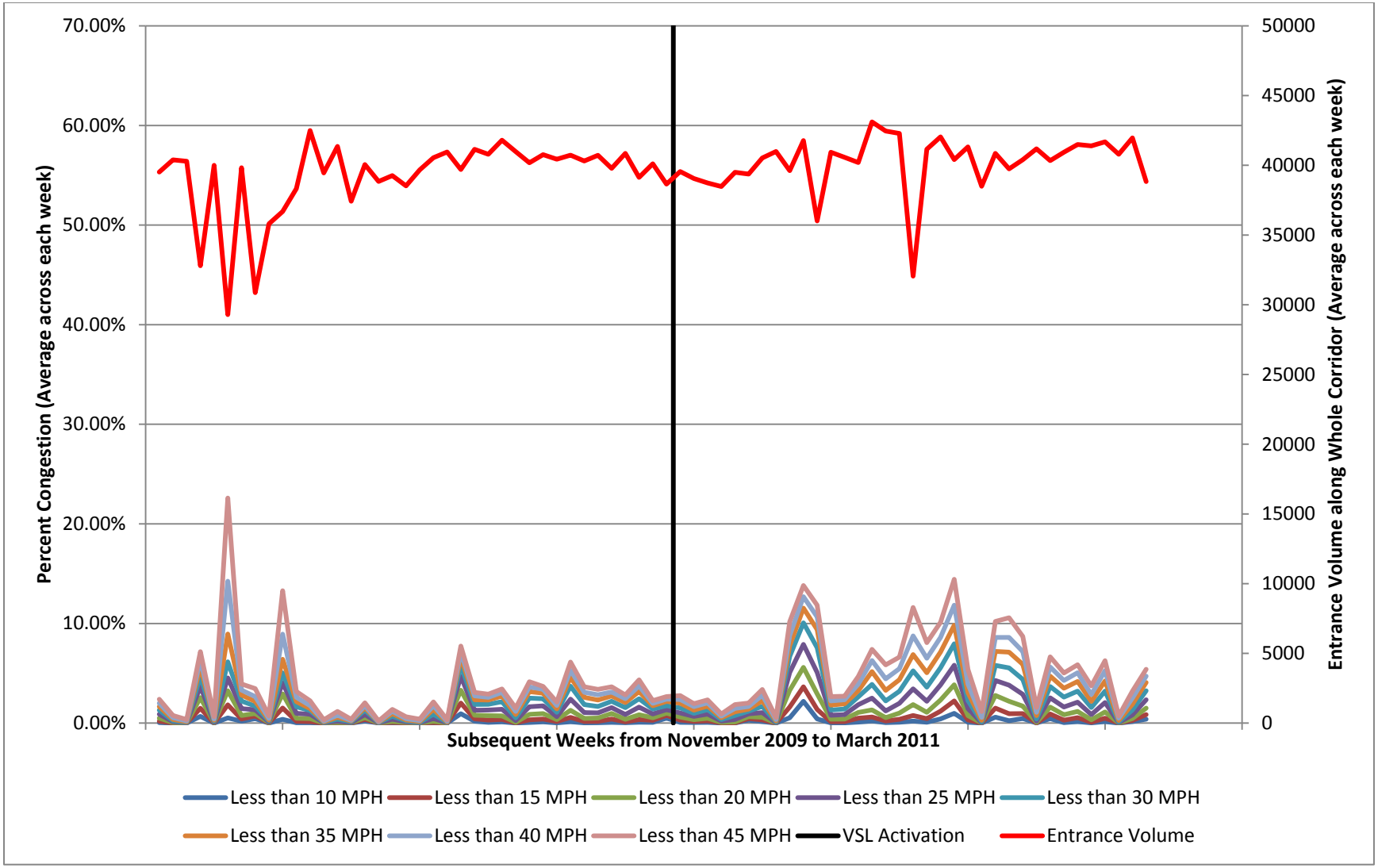

Figure 2.30: Average weekly speed-based congestion for all days between November 2009 and March 2011 for the Cliff Road and 98th Street bottleneck regions combined.

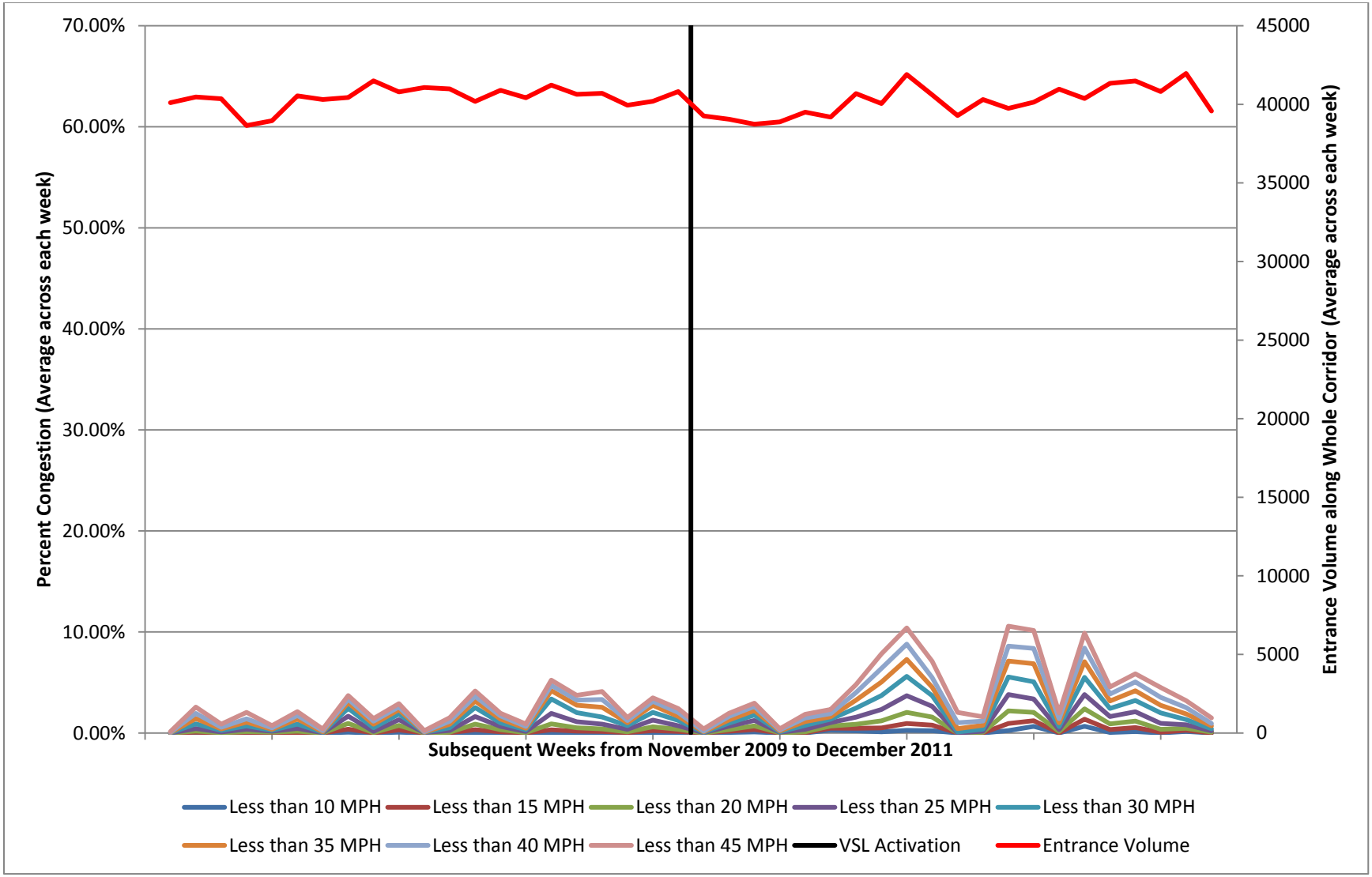

Figure 2.31: Average weekly speed-based congestion for correlated days for the Cliff Road and 98th Street bottleneck regions combined.

Table 2.14: Average percent of PM peak below speed thresholds from 10 mph to 45 mph for the Cliff Road and 98th Street bottleneck regions combined based on correlated days before and after VSL implementation.

	Speed Threshold (mph)							
	10	**15**	**20**	**25**	**30**	**35**	**40**	**45**
Before VSL Implementation	0.03 %	0.13 %	0.34 %	0.70 %	1.16 %	1.56 %	1.87 %	2.23 %
After VSL Implementation	0.17 %	0.46 %	0.94 %	1.67 %	2.53 %	3.34 %	4.12 %	5.02 %

Among well correlated days for the segment, after the VSL system was implemented, the southbound side of I-35W showed an increase in overall congestion of approximately 2.8% of PM peak. Table 2.15 puts the percentages in terms of minutes per PM peak for reference.

Table 2.15: Minutes per PM peak for each speed threshold for the Cliff Road and 98th Street bottleneck regions combined based on correlated days before and after VSL implementation.

	Minutes at Speeds Under							
	10	**15**	**20**	**25**	**30**	**35**	**40**	**45**
Before VSL Implementation	0.1	0.4	1.0	2.1	3.5	4.7	5.6	6.7
After VSL Implementation	0.5	1.4	2.8	5.0	7.6	10.0	12.4	15.0
Absolute Change	0.4	1.0	1.8	2.9	4.1	5.3	6.7	8.4
Percent Change	578.2%	258.6%	174.5%	138.4%	118.9%	114.0%	120.2%	125.4%

On average for the correlated days for the southbound PM peak, congestion for each speed threshold (except for 10 mph and 15 mph) was around 125% to 150% greater than before. However, the large percentages are due to the extremely low congestion rates prior to VSL activation. The absolute changes are only on the order of a few minutes and the total congestion remains small.

The speed range breakdown in Table 2.16 shows that each speed range contributed between two and three times more congestion after VSL implementation, consistent with the growth shown in Table 2.15.

Table 2.16: Average percent of PM peak in speed ranges for the Cliff Road and 98th Street bottleneck regions combined based on correlated days before and after VSL implementation.

	Non-Inclusive Contributions							
	0-10	**10-15**	**15-20**	**20-25**	**25-30**	**30-35**	**35-40**	**40-45**
Before VSL Implementation	0.03%	0.10%	0.21%	0.36%	0.46%	0.41%	0.31%	0.35%
After VSL Implementation	0.17%	0.29%	0.48%	0.72%	0.87%	0.81%	0.78%	0.90%

3. Evaluation of UPA Corridor Operations during Inclement Weather Conditions

3.1 Introduction

From safety perspective, this evaluation process focuses on the analysis of severe weather condition effects on the safety of the traveling public and the effectiveness achieved by the design-build process of the UPA corridor. Often, roadway geometric design practice applies a uniform nationwide standard in terms of assumed weather impacts on geometric design. The Minneapolis UPA project is not an exception to this rule. Presumably, much could be gained by adjusting this standard to account for weather conditions that may deviate greatly from the norm. Adverse weather is often considered as an external factor that can affect freeway traffic operations. Moreover, standing/moving water can unexpectedly hydroplane light and medium size vehicles moving at about 50 MPH or higher speed and lead to loss of control of the vehicle resulting in catastrophic events. It is known that adverse weather is the second largest cause of non-recurring congestion, accounting for about 25% of freeway delays. From a safety perspective, the Federal Highway Administration (FHWA) is advancing advisory, control, and management strategies that include information dissemination and methods to regulate or optimize the traffic stream and ensure that roads are clear of obstructions. In addition, the Highway Capacity Manual (HCM) considers that adverse weather can reduce free-flow speeds and uses evidence that different weather conditions can impact the form of speed-flow relationships, [24]. Along the UPA corridor, there are a number of sag points. However, at this time, the focus is put on the evaluation of probable major flooding risks around 42nd Street as shown in Figure 3.1.

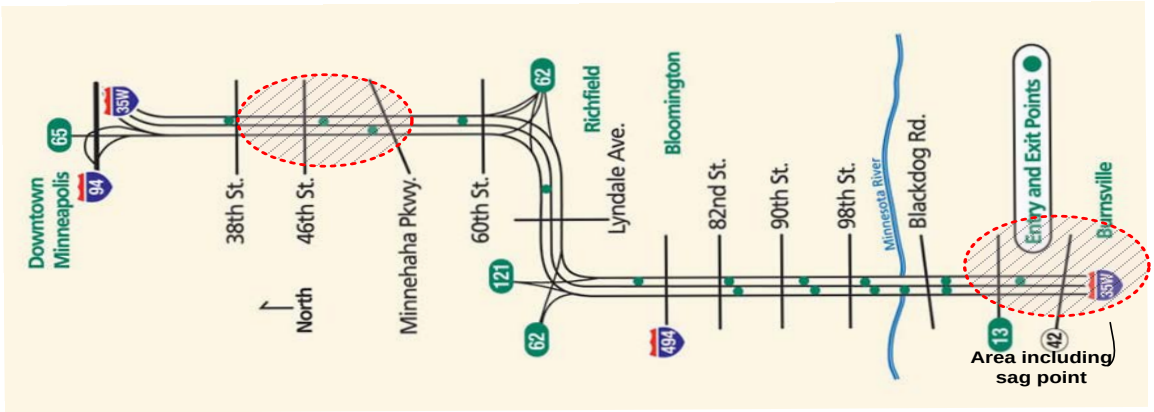

Figure 3.1: Area of concerns around the sag point.

The objective of this part of the project is to evaluate to what extent inclement weather conditions may affect road safety and formulate recommendations that can help improve traffic operations and the safety of the traveling public. Heavy rain conditions may also have great effect on traffic flow and road safety as congestion worsens, resulting in vehicles crashes. Most of the literature describes the impacts of snowy conditions on highway transportation, while only a few references were found to estimate the impacts of rain, standing water, and reduced

visibility, [19], [23], [12]. This evaluation process is based on the worst-case scenario where the existing storm drain systems design data is considered as initial conditions for the prediction model of the storm rain accumulation. The method used in this analysis considered visual and technical design data of the highway, rainfall frequency and duration relationships throughout Minnesota areas, and a modified Gallaway's hydroplaning equation, [22], [10], [8], [9]. Continuity equation and control volume principle [7], is used to develop storm rain accumulation model and predict the depth of standing water on the roadway.

Both the rainfall water accumulation rate and the hydroplaning models describe the ways that aggregate inherent risk factors which are calculated can be used to implement a weather-responsive algorithm that can help make informed decisions: (1) Determine under what rainy conditions the PDSL should be closed; (2) Provide a set of performance measures for the monitoring of the operation of the speed harmonization system on the highway section between Blackdog Road and 90th Street based on the prediction of rainfall accumulation; and (3) Improve mobility and roadway safety.

3.2 Problem Statement and the Existing Storm Drains Design Criteria

3.2.1 Problem Statement

In general, the geometric aspects of a highway which are seen to be one of the risk factors in this study include features that affect or relate to the roadway operational quality and safety. These features, which are visible to the driver and affect driving performance, include elements of the roadways and shoulder. Specific roadway features which pertain to this study are physical features of the roadside such as obstacles, flooding water, and other miscellaneous features (embankment slopes, ditches, etc.). The shortcomings of the UPA corridor design due to a number of constraints can be overcome by adopting a direct or optimal design procedure. Although the intent of the research project is to use a theoretical and scientific base, it has no means to redesign the existing hydrologic and hydraulic systems designed for the UPA corridor.

Probable flash floods during heavy rain are major problems of this study. They tend to be quite local and it is difficult to provide effective forecasting because of their rapid onset. It particularly becomes a serious problem in the corridor areas where drainage systems may not cope and in very small creeks and streams. Hydrology is not an exact science. The models underlying these design standards have not, therefore, as a rule, included variations to account for the main roadway traffic stream behavior and parameters. However, it is possible to obtain solutions which are functionally acceptable to form the basis for design of highway drainage facilities. To choose the analytical method for informed decision-making, it was determined: *(1) What level of hydrologic analysis is justified? (2) What data are available? and (3) What methods of analysis are available, including the relative strengths and weaknesses in terms of safety and reliability?*

Often highway design engineers assume that a given frequency storm always produces a flood of the same frequency. The author believes that a statistical analysis of extensive past rainfall records should be made before this hypothesized assumption is used and any analytical techniques for ungagged watersheds are accepted as a correlation means. On I-35W MnPASS, a similar design approach has been used. It was found that on narrow shoulder segments of the northbound of I-35W hydrologic design exceptions have been applied to allow (State Trunk

Highway versus Interstate Highway design standards) spread into 1/3 of the 11ft. lane width during the 10-years event instead of confining spread to the reduced 3ft. shoulders. This type of design approach raises safety concerns for the traveling public in circumstances of standing water in case of severe rainfall.

However, integrating of various engineering risk control technologies can substantially help monitor the risk to A Limit as Low as Reasonably Practicable (ALARP) and gain transportation system performance and operation management effectiveness. In this regard, the first step in this study is to quantify critical threats from severe weather to the roadway safety based on multivariate analysis of the entire corridor, encompassing the roadway geometrics, design exceptions and assumptions, weather, and other seasonal effects.

3.2.2 Purpose and Scope

Considering the project size and complexity, the problem statement of this research part focused on the evaluation of the effect of rain on the *MnPASS HOV/HOT lane (leftmost lane).*

This evaluation report is to provide a comprehensive analysis of the relative crash susceptibility in various segments of the MnPASS lane based on knowledge of local geography, topography, rain intensity, and other risk factors. It also provides product modeling as a computer-aided decision-making tool for operations management and mainline traffic flow control, including flooding risks assessment the sag point around 42nd Street and I-35W as illustrated in Figure 3.2.

Figure 3.2: Configuration of the sag point around 42nd Street.

(©2013 Google - DigitalGlobe, GeoEye, U.S. Geological Survey)

In this evaluation process, the two specifically targeted objectives are to:

- Review the configuration of the redesigned I-35W corridor following hydrology practices and predict probable standing water issues during intense rainfall which can impact the safety of the Interstate 35W section around 42nd Street, considered as the sag (low points) with probable major flooding risks along the UPA corridor, Figure 3.2.

- Develop recommendations for the PDSL segment closing decision-making during inclement weather conditions and better traffic operations monitoring, through the use of decision-making tools and coordination with the MnDOT operations team

The success of this approach towards our aim is measured using open-loop monitoring indicator (i.e., a rain gauge, traffic control systems).

3.2.3 Background

The Minnesota Department of Transportation (MnDOT) recognizes that infrastructure is only one of many elements necessary to achieving a high quality of life, a competitive economy, and a healthy environment. Therefore, MnDOT launched the reduction of incidents and road congestion to better align the transportation system with what Minnesotans expect for their quality of life, road safety, economy, and natural environment. The effort is based on an understanding that transportation is a means to other ends, not an end in itself.

More importantly, it was recognized that safety and security are top priorities as are efficiency of operations, O&M costs, and capacity and ridership and that the system provides an overall benefit to the regional system. This belief and recommendations are incorporated into the UPA project: a vision of creating a project that enhances the lives of residents by improving the safety, well-being, and cohesion of the neighborhoods adjacent to I-35W in Minneapolis areas. To avoid creating too cumbersome of a document, this evaluation report typically does not identify the underlying issues and the rationale for these recommendations. Those underlying issues and the rationale are documented for public access.

Design of storm drains always involve risks associated with hydrologic and non-hydrologic technical and nontechnical reasons. The traditional method of considering only the design rainfall frequency gives a partial and distorted view of the truth. These constraints significantly impact the road safety and may involve severe crashes. As a result, engineering design is needed to control the risk of flooding. In regard to probable flooding and hydroplaning risks, questions have been asked, such as, what if an expected decision for closure of the PDSL is made due to catastrophic events or weather conditions or what are emergency preparedness and recovery actions? However, few of them have explicit answers.

Therefore, to evaluate the effectiveness of the UPA project so that it is possible for decision-makers to refer to a set of practical recommendations from the perspective of traffic safety, operations, and maintenance, it is important first to develop an understanding of the factors that have historically contributed to the likelihood of an accident in the study area. However, the objective of this study is to focus on the non-behavioral determinants of accident risks, specifically roadway geometrics and severe weather conditions for informed safety decision-making.

The study begins with a review of previous research on weather-induced accident frequencies in terms of their relationship to geometric and weather-related elements. On the basis of this review, appropriate methodology to establish an explicit relationship between geometric and weather-related elements which may lead to critical events is presented. This is followed by a description of available data and a discussion of model estimation results. Prolonged heavy rain

can produce flooding in underpasses and inundate entire road sections. Heavy rain may cause a sudden rise of water in small streams and creeks (known as flash flooding) that can overflow onto roads.

One of the greatest threats to public safety is driving a vehicle through moving water of unknown depth. Each year, many fatalities are attributed to floods from heavy rain, which can occur from localized storms to major cyclones. Even though the study is to evaluate the entire UPA's project, we focused on the sag points for which traveling public safety may be impacted from standing water, residual melting snow and ice accumulated on the ground. Particularly, this can contribute to adverse driving conditions in the area where restricted (nonstandard) hydrologic design has been used for storm drains.

3.2.4 Data Sources for Impacts Simulation

In the reviewed shoulder area on I-35W, the author assumed that an engineering feasibility study for designing route opportunities exists. Therefore, data of various kinds is being collected and has turned out to be relevant to the question of interest: In heavy rain conditions, how probable is vehicles' hydroplaning to happen on the roadway? However, the general area of concern (i.e., the segment from Blackdog Road to 90th Street and the north bound segment between 42nd Street and 38th Street), visually reviewed on maps, showed that the shoulder environments vary so that related topology and factual data is very high-dimensional or has more missing information (missing data), which severely restricts a conclusive analysis and any interpretation.

Limited portions of the MnPASS lane may not offer feasible driving route opportunities and designs of standard storm drains because they have space constraints in the directions desired and are too narrow or irregular in width (i.e., non-standard design). To understand the connectivity of all safety attributes in the study areas and methods for dealing with the hydroplaning properties mentioned above, the underlying approach of the study deals with qualitative geometric information

Existing drawings and electronic maps were obtained and thoroughly examined as a part of the UPA corridor for the study. These included various state and county road maps, speed detector locations, and other map resources. The use of these data allow for the consideration and efficient use of a wide variety of information that would otherwise be unavailable or impractical to consider for a comprehensive synthesis of this scope. Nevertheless, these obtained data sources vary widely with respect to accuracy and precision, and presentation, analysis, and calculations that may be derived from these sources require careful consideration when used for safety constraint considerations.

3.2.5 Research Methodology

Both the I-394 and I-35W MnPASS projects were implemented with the primary purpose being congestion management. In many segments, the limitation to only two HOV corridors converted to managed lanes, without new capacity (i.e., addition of new lanes) pose engineering design challenges. One rational order of steps by which we investigate these challenges is the application of an engineering process to evaluate the effects of heavy rain on the roadway performance (i.e. the safety of the travelling public) as follows:

- **Step 1**: This first step is performed to analyze the existing hydrologic and hydraulic system. It should be understood that there are no exact methods for hydrologic analysis. Different methods that are commonly used may produce significantly different results for a specific site and particular situation. The hydraulic design approach estimates the discharge (rate of runoff) or volume of runoff of the drainage facility in the sag point of probable major flooding risk in the UPA corridor (i.e., the section around 42nd Street). In this step Manning's equation is considered to determine fundamental characteristics of the existing storm drains design configuration, including the rainfall intensity and duration, the frequency, and the discharge rate. These relevant characteristics are set as initial conditions to develop the storm rain accumulation model based on continuity equation and control volume principles.
- **Step 2**: This second step is used to predict hydroplaning conditions based on worst-case scenario of storm rain. From safety perspective, this approach is used to evaluate the extreme circumstances that may the safety of the traveling public at risk. That is when the set of hydroplaning relevant parameters exceed the range of those used for both hydrologic system and the highway design safety and reliability.
- **Step 3**: The prediction of the rate of water rain accumulation algorithm for risk management decision-making. The flooding risks are predicted considering the volume of rainfall accumulation calculated in step 2 for the worst-case scenario of weather conditions: (1) Low rainfall intensity and long duration; and (2) Short duration and high rainfall intensity that exceed those considered for the existing drainage design. Therefore the developed flooding risk model focused on one of the important hydroplaning factors: the increase of the depth of the standing water on the roadway from initial conditions that are set in step 1. This analysis characterizes vehicles hydroplaning due to water spread on the roadway and the probable risk of truck-car crashes leading to a closing decision of the corridor without emergency response.

3.2.6 Hypothesis

- **Design**: We assume that the existing storm drain design characteristics have been improved enough to efficiently and accurately contain weather events associated to the type of the storm rain in the area of study. Therefore, any storm event similar to a type of storm of 6in./hr which has been identified in the area of study [5], and used in the existing storm drains design of 10 year frequency, should not jeopardize the safety of the traveling public. As a result we can set these fundamentals as initial and boundary conditions to determine the extent to which standing water on roadways may lead to vehicle hydroplaning and result in catastrophic crashes.
- Since the objective is not to redesign the existing hydrologic and hydraulic systems, the above hypothesis is assumed true and used as initial conditions for flooding risks from storm rain events of the intensity higher than 6in./hr. Although the hydrologic analysis developed is relevant in establishing the quantity of surface water that must be considered in the design of the drainage facilities, the extent of such studies are commensurate with the importance of the highway flow density, the potential for damage to the roadway, and the potential risk to traveling public life, this evaluation concept was not considered as an absolute approach for designing the hydrologic and hydraulic systems.

- **Control**: The flooding risk management process we are dealing with is not a closed-loop prediction process (i.e. the rain gauge sensor is not in the control-loop). Therefore, we assume an operator is in the control-loop to supervise the process. However, the study is not developed to account for human factors to react to the flooding threats. The accuracy of the prediction depends on the accuracy of the inputs of the rain sensor data by the operator and adjustment to any delay in the prediction process. The developed flooding risks model focused on one of the important hydroplaning factors which is the increase of the depth of water pond on the roadway. Ensuring exemplary operator's supervision, the storm rain accumulation can be predicted to a reasonable accuracy and nonrecurring incident occurrences that may pose safety threats to the traveling public.
- **Minors drains**: Minor drains (helpers) installed within the sag point area have efficiency $\varphi_{d,m} = 0.70$, primary drains' efficiency is $\varphi_{d,m} = 0.85$; the clogging factor in the area is $C_g = 0.55$.
- Federal Motor Carrier Safety Regulations indicates that a driver of a vehicle who is using tires in service must be in compliance with the Motor Carrier Safety Standards in regard to the application, usage and condition of those tires. Therefore, we assume that tires in use are in good conditions and exclude any involvement of worn tires. We only evaluate circumstances where flooding roadway may potentially impact the safety of the traveling public.

As a result in the following sections, the evaluation process will provide, a sustainable rainfall intensity threshold over a period of time that equals the storm rain duration, as a set point for decreasing the speed limits in order to avoid cars hydroplaning.

3.2.7 The Existing Hydrologic System Characteristics

The section considered along the Interstate 35W is the sag point around 42nd Street and the northbound, Figure 3.2. They are also stretches of road suffering from a chronic flash flooding problem during heavy rain. Heavy rainfall events are important in the design of water-related structures (e.g., storm sewer systems). In general, more of the heavier storms occurred in summer than in any other season, while the least number occurred in winter for shorter durations.

In completion of these challenging UPA projects in Minneapolis, engineers used in many segments of the northbound of I-35W hydrologic design exceptions to allow (State Trunk Highway versus Interstate Highway design standards) spread into 1/3 of the 11ft. lane width during the 10-years event instead of confining spread to the reduced 3ft. shoulders. This type of design approach raises safety concerns for the traveling public in circumstances of standing water in case of severe rainfall. Moreover, based on human activities related to improper maintenance and management impacts, the flood issue is recognized as a complex problem involving uncertainties and optimization of protection measures. Minor drains (helpers) are used to reduce the runoff flow from top-to-bottom point of the sag, Figure 3.3. This method helps to collect as much as possible the transverse flow and reduces the carryover $\mathbf{Q_c}$ to the sag point.

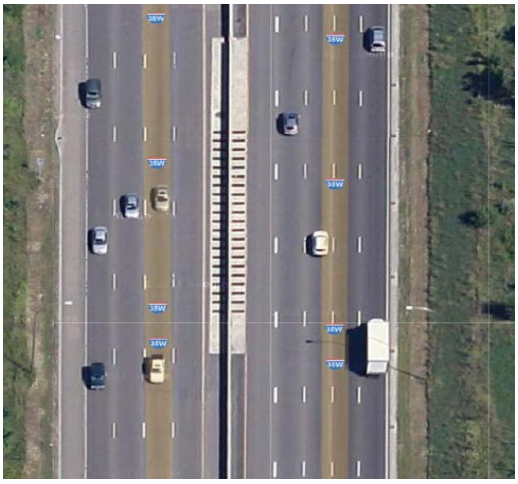

Figure 3.3: Configuration of minor drains (helpers) to reduce runoff bypass.

(©2013 Google - DigitalGlobe, GeoEye, U.S. Geological Survey)

Storm rain variability and non-representative effects of the expected rainfall for a given recurrence interval and storm duration, due to various causes, such as observational and processing errors, have been minimized by using the individual frequency distributions, rather than the raw data observations, to measure rainfall dispersion around the sectional mean frequency distributions. The identified area around the sag point in the UPA corridor is located in rainfall sectional area 01 which data is presented in Table 3.1 of frequency distributions for various storm periods and recurrence intervals in Minnesota, [5].

Table 3.1: Rainfall (in.) for given recurrence interval.

Sectional mean frequency distributions for storm period of 5 minutes to 10 years and recurrence intervals of 2 months to 100 years in Minnesota (zone 01) **Rainfall (in.) for given recurrence interval**								
Section	**Duration**	**2-month**	**4-month**	**9-month**	**1-year**	**5-year**	**10-year**	**25-year**
01	**5-day**	1.27	1.73	2.30	2.50	4.11	5.01	6.12
	48-hr	1.03	1.34	1.78	1.94	3.25	4.05	5.13
	18-hr	0.89	1.13	1.48	1.61	2.76	3.47	4.30
	12-hr	0.82	1.04	1.37	1.49	2.56	3.21	3.98
	3-hr	0.60	0.76	1.00	1.09	1.88	2.36	2.92
	2-hr	0.54	0.69	0.91	0.99	1.71	2.14	2.65
	1-hr	0.44	0.56	0.74	0.80	1.38	1.73	2.15
	30-min	0.35	0.44	058	0.63	1.09	1.37	1.69
	15-min	0.25	0.32	0.42	0.46	0.79	1.00	1.23
	10-min	0.20	0.25	0.33	0.36	0.62	0.77	0.96
	5-min	0.12	0.15	0.19	0.21	0.35	0.44	0.55

Table 3.1 portrays empirical result of rainfall for given recurrence interval in Minnesota area (zone 01). As it can be noted in Table 1, the prediction of the rainfall variability in a simple

linear relationship in time is almost impossible to quantify. Therefore, a constant rainfall for a given recurrence interval is used for the analysis (i.e. 0.77 inches or 4.62in./hour).

3.2.7.1 The Existing Hydrologic System Design Concept

The issue of concern at the end of the UPA project was whether the reliability and safety of the final plans and as-built would be higher than the standards of traditional design-bid-built projects. Although it is known that all development comes with a residual risk, there is no doubt that the project is of high quality.

Safety, engineering designs, and risk analysis considered the corridor length and general design features. The assessment of the hydrologic design concept used in the UPA project reveals that a standard design concept such as Manning's Equation was used. Although design practice that uses a generally accepted concept is not unusual, it can adversely affect the design reliability and safety. Runoff models used in the design of roadway water-control structures necessitate defining the time distribution characteristics within heavy rainstorms. Such information is also pertinent to the use of the frequency distributions presented in this report.

In the UPA corridor, converting narrow bus-only shoulder lanes along the northbound portion of I-35W to wider, priced dynamic shoulder lanes (PDSLs), and moving these lanes from the right-most to the left-most portion of the roadway facilitate minimizing conflict with entering vehicles. However, variable lanes of 12ft mixed use and a 10ft right shoulder are assumed to be standard. To accommodate such a design configuration, the distance between left edge lane lines needs to be a minimum of 39ft.

Corridors that largely met these qualifications were classified as "*Standard Design*" corridors and were assumed to meet state and federal design requirements in most locations throughout the corridor. By visual inspection of aerial maps, pavement widening in many segments of the I-35W did not fit into standard design qualification, Figure 3.4.

These sections are particularly risky regarding issues such as the expansion of the roadway width and roadway hydrology and have little transit service. It has a challenging mix of short and long trips which could complicate operations when subject to a more detailed micro-simulation analysis. These problem areas have not been evaluated in detail, and no solution has been sought to assess/mitigate the risk that is involved. Because many of these problem sites may pose a public safety hazard to the general traveling public, the already identified drainage problems need to be evaluated, prioritized, and mitigated.

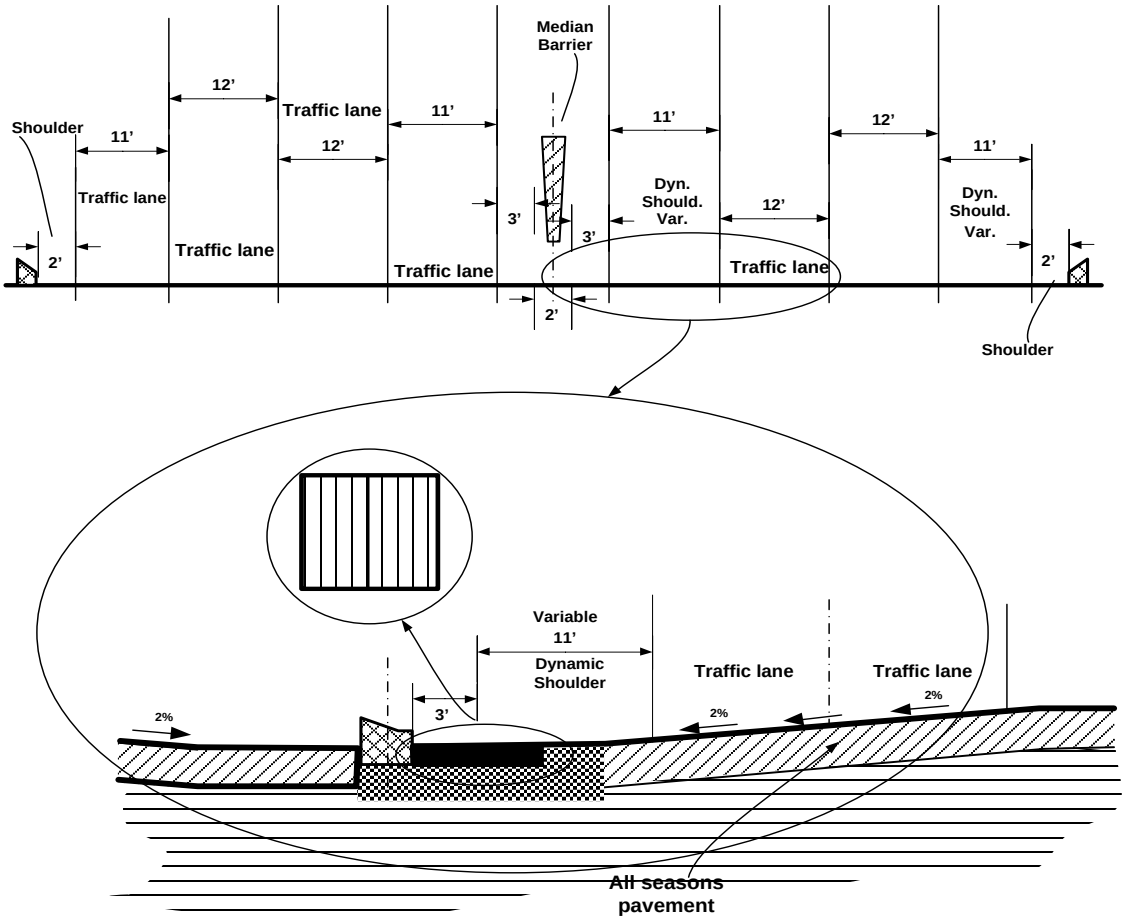

Figure 3.4: Storm inlet at the low point: Design exception.

Hydrologic design concepts have not changed much through the years. The street hydraulic capacity includes two aspects: (1) *hydraulic conveyance capacity*, and *hydraulic storage capacity*. NOAA technical memorandum NWS Hydro-35 or the Technical Paper No. 40 has not been updated since 1977. In the existing hydrologic and hydraulic systems design, the shoulder is viewed as a means of conveyance as given by Manning's equation (1) for the cross sectional area of the shoulder/gutter below the elevation of the edge of lane and the longitudinal slope of the gutter. Table 2 illustrates some of relevant parameters used for the design of the existing storm drains system.

$$\begin{cases} Q = VA \\ Q_{10} = Q = \dfrac{\varphi}{n} AR^{2/3}\sqrt{S} \\ n = 0.016 \end{cases} \qquad (1)$$

where: $\boldsymbol{Q}$ is flow rate (ft^3/s); $\boldsymbol{V}$ is the average velocity in the culvert barrel (ft/s); $\boldsymbol{A}$ is a cross sectional area of the flow (ft^2); $\boldsymbol{n}$ is Manning's Roughness Coefficient; $\varphi = 0.56$ is constant; $\boldsymbol{R}$ is the hydraulic radius (ft); $\boldsymbol{S}$ is the longitudinal slope.

Table 3.2: Storm drain system design parameters.

Existing storm drains design parameters		
Items	**Definition**	**Data**
$\mathbf{I_r}$	Rainfall intensity for drains storm design	6 in./hr
f	Minnesota zone 1 (IDF) curves: Design storm frequency	10 year
$\mathbf{T_c}$	Storm duration	10 min
$\mathbf{V_d}$	Highway design velocity	70 mph
$\mathbf{k_r}$	Runoff coefficient (asphalt and concrete)	0.90
$\mathbf{S_x}$	Street cross slope	2%
S	Longitudinal slope	3%

Geometric constraints at the sag point restrict this design concept to fully comply with storm drain design standard such as Technical Memorandum No.0626B02. Federal highway standards and specifications for construction indicated that at locations where the vertical alignment of the roadway creates a sag condition in either a depressed roadway section or a roadway section utilizing concrete barriers, and ponded water on the roadway can only be removed through the storm drain system, a 50-year storm frequency and the actual time of concentration should be used as the design criteria for both the drop inlet and the pipe system. In this regard, the restricted physical characteristics of the location and the use of 10 year storm frequency at the sag points pose non-negligible flooding safety threat to the traveling public.

3.2.7.2 Gutter Hydraulics Design Analysis

In general for design standard, a greater longitudinal slope results in higher velocities, less spread, and generally higher inlet efficiencies. Figure 3.5 illustrates a safety-driven design concept and provides allowable spread thresholds by establishing for both rainfall runoff evaluation and management with the basic fundamentals of safety for informed decision-making. The crucial step necessitates a definition of time distribution characteristics for heavy rainstorms. The street hydraulic conveyance capacity depends on street geometry and hydraulic parameters such as roadway surface roughness coefficient. Storm water flowing through a triangular gutter section can be described by the revised Manning's equation (Technical Memorandum No.0626B02), as follows:

$$\begin{cases} Q_o = \dfrac{0.56}{n} S_x^{1.67} S^{0.5} T^{2.67} \\ T_{\max} = 3 + \text{shoulder width} \cong 6\text{ft} \end{cases} \qquad (2)$$

where: $\boldsymbol{Q_o}$ is flow rate (ft^3/s); $\boldsymbol{S_x}$ is the street transverse slope (%); $\boldsymbol{S}$ is the street longitudinal slope (%); $\boldsymbol{n}$ is Manning's Roughness Coefficient; $\boldsymbol{T}$ is the spread width (ft); $T_{\max}$ is the maximum allowable spread at sag point

The maximum allowable spread, in general, is presented in Figure 3.5. Characteristic values of the roadway geometry at the sag point is described as: $S_x = 0.02$, $S = 0.03$ and the gutter width is $W = 2\,\text{ft}$.

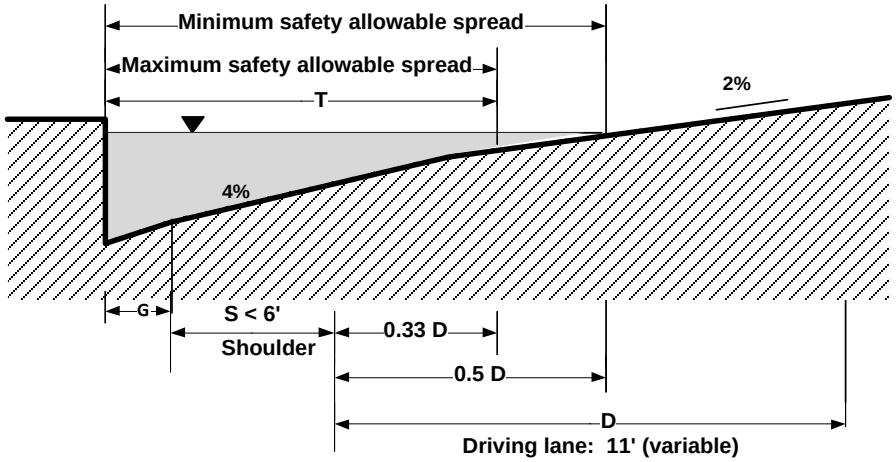

Figure 3.5: Storm drain: Allowable spread for restricted design.

Since design exception was used on the sag point area to allow (State trunk highway versus Interstate highway standards) spread into 1/3 of the 11ft lane during 10 year event instead of confining spread to the reduced shoulder of 3ft, the ratio of flow capacity R_Q, is determined using equation (2) as follows:

$$\left.\begin{aligned} Q_o &= \frac{0.56}{n} S_x^{1.67} S^{0.5} T^{2.67} \\ Q_{or} &= \frac{0.56}{n} S_x^{1.67} S^{0.5} T_r^{2.67} \end{aligned}\right\} \Rightarrow R_Q = \frac{Q_o}{Q_{or}} = \frac{T^{2.67}}{T_r^{2.67}}$$

$$R_Q = \left(\frac{0.33 \times 11 + 3}{3}\right)^{2.67} = 8.44 \qquad (3)$$

where T is the maximum spread; T_r is the reduced shoulder width

Using equation (3), lumped hydroplaning analysis involving restricted physical characteristics of the location of the sag points and the hydrologic data in Table 2 (e.g. frequency, duration, intensity) shows that the reduced 3ft shoulder would approximately carry storm rain intensity I_e, as follows:

$$\left.\begin{array}{l} f = 10 \text{ year} \\ I_r = 6"/\,hour \\ R_Q = 8.44 \\ T_d = 10\,\text{min} \end{array}\right\} \Rightarrow I_e = \frac{I_r}{R_Q} = \frac{6"/\,hour}{8.44}$$

$$I_e = 0.7"/\,hour \qquad (4)$$

I_e is an estimate of the storm rain intensity carried over the reduced shoulder if the shoulder with spread into the driving lane will carry runoff from 10 year event frequency based on the design storm rain intensity $I_r = 6"/\,hour$ for a 10 minute duration (i.e. $T_d = 10\,\text{min}$). This lumped analysis helps determine foreseeable initial hydroplaning conditions, the sensitivity of the rain gauge, and storm rain intensity threshold setting for informed decision-making to reduce the speed limits.

Consider the data from Rainfall Frequency Atlas of the Midwest (Midwestern Regional Climate Center) for a 100 year frequency and 1hour duration. The 2.75 inches contour, given in the Atlas in the area around both sag points of the UPA corridor, means that a 100 year storm drops rainfall totals that had a one percent probability of occurring around the sag point that year (i.e. 2.75in./hr.). As a result, adopting a setting for speed limits using the estimate rainfall intensity $I_e = 0.7\,\text{in/hr}$ would not create the expected results. The rainfall concentration time is determined in the next section.

3.2.7.3 Storm Rain Events around the Sag Points

This section provides a review of historical flood data around the sag points that could potentially be used in the tuning of the backwater model with reasonable details. The energy equation can provide valuable information to positively benefit this analysis. It was considered in this hydrologic analysis that establishing the quantity of surface water that must be considered in the design of the roadway drainage facilities in the area of the study is necessary. Furthermore, the extent of such studies are commensurate with the importance of the corridor, the potential for damage to the traffic network, loss of property, and hazard to life associated with the I-35W facilities. To make an informed management decision, including emergency actions, as critical weather related event arises, we must determine:

- *What level of hydrologic analysis is justified, including the relative strengths and weaknesses in terms of accuracy*
- *What data are available or must be collected*

The review of historical flood data around the sag points is viewed as a test for inundation criteria that have been used. One of the consequences of the hydrological regime change is that more of a stream's annual flow is delivered as storm water runoff rather than base flow. Depending on the watershed impervious cover, the annual volume of storm water runoff can increase by up to 16 times that for natural areas and pose significant flooding threat to the roadway safety.

It was reported that in June 2010, cars were stuck when heavy rain poured. People had to push their cars out of the rising water because the water was about 3 inches deep, Figure 3.6. Most of the construction contracts were done under a lump-sum contract. Therefore, we have not found documents as pay items with final drawings which would have been submitted by the design-builder.

Figure 3.6: Storm water runoff.

This assessment of the project quality performance would be performed in a more traditional way as in a common engineering design reviews submittal process if comments on the design-build project reviews were available during this evaluation process. This historical data review shows the importance of the performance measure in use to assess the storm drain retention effectiveness to understand the awareness of the causes and remedies for water flooding.

3.2.7.4 Storm Rain Accumulation Rate Calculation

From a safety perspective, the highway engineers are becoming familiar with the many factors or characteristics that affect runoff before making a hydrologic analysis. Meteorological phenomena are considered the more important factors affecting runoff and flood predictions. In general, rainfall event characteristics which are important to highway drainage design are:

- *Intensity (rate of rainfall) and duration (time rainfall lasts)*
- *Frequency (statistical probability of how often rainfall will occur)*
- *Time distribution (intensity hyetograph) and storm type (orographic, convective, or cyclonic)*
- *Storm size (localized or broad areal extent) and movement (direction of storm)*

Analytical description of the effects of many of these factors known to influence surface runoff only exists in empirical form. Relating flood flows to some causative factors has not yet advanced to a level of precise mathematical expression. Some of the more significant factors which affect the hydraulic character of surface water runoff need be understood and properly evaluated for the selection of design storm frequency and flood probability. However, it is important to recognize that the factors discussed in this study may exist concurrently within a watershed and their combined effects may be very difficult to quantify.

The MnPASS lane enables bus speeds to increase to 50 mph from the current bus-only shoulder lane speeds of 35 mph or less. In this regard, the cognizance of engineering standards such as those included in the *SCS National Engineering Handbook* (SCS, 1985) and safety standards are mandatory to achieve drainage structures design with risks as low as reasonably practicable (ALARP). In general, designing highway drainage structures, floods are measured in terms of peak runoff or a hydrograph having a discharge Q in cubic feet per second (cfs). Structures designed to control volume of runoff, like detention storage facilities or situations where flood routing is used the entire discharge hydrograph will be of interest.

The existing hydrologic and hydraulic systems are designed for ten year recurrence frequency and thirty minutes. More importantly, we assumed that these storm drains design conditions were developed for a minimum roadway safety requirements compliance (i.e., the runoff should not encroach onto the highway so as to cause a significant traffic hazard or limit traffic to an unreasonable extent). However, in respect to the allocated resources for hazards control in this project, the general public expectation is that the UPA project would make significant difference in motorist safety (i.e., beyond the minimum standard safety compliance).

As a result, in order to perform a design beyond the minimum standard safety compliance as shown in Figure 3.5, the major challenge arises from the need to use detailed simulation model that takes into account equation (4) to assess the flooding and hydroplaning risks. We use therefore the energy equation where the accumulation of the flow prevails to determine the maximum rainfall spread.

In this analysis, we assumed, without loss of generality, that storms can be combined into one distribution. The question of whether a distribution of extreme rainfall is a function of storm type (tropical or non-tropical storm) would be nice to elaborate. However, this is not in the scope of this study. Although there may exist between the hydrologic characteristics of a hurricane or tropical storm rainfall and those of rainfall from other types of storms, the conventional procedure of analyzing the annual maxima without regard to storm type is preferred because it avoids nonsystematic analysis. Also, it eliminates having to attach a storm type label to the rainfall, which in some cases of an intermediate storm type (as when a tropical storm becomes extra-tropical) is arbitrary.

Due to the diversity of the surrounding environment of the sag point (i.e. variable terrain, residential area, concurrent roads, etc.), the tributary area to the flow is complex to be determined precisely. The notion of control volume is used to map the tributary area to the flow as shown in Figure 3.7. It illustrates a theoretical configuration of continuity and control volume principles for prediction of storm rain accumulation on roadway surface at the sag point.

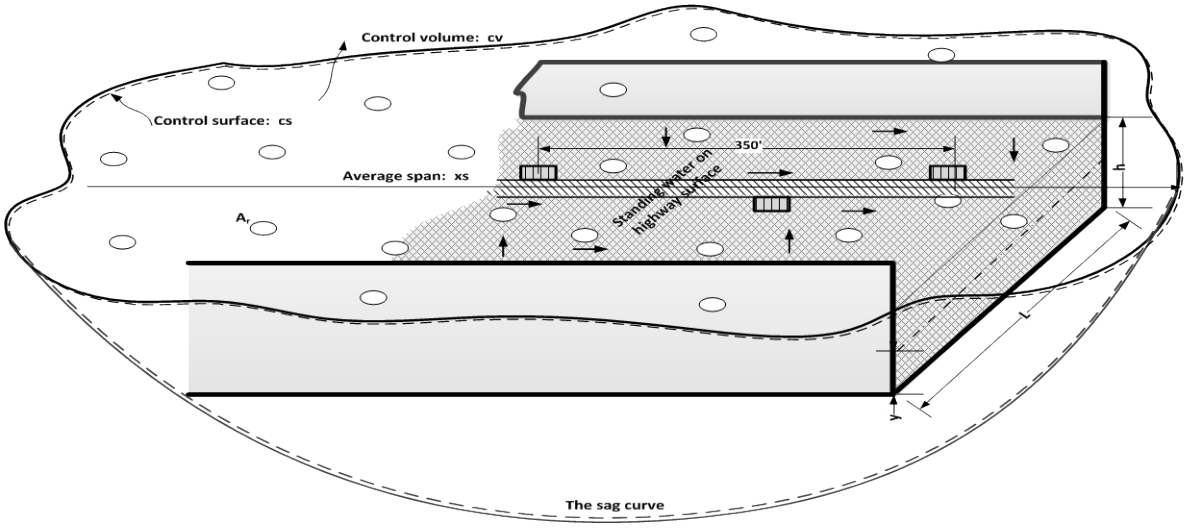

Figure 3.7: Control volume of storm rain accumulation.

We assume the geometry is uniform from the upstream to downstream extent so that we can make use of the cross section interpolation tool to compute the geometry with the specified cross section spacing. Moreover, we assume the design exception is the same as in the case of Burnsville and Bloomington. Therefore the design criteria for the speed limits setting and the rainfall accumulation will be the same.

Practical evaluation of this hydrologic problem requires analysis of the behavior of the contents of a finite region in space surrounding the sag points (a control volume). The control volume formulas are derived from the equations representing basic laws applied to a collection of mass flow rate (i.e. Reynolds Transport Theorem). This concept of a control volume and mechanism occupying the same region of space at an instant (coincident condition) and use of the Reynolds Transport Theorem are key elements in the derivation of the control volume equations. Note that storm drains are designed for ten year retention capacity with allowable spread for minimum safety, as shown in Figure 3.5. Method for estimation of water accumulation rate on the roadway surface requires an assumption concerning the parametric form of the distribution function of the rainfall. For the control volume identified around the sag points and depicted in Figure 3.7, the Reynolds Transport Theorem [6] is as follows:

$$\frac{D}{Dt}\int_{sys}\rho d\forall = \frac{\partial}{\partial t}\int_{cv}\rho d\forall + \int_{cs}\rho V.\vec{n}dA \qquad (5)$$

where ρ is water density; $\forall$ is total volume; V is average rainfall velocity; A is drainage area; subscript ***cv*** stand for control volume; subscript ***cs*** stand for control surface

Consider the initial condition of water accumulation rate on the roadway is when rain intensity equals the estimate of the storm rain intensity carried over the reduced shoulder I_e, (equation 4). Since this corresponds to the condition that creates the allowable minimum spread in a 10 minute period, a storm rain intensity $I_r < I_e$ sustained in the same time range should normally be

contained by the existing storm rain design and should not constitute a threat to the traveling public. As shown in Figure 3.8 the maximum allowable spread would not create total hydroplaning conditions (i.e. complete separation of tire from roadway by fluid). As shown in Figure 3.8, helpers are used to retain maximum runoff from the top-to-bottom point of the sag.

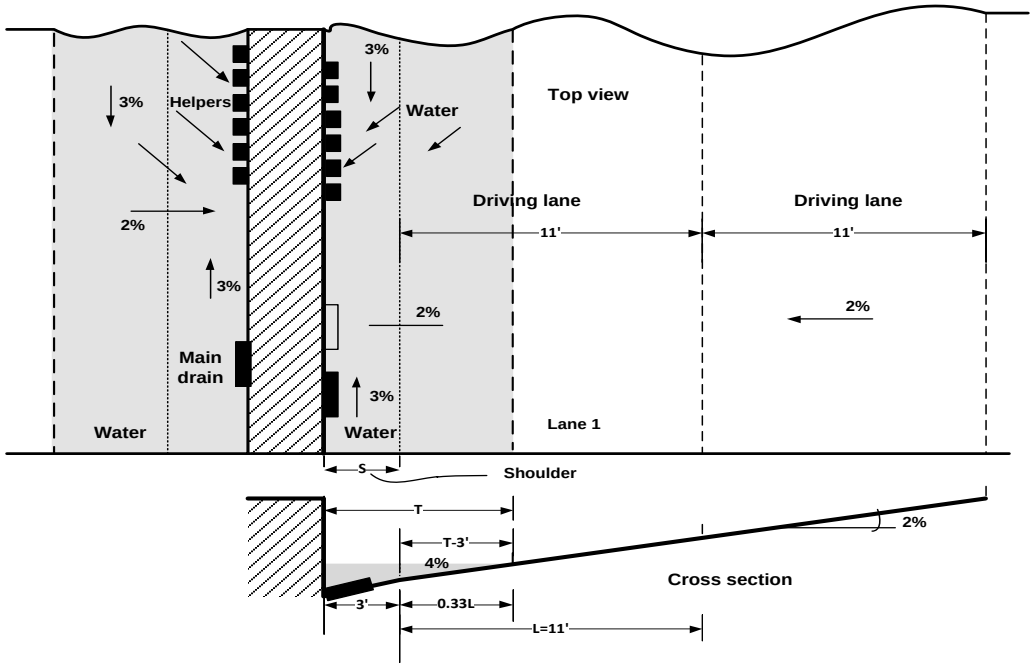

Figure 3.8: Lower threshold of storm water spread conditions at the sag point.

In this circumstance, the mass volume and viscosity of water spread on driving lane is not sufficient enough to generate lifting forces to completely support the load on the tire, and a full dynamic hydroplaning is evidently going to occur. The design water spread for determining the roadway hydraulic conveyance capacity evaluated in the safety criteria section below. However, safety attributes related to the rainfall depth increase is analyzed based on continuity equation. The material derivative (i.e. the term in the left side of the equation (5)) equals to zero from continuity equation principle. That is:

$$\frac{D}{Dt}\int_{sys}\rho d\forall = 0 \tag{6}$$

Therefore, the continuity equation (5) becomes:

$$\begin{cases}\dfrac{\partial}{\partial t}\int_{cv}\rho d\forall + \int_{cs}\rho V.\vec{n}dA = 0 \\ \int_{cs}\rho V.\vec{n}dA = \dot{m}_{in} - \dot{m}_{out}\end{cases} \tag{7}$$

where $\dot{m}_{in}$ is the rainfall mass flow rate received in the control volume; $\dot{m}_{out}$ is the rainfall mass flow rate discharged by storm drain systems.

If no rainfall rate is discharged by storm drains within the time frame of 10 minutes of the rainfall duration or the rainfall intensity is less or equal to the rainfall intensity used for hydrologic and hydraulic systems design, the equation (7) becomes:

$$\dot{m}_{out} = 0 \Rightarrow \int_{cs} \rho V.\vec{n} dA = \dot{m}_{in} \tag{8}$$

In worst-case scenario, the probable hydroplaning is evaluated in the circumstance of a non-steady state flow discharged (i.e. increase of water accumulation in the control volume). Therefore, equation (7) becomes:

$$\left.\begin{array}{l} \dot{m}_{out} = 0 \Rightarrow \dot{m}_{in} = \dot{m}_{acc} \\ \dot{m}_{in} - \dot{m}_{out} \neq 0 \end{array}\right\} \Rightarrow \begin{cases} \dot{m}_{in} = \dot{m}_{acc} \\ \dfrac{\partial}{\partial t}\int_{cv} \rho d\forall = \dot{m}_{acc} \end{cases} \tag{9}$$

where $\dot{m}_{acc}$ is water mass flow rate accumulated in the control volume

$$\left.\begin{array}{l} \dot{m}_{acc} = \rho Q_{acc} \\ Q_{acc} = k_r I_r A \\ \dot{m}_{acc} = \rho k_r I_r A \end{array}\right\} \Rightarrow \frac{\partial}{\partial t}\int_{cv} \rho d\forall = \rho k_r I_r A \tag{10}$$

where Q_{acc} is rainfall volumetric flow rate [cfs]; A is drainage area (acre) [Ac]; I_r is rainfall intensity [in/hr]; k_r is runoff coefficient [-]

The peak rainfall flow Q_{acc} is determined using the modified rational method, [4]. Equation (10) is used to determine the water pond rate $\frac{\partial h}{\partial t}$ on a roadway surface. Worst-case scenarios and contests are described in section 3. This calculation is the basis for systems control volume-related engineering analyses. It also integrates hydrographs' rational method for rainfall runoff discharge calculation. The integral term of the equation (10) is to estimate the time of change of the depth of standing water on a roadway surface $\frac{\partial h}{\partial t}$ at any instant.

Although hydroplaning is a very complex phenomenon, it is known to be associated with several physical and fluid dynamics factors. This makes it an extremely complex analysis, since the number of variables is large and subject to uncertainty (e.g. rainfall intensity variation in time). Moreover, each variable affects the other in a variety of ways, for instance, the rain intensity may suddenly change within the time.

The likelihood of hydroplaning on wet pavements increases with roadway and environmental factors that increase water depth and with driver and vehicle factors that increase the sensitivity to water depth. To solve this complex problem analytically an iterative approach is used. In the next section a short write-up explains the flowchart of the algorithm used for water depth estimation. Rain gauge data and traffic data from single loop detectors installed on freeway lanes

around the sag points were available in addition to the water depth estimation model in order to make informed decision for highway closure. In this regard, sensitivity analysis is a key.

3.2.7.5 Sensitivity Analysis of the Model

Vehicular hydroplaning speed is affected by the thickness of water film on the pavement surface. For US road design projects, AASHTO recommends a geometric design that accounts for 0.095 in. (2.4 mm) water film in order to determine the relationship between the velocity at which hydroplaning initiates and standing water film. In this study, the use of the empirical formula developed by Gallaway (1979) is a widely accepted model for water film depth estimating.

Due to geometric constraints and a non-standard design of the UPA corridor at the sag points, and the hydrologic and hydraulic systems around the sag points, consideration is given to rainfall accumulation dynamics to account for Gallaway's equation and time in order to provide realistic evaluation of hydroplaning risks.

As a result, the proposed simulation model is most sensitive to the rainfall intensity at high values but more sensitive to slope when slope gets very low. Moreover, the model evaluates more variables, and is valid for roadway texture depths above 0.0079in. (0.2mm). It predicts a decreasing water film thickness of approximately 0.028 in. (0.7mm) per millimeter increase in texture. The rate of water accumulation depth $\frac{\partial h}{\partial t}$ is determined from the control volume equation (7) as follows:

$$\left.\begin{aligned} &\frac{\partial}{\partial t}\int_{cv}\rho d\forall = \rho Q_{acc} \\ &\rho\left(xL-\sum A_r\right)\frac{\partial h}{\partial t} = \rho k_r I_r A \end{aligned}\right\} \Rightarrow \frac{\partial h}{\partial t} = \frac{k_r I_r A}{\left(xL-\sum A_r\right)} \qquad (11)$$

where x is optimum span of the sag of the flooded segment (e.g. section between Blackdog Road and I35W); L is width of the flooded segment at the sag point.

Total hydroplaning on water film (i.e. inability of tires to develop resistive ground forces to overcome external forces) occurs on a distance which is about three times of braking distance on a dry-way.

Parameters used for hydroplaning hazard analysis		
Items	**Definition**	**Data**
A	Drainage area	2.1 Ac (acre)
p	Tire pressure	165 kPa
T_d	Tire thread depth	0.5 mm
Q_{peak}	Upper flow rate threshold	11.5 cfs
Q_{min}	Lower flow rate threshold	7.28 cfs
T_{max}	Storm duration upper threshold	18 min
T_r	Design storm duration	10 min
V_{st}	Storage volume	4140 cf

Figure 3.9: Sag point around 42nd Street and I35W.

Equation (12) can be used to determine the depth h of water accumulated on the highway surface at the sag point:

$$\begin{cases} \dfrac{\partial h}{\partial t} = Q_{acc}\dfrac{1}{\left(xL-\sum A_r\right)} = \dfrac{k_r I_r A}{\left(xL-\sum A_r\right)} \\ \displaystyle\int_{h_0}^{h} d\tau = \int_0^T \frac{k_r I_r A}{\left(xL-\sum A_r\right)}dt = \frac{k_r A}{\left(xL-\sum A_r\right)}\int_0^T I_r dt \end{cases} \qquad (12)$$

As shown in Figure 3.9, equation (12) may be simplified assuming $\sum A_r \approx xL$. The peak rainfall flow Q_{acc} is determined using the rational method. The basic concept in the volume-based method is to find the maximum volume difference between the inflow and the outflow volumes under a series of storm events with different durations. The Intensity-Duration-Frequency (IDF) curves are used to determine the rainfall intensity I_r, [17].

Parameter values in the above table are used to solve equation (12) with initial conditions as storm drains design parameters (i.e., reference for water accumulation rate). In addition to both rigid and flexible cells included pavement design factors that could be evaluated as to their

influence on load equivalency and contributing factors to hydroplaning, rough vehicle factors such as load, tire type, tire pressure, vehicle speed, environmental conditions, and other quantifiable factors were included as part of the model simulation.

3.3 Hydroplaning Model

When road surfaces become flooded or puddle with water, vehicles such as automobiles can at some critical ground speed encounter the phenomenon of tire hydroplaning. To describe the contributing factors of hydroplaning phenomena at the sag points of study, we applied the worst-case scenario concept. This approach considers the extreme physical characteristics applicable to either one of sag points in addition to the spatial representation and the occurrence of the flooding risks. Using a proportioned estimated impact analysis rather than performing detailed hydrology, the approximate area of study boundary includes 2.1 acres around the sag point, roughly bound by the minimum hydroplaning distance and the width of the roadway, Figure 3.9.

The average rainfall intensity (I_r) is defined as the intensity of rainfall in inches per hour for the duration equal to the time of concentration, [15]. In general, the rainfall intensity determined with a rational equation is based upon the duration and not the time of concentration; however, hydrographs initially peak at the original time concentration. The time of concentration is the time required for water to flow from the hydraulically most remote point of the drainage area to the point under investigation.

The lumped analysis, equations 2-4 provides some incentive for the allowable spread thresholds by establishing for both rainfall runoff evaluation and management with the basic fundamentals of safety for informed decision-making. Having set the threshold for the allowable spread and maintaining the 10 year design frequency, the next step is to analyze the rain rates in worst-case scenarios and evaluate the efficiency of the existing storm drains structure to reduce flooding and hydroplaning risks. The crucial step necessitates a definition of time distribution characteristics for heavy rainstorms. Previous attempts to describe the process have been only partial.

3.3.1 Factors Contributing to Dynamic Hydroplaning

Hydroplaning is known to be a major cause of wet-weather road accidents, which occurs when the traveling speed of a vehicle becomes so high that the hydrodynamic pressure of the water between its tires and the pavement surface rises and equals the tire inflation pressure. When this condition prevails, the amount of water encountered on the roadway by a rotating tire exceeds the combined drainage capacity of the tread pattern of the tire and the texture of the pavement. The tires become supported on the water film, and the driver may lose braking and steering control of the vehicle, Figure 3.10, [14].

Figure 3.10: Hydroplaning condition.

The water pressure build-up under the tire originates from the effects of fluid density and fluid viscosity. The following physical factors are involved in the occurrence of hydroplaning of automobile tires:

- *Tire construction type, size, and loading*
- *Tread depth and pattern*
- *Inflation pressure*
- *Pavement surface texture*
- *Length of the path and depth of standing water*
- *Vehicle speed*

Two types of hydroplaning can be distinguished: dynamic hydroplaning and viscous hydroplaning. In general, both types of hydroplaning can occur at the same time. This study focuses on dynamic hydroplaning because this is the most important one. Dynamic hydroplaning is the result of the hydrodynamic forces developed when a tire rolls on a water-covered surface, Figure 3.11. This is a direct consequence of the tire impact with the water that overcomes the fluid inertia. The magnitude of the hydrodynamic force varies with the square of the tire forward ground speed and with the density of the fluid. Dynamic hydroplaning is influenced by tire tread, water layer thickness, and roadway macrotexture. Figure 3.11 depicts different phases of the occurrence of hydroplaning.

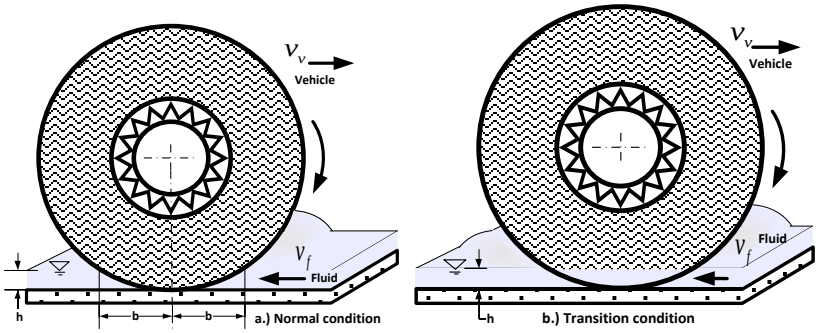

Figure 3.11: Hydroplaning development phases: Normal, and transition hydroplane condition.

As shown in Figure 3.11, a normal hydroplaning condition (a.) prevails when water film and car velocity are below the minimum safety hydroplaning limits. Figure 3.11b. presents the transition condition (i.e., initial condition of the lifting force). Figure 3.12 illustrates a hydroplaning condition where the vehicle is lifted above the highway surface.

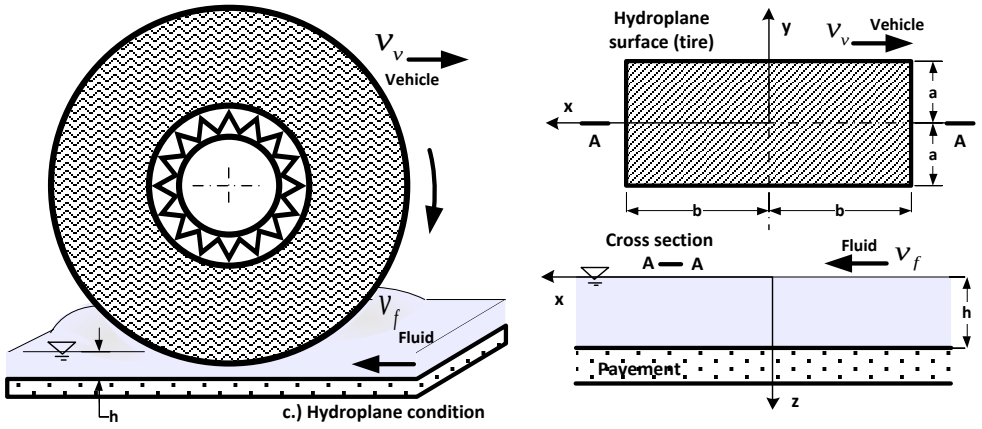

Figure 3.12: Total hydroplaning condition.

As shown in Figure 3.12, when hydroplaning occurs, more than one factor often contributes to the loss of control of the vehicle. Hydroplaning occurs during a moderate to heavy rainfall on roadways with 50-mph speeds or higher. But other factors also need to be present either to create a sufficient water depth or to reduce the resistance to lesser water depths. These factors are developed in the following section.

3.3.1.1 Safety Criteria

From safety perspectives in this study, we evaluate the case where factors that the most increased dynamic hydroplaning risks are related to: (1) heavy rain, (2) high volume of water arriving on the roadway due to the design restriction of storm drain systems, (3) poor texture of the pavement, (4) poor drainage capacity of the tread pattern of the tire, and (5) drivers' behavior in inclement weather conditions.

A very important feature of road construction is drainage. Flooded and waterlogged roads result when the amount of water arriving on the road due to heavy rain or flooding from a main river is greater than the capacity of the drainage facilities. The risk of hydroplaning in wet-weather driving is a function of various parameters. The non-exhaustive list of parameters considered in this analysis includes thickness of water film on the pavement, pavement texture properties, tire characteristics and inflation pressure, wheel load, and vehicle speed. With the aim to improve and ensure wet-weather driving safety, first of all, we considered experimental results and the values of these parameters provided in the literature for the hydroplaning speed analysis [18], [16], [2], [22].

Second, the traffic dynamics, rainfall intensity, and visibility have been considered in the analytical studies to understand how tire characteristics (in particular, tire tread depth) would affect hydroplaning dynamics in the analysis for a hydroplaning risk. In this regard, the analysis

of the existing hydraulic capacity at the sag points will be used to set the lower and upper flooding safety threshold at the sag points.

3.3.1.2 Runoff Capture Analysis

When the amount of water encountered on the roadway by a rotating tire exceeds the combined drainage capacity of the tread pattern of the tire and the texture of the pavement, the mass and viscosity of the water cause it to resist being displaced from between the tire and the pavement, thus generating lift forces on the tire which reduce tire contact with the pavement. If the lift forces are sufficient to completely support the load on the tire, contact with the road is no longer made and full dynamic hydroplaning is evidently going to occur. In this section we analyze the existing hydraulic storage and conveyance capacity.

Since the simulation tools that will be linked to the instrumentation and operation monitoring systems require values for all input parameters such as traffic flow, volume, vehicles' technical characteristics, and weather conditions, in the following we: (1) develop a schema that assigns "smart" default values to all those parameters that cannot yet be simultaneously defined by the user; and (2) treat these variables as exogenous only for considerable rainfall threshold identification. Furthermore, these default values represent proactive safety action decisions. However, water pond depth on the roadway, should be clearly indicated to the management whose task is to decide upon operation controls expertise and appropriate ITS means available to warn/close or limit the traffic flow.

Figure 3.13 illustrates a worst-case scenario of the flooded roadway at the sag points. It can be seen that based on the street transverse slope, driving lane 1 can be used as the monitoring point because the highest water pond is within the driving lane 1. Since risk-based approaches are applied to this study, a selected risk level shall be applied to the entire region of the sag point. Often, inconsistent parameters add random uncertainties to the selected risk level. Therefore, discharge reduction factor is used to alternatively evaluate the depth of the gutter in case of minor and major events:

$$\begin{cases} \mathrm{R}_{ed} = \dfrac{Q_{red}}{Q_{full}}; \quad 0 < \mathrm{R}_{ed} \le 1 \\ \qquad = \dfrac{1}{(T_{\max,s} S_x)^{2.67}} \left(\dfrac{np_{vd}}{2kS^{0.5}} \right)^{1.60} \end{cases} \tag{13}$$

where R_{ed} is the reduction factor (see Appendix A.2)

Observation of the area around the sag point indicated that the real problem in this design is a runoff volume problem not a peak problem (i.e. in worst-case, a highly developed portion of the watershed produces a higher rate of runoff than the overall drainage area) that overloads the sewer systems capacity.

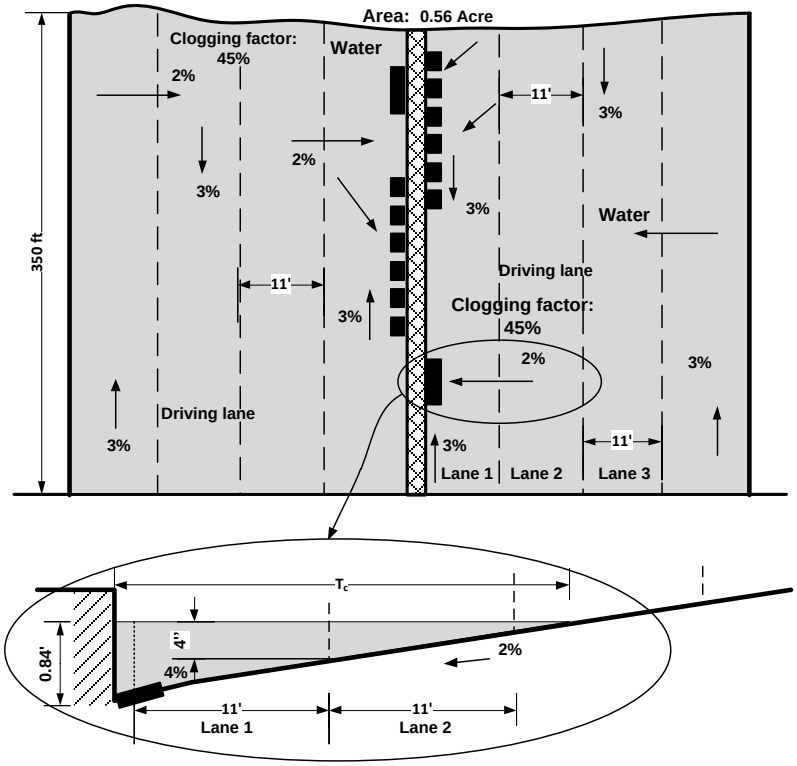

Figure 3.13: Flooded road scenario at the sag points.

Additional runoff collectors (helpers) were constructed to collect maximum flow that attempt to bypass main drains. Their number increase from the top to bottom of the sag. In Appendix A.2 the drain reduction factor ic calculated to determine if main drains scaled accurately. The reduction factor determined in Appendix A.2 shows that the reduction factor $\mathrm{R}_{ed} > 1$, indicating that the street gutter can carry the design discharge without exceeding the permissible product $VD = p_{vd}$, (i.e. the product of runoff velocity V and the depth of the curb D) if a maximum spread is maintained to $T_{\max,s} = 0.5L$ in order to monitor the flooding risks.

3.3.1.3 Analysis of the Design Time Duration

In the analysis of the existing design for determining the roadway hydraulic conveyance capacity, the full water spread is defined as follows:

$$T = \min\left(T_m, \frac{D_m - D_s}{S_x}\right) \tag{14}$$

where T_m is the available water spread; D_m is the gutter-full depth; D_s is the gutter depression; $\boldsymbol{S_x}$ is the street transverse slope (%)

Consider the worst-case scenario where the water spread into the traffic lane is limited to 14ft (i.e. $T_m = L + 3 = 14\text{ft}$), Figure 3.10. The capacity of type D4 grate (standard plate 4154) is

calculate considering debris clogging factor $C_g = 0.55$. For 10 year frequency the capacity of the sump inlet for one unit is determined as:

$$\begin{cases} Q_s = \left(1 - C_g\right) KD^{5/3} \\ \quad = \left(1 - 0.55\right) \times 14.5 \times 0.34^{5/3} = 1.08\,\text{cfs} \end{cases} \tag{15}$$

where $D = 0.34\,\text{ft}$ is the depth over the grate; $K = 14.5$ from CAT. No. 3250CV

Based on the IDF's 10 year frequency curve the rainfall intensity curve in in./hour is determined as follows:

$$I_r = 8.4 - 295 \times 10^{-3} t_m^{0.982} + 53 \times 10^{-4} t_m^{2.01} - 28 \times 10^{-5} t_m^{2.54} \tag{16}$$

Using equation (16) in Appendix A.3, the optimum detention time $T_{opt} = 28$ minutes and storm water detention volume $V_d = 3586\,\text{ft}^3$. With these results, we will maintain in the next section $T_{opt} = T_c$ (i.e. detention time equals to rainfall duration) for a given intensity I_r in order to predict rainfall accumulation.

Since at the sag point three units are used the optimum detention time becomes $T_{opt,s} = 10$ minutes approximately. This time corresponds to the concentration time $T_c = 10$ minutes used for the hydrologic system design.

As developed in Appendix A.1, the total hydraulic system capacity without minor drains (helpers) is:

$$\begin{cases} Q_{L,T} = 3C_g \left(\varphi_d Q_x + Q_w\right) \\ \quad = 3 \times 0.55\left(0.85 \times 5.32 + 7.92\right) = 20.53\,\text{cfs} \end{cases}$$

The next section is to evaluate the flow condition from manholes.

3.3.2 Hydroplaning Models

The experimental study developed by Gallaway et al. [8], provides insights to understanding and control hydroplaning phenomena. At a given operating condition on wet pavement, the effective friction coefficient is reduced by worn tires. The rainfall water accumulation model developed above (equation 12) will be integrated into Gallaway's equation to evaluate the safety limit of vehicles' speeds and wet roadway surface conditions.

Safety requirements have been taken into account to set the maximum design speed of the highway in the area of study to 70 mph. In inclement weather conditions, vehicles' speed may varies over a large range, from 30 to 70 mph. In these conditions, the magnitude of vehicles' speed depends on the vehicle type, environmental conditions (such as wind conditions, rainfall intensity, visibility, etc…), and traffic volume. To assess probable hydroplaning risks, a

probabilistic distribution of traveling speed is established for each vehicle type. Vehicle characteristics and drivers' behavior are also important factors in hydroplaning.

Dynamic hydroplaning of middle size vehicle tires occurs on relatively thick water films, generally greater than 0.08 in. deep, and at speeds greater than 40 MPH [16], [20], [11]. Prior to the onset of full tire hydroplaning, a transitional condition occurs in which the surface contact area of the tire footprint is decreased as the vehicle speed is increased. This condition is sometimes referred to as "partial hydroplaning" and it is associated with a reduction in the effective friction coefficient, Figure 3.14.

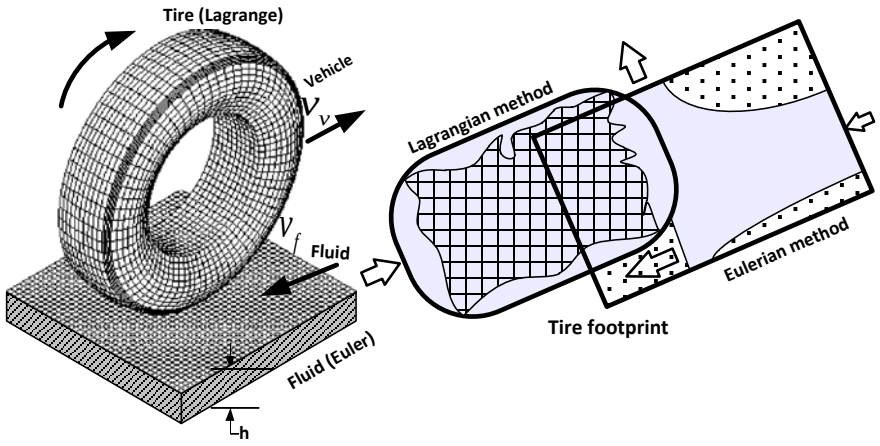

Figure 3.14: Partial hydroplaning model.

The evaluation of hydroplaning risks becomes complex as a result of the combination of factors involved. The capacity of the tire tread grooves for water flow is an important factor in limiting the development of partial hydroplaning. Vehicles with worn tires are the most at risk. The tire-pavement model obeys to the Coulomb principle as follows:

$$F_T = \tau \mu F_n \tag{17}$$

where F_T is tangential force; F_n is normal contact force; μ coefficient of friction; τ is a dimensionless variable.

The variable τ can be further characterized as follows:

$$|\tau| \le 1 \Rightarrow \begin{cases} |\tau| < 1 \Rightarrow \dot{u} = 0 \\ |\tau| = 1 \Rightarrow sign(\dot{u}) = sign(\tau) \end{cases} \tag{18}$$

where $\dot{u}$ is the sliding velocity

Manifestations of tire hydroplaning which have been experimentally observed are presented and discussed, [9]. These manifestations are: detachment of tire footprint, hydrodynamic ground pressure, spindown parameter (i.e. change of in rotational velocity of a wheel due to the loss of

contact with the pavement surface), scouring action of escaping fluid in tire-ground footprint region, peaking of fluid displacement drag, loss in braking traction, and loss of tire directional stability. The hazards of tire hydroplaning to ground performance in terms of braking coefficient as a function of the tire groove ratio is illustrated in Figure 3.15. Procedures to minimize these effects are developed in the next section. In these conditions, the hydroplaning distance on wet surface is almost three times the braking distance on dry-ground.

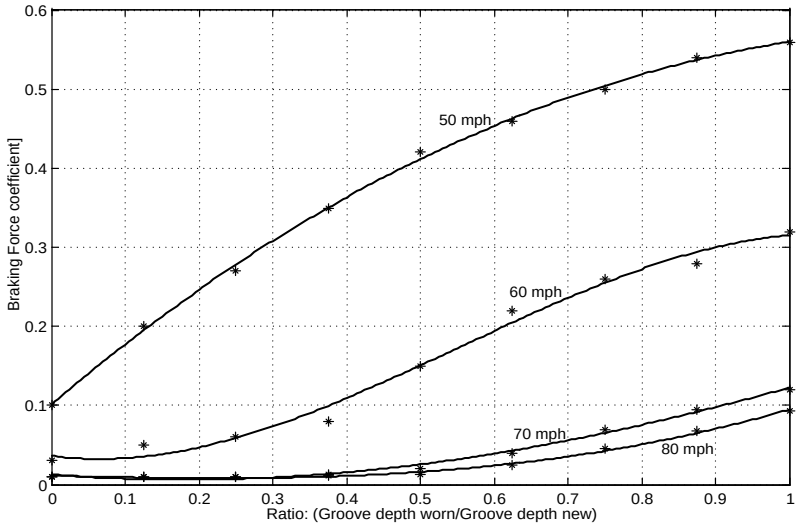

Figure 3.15: Braking coefficient as a function of the groove ratio.

A function that determines the critical hydroplaning speed as a function of tire pressure, when the steering ability of the tire is completely lost and the braking ability drops dramatically is derived by NASA Langley Research Center, [22], [13] as follows:

$$V_p(p) = 10.35\sqrt{p} \tag{19}$$

where V_p is vehicle speed [mph]; p is the tire inflation pressure [psi]

Figure 3.16a depicts experimental hydroplaning speed as a function of water depth while Figure 3.16b illustrates the graph from empirical hydroplaning speed as a function the tire pressure, [13].

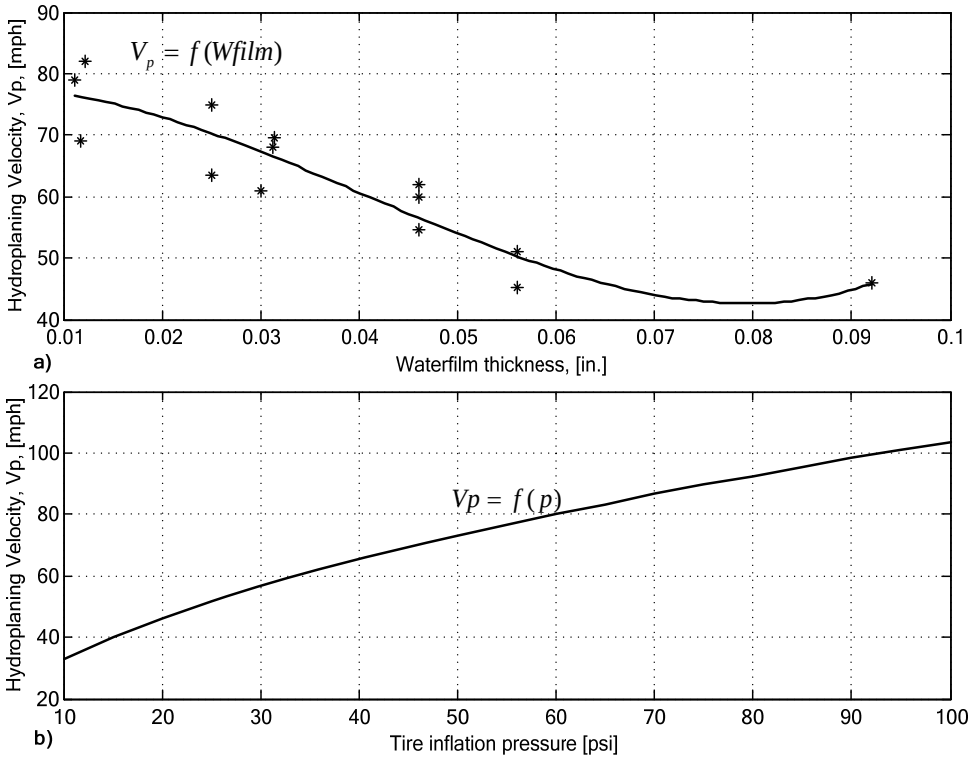

Figure 3.16: Hypothetical hydroplaning speed: a) $Vp = f(Wfilm)$; b) $Vp = f(p)$ **.**

From different aspects of hydroplaning conditions, we noticed that if NASA hydroplaning equation (19) is applied to predict hydroplaning behavior of trucks, two major discrepancies are observed:

a) Equation (19) grossly overestimates truck hydroplaning speeds (i.e., underestimates the risk of hydroplaning) for the range of normal operating tire inflation pressures of trucks, and
b) Equation (19)is unable to explain the tendency of empty trucks (i.e., trucks with lower wheel loads) to be involved in wet-pavement accidents more than loaded trucks (i.e., trucks with higher wheel loads)

As stated in the hypothesis, driving on worn tires which characteristics may increase hydroplaning risks is not evaluated in this analysis. The speed at which a vehicle needs to travel to begin hydroplaning is determined by water depth but also by the vehicle's weight, and tire characteristics. More importantly, the vehicle weight determines how much uplift force is needed to induce separation and it follows that a lighter vehicle will aquaplane at a lower speed. Also, higher tire pressures increase the hydroplaning speed by reducing the contact area between tire and road, increasing the vehicles weight to area ratio.

Tire tread depth significantly affects hydroplaning the same way as pavement texture, with deeper tread moving the water away from the area of contact more effectively. While minimum tire tread depth and maximum speed are often both specified by law, minimum weight and tire pressure are not. For safety purposes, an automobile driver should allow at least 3 times the

normal spacing between his car and the vehicle ahead to allow for this reduced braking traction for there may be a truck or bus ahead that is not hydroplaning and therefore not experiencing low braking traction.

In line with these safety issues and the hydrodynamic theory, the model of tire behavior under partial and total hydroplaning conditions is developed by Gallaway et al. in a better light, [8]. The equation is derived as a function of the water pond depth on a roadway surface and vehicle tire pressure.

$$\left\{\begin{array}{l} V_p = 0.9143 k_a \times S_d^{0.04} \times p^{0.3} \times \left(T_d + 0.794\right)^{0.06} \\ k_a = \dfrac{12.639}{h^{0.06}} + 3.50 \\ \text{or} \\ k_a = \left(\dfrac{22.351}{h^{0.06}} - 4.97\right) \times \delta_d^{0.4} \end{array}\right\} \text{whichever is greater} \qquad (20)$$

$$S_d = 100\left(1 - \frac{w_w}{w_d}\right)$$

where V_p is hydroplaning speed [km/hr]; h is accumulated water depth on the roadway surface in [mm]; δ_d is pavement texture depth [mm]; T_d is vehicle tire tread depth [mm]; p is the tire inflation pressure [kPa]; S_d is the spindown speed (at initiation of hydroplaning); w_w rational velocity of wheel after spindown due contact with wet surface; w_d rational velocity of wheel on dry surface;

These parameters are carefully selected for the analysis in order to be consistent with weather data around the sag points area and the storm drains design. However, in the context of various climate changes, it is not feasible to capture all contributing factors involved in hydroplaning. We examine only those weather parameters that have significant effects on maintenance management, emergency management, and traffic management, and road users' behaviors are identified and prioritized for decision support.

The rainfall IDF's data analyzed were restricted to reasonably as practicable traffic flow for different weather conditions (light and heavy rain and heavy wind). The traffic operation was evaluated statistically for different types of weather as shown in Table 4, [22]:

Table 3.3: Average impact of weather on highway speed limit.

The average impact of weather on freeway speed and capacity

Weather variable	Intensity	Speed (mph)	Reduction ratio	Capacity (Veh./hour)	Reduction ratio
Wind speed	< 9.95 mph	67.9		2334	
	9.95 - 19.9 mph	67.6	1 %	2309	1 %
	> 19.9 mph	67.2	1 %	2300	1%
Visibility	> 1 mile	69.8		2342	
	1 – 0.5 mile	65.1	10 %	2115	10 %

Excluding worn tires, Figure 3.17 illustrates results of the two proposed models for estimating hydroplaning velocity for four different tire pressures. Where assumption is made that, taking the highway design parameters including rainfall intensity as a threshold, if the depth of the standing water on pavement surface starts to increase, passenger car will hydroplane before a truck at the same speed. Moreover, conservative approximations were made to compute flow estimates. Graphs in Figures 3.17a and 3.17b show that the risk of hydroplaning decreases with the increase of the depth of water on pavement surface when the rainfall intensity is respectively 1in/hr and 3in/hr. In these circumstances with reduced speed the traffic flow will be reduced significantly.

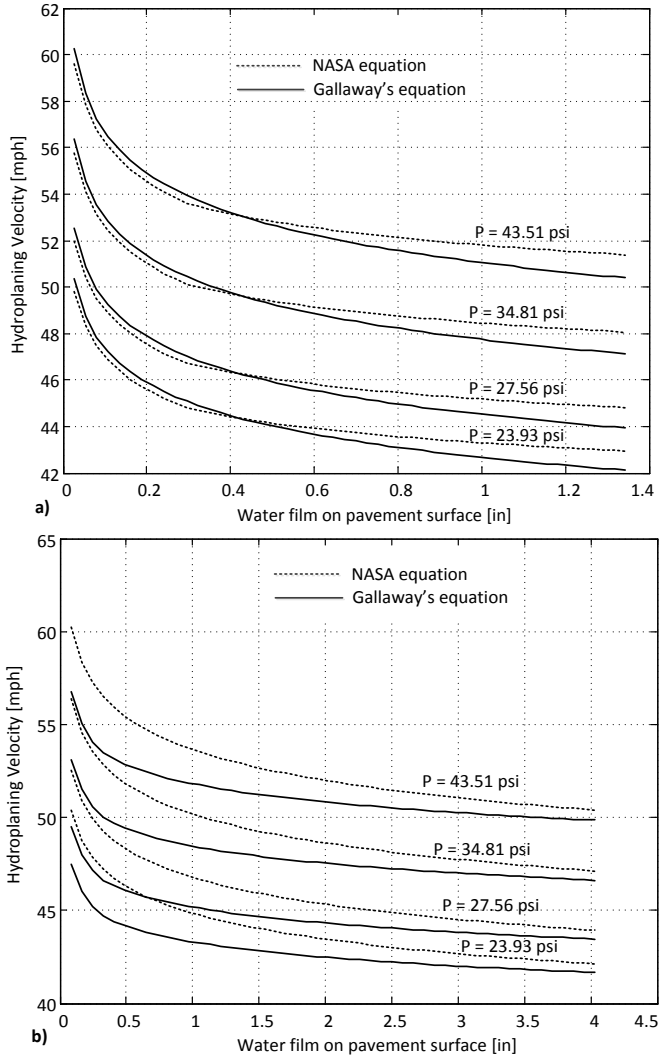

Figure 3.17: Two models for the estimation of hydroplaning velocity as a function of tire pressure

Given the experimental results depicted in Figure 3.17 from NASA and Gallaway's equations, section 3 will use relevant causal constructs around the sag point (i.e. Blackdog Road and I35W) to predict hydroplaning events. More precisely, the algorithm developed in section 3 is based on the physical characteristics of the existing storm drains presented in section 2, and the assumptions presented in the next section. However, these factors may not be enough to reconstruct the multifactorial path to unwanted energy transfers and their relationships to each other and to the traveling public. Human factors play important role, but they are out of the scope of this study.

3.4 Prediction Algorithm of Rainfall Accumulation and Analytical Results

3.4.1 Assumptions

- Since the UPA corridor hydrologic and hydraulic systems are designed for 10 year frequency, we assume during the 10 year event, must maintain a minimum of 11ft traffic lane free from the storm runoff and the gutter water depth is not to exceed the curb of 6inches. Moreover, for safety, the product $VD = p_{vd}$, (i.e. the product of the runoff velocity V, and the depth of the curb D) should not exceed 2cfs/ft.
- The depth of rainfall used is one that occurs from the start of storm rain to the time of concentration calculated using actual data inputs from the rain sensor. The rainfall depth has a level distribution over the duration of the storm, meaning the rainfall intensity is constant throughout the storm. In these circumstances the analysis time not the design time concentration becomes a threshold for flooding risks management.
- The maximum runoff rate occurs when a low developed portion of the watershed with a longer time of concentration or a more intensely developed portion of the watershed with a shorter time of concentration produces a higher rate of maximum runoff than the entire watershed with a longer time of concentration. The maximum runoff rate occurs when the entire area is contributing to the flow. Then, the prediction is initiated when the rainfall intensity and duration is high enough to fill up the basin and gutter storage volume.

3.4.2 Analytical Results

The prediction of water pond accumulation on the roadway uses the average rain sensor data inputs provided by the operator due to complex variability of storm rain intensity in real time. The prediction process is open-loop process. Therefore the time synchronization of the sensor is crucial for the algorithm to accurately predict the rainfall accumulation. The following two scenarios are analyzed to determine the extent to which the rainfall intensity level should rich so the traffic operation management decides to warn safety speed limit or close the highway segments including sag points.

3.4.2.1 Low Intensity and Long-Time of Concentration

Upon the characteristics of the sag points as described in section 2 the choice of elements associated to risk-based scenarios strictly depends on the configuration of the drainage system. Based on equation (4) which provides the minimum rainfall intensity $I_e = 0.7\,\text{in/hr}$, storm events that produce $h_r \le 0.7\,\text{inch}$ of rain within 3.0 hours period of time is classified as *low intensity and long-time of duration*. Otherwise it is classified as high intensity event by the algorithm to test the capacity of capture of the basin.

Complicating the issue is the design of UPA corridor assuming that the existing drainage system is adequate. Based on 10 year event frequency it was shown in the Appendix A.3 that because the actual runoff hydrograph is not truncated like a simple triangle **v**olumes are set too low. As a result, the existing 10-year design control does nothing for two-year downstream flooding problems. This is referred to as a runoff volume problem not a peak discharge problem. Under

constant flow conditions, the principle of flood routing is used to solve aspects of fluid dynamics as shown in Figure 3.7 with consideration of changes of the basin storage volume.

It is not easy to predict variation of rainfall intensity of the tributary area that contributes to the change of the storage volume. However, since 10 year event frequency was used for drain design, rainfall intensity extrapolation from the IDF curve (zone 2 Minnesota) is developed in Appendix A3. In order to formulate the variation of rain intensity, the rainfall intensity I_r , Figure 3.18, is determined as a function the duration time t_m as follows:

$$I_r = 8.4 - 295\times10^{-3} t_m^{0.982} + 53\times10^{-4} t_m^{2.01} - 28\times10^{-5} t_m^{2.54} \qquad (21)$$

For different type of events (either sort time or long time), the basin capacity of capture is important. The equation (21) provides the minimum rainfall intensity $I_{r\min} = 2.6\,\text{in/hr}$ and $t_{d,\min} = 54\,\text{minutes}$ of duration. In another word, this 10 year frequency of rainfall events (i.e. 10% of probability of occurrence in any given year) will produce a minimum rainfall $I_{r\min} = 2.6\,\text{in/hr}$ and $t_{d,\min} = 54\,\text{minutes}$ of duration while the drain is designed for $I_r = 6\,\text{in/hr}$ and $t_d = 10\,\text{minutes}$ duration.

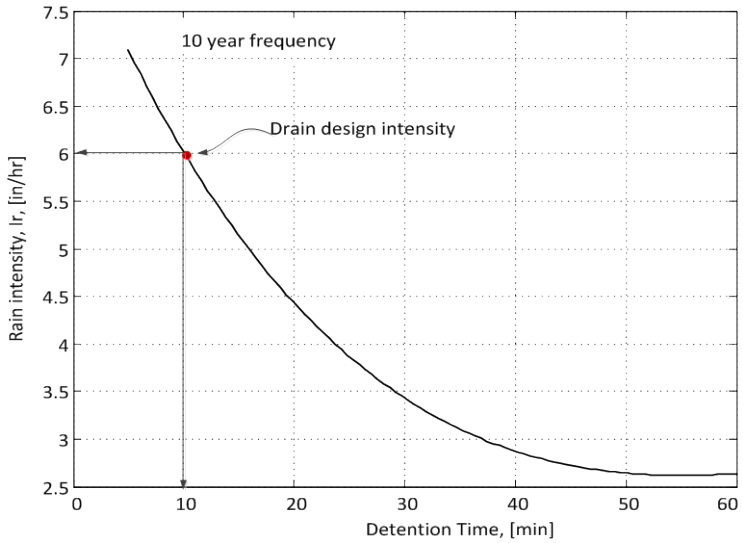

Figure 3.18: Rainfall intensity based on IDF's curve for 10 year frequency.

3.4.2.2 High Intensity and in Short Time of Concentration

This is the critical scenario for the evaluation. Throughout the analysis of the existing drainage system, few questions on reengineering the hydrologic system are less fundamental to the risk control planning than the question of how exactly rainfall variations influence landscapes and road safety – the extent of weathered pavement (all season pavement), the morphology of landscapes (e.g. channel slopes, transverse and longitudinal slope gradient at the sage point), the efficiency and the relative flux of mass in sediments.

Despite the foundational nature of the question of the overflow risk associated with the manhole and methods used to choose storm drains' design strategy, much remains un-quantified and undocumented. We assumed that, as is generally the case for standard design, the drainage structure for minor and major flood control is sized for extreme events using the prescribed relationship between design capacity and overflow risk (US Water Resources Council 1981).

Therefore, to quantify the overflow risk for the installed manholes and their drain time, the most deductive analytic method is that empirical model parameters absorb all rainstorm variations (climatic) influence, but remain un-calibrated to measureable climate attributes such as mean annual precipitation, time distributions, frequency, return-period, seasonality, and storminess. Thus we consider that during an event the manhole is operated under the dynamic processes of filling and draining and the manhole is partially or fully occupied by the event runoff.

In Appendix A.1 the total hydraulic system capacity $Q_{L,T}$ is determined without minor drains (helpers) capacity as follows:

$$\begin{cases} Q_{L,T} = 3C_g\left(\varphi_d Q_x + Q_w\right) \\ \qquad = 3\times 0.55\left(0.85\times 5.32 + 7.92\right) = 20.53\,\text{cfs} \end{cases}$$

Consider the efficiency $\varphi_{d,m} = 0.70$ for minor drains (helpers) along the sag point area, Figure 3.19.

Figure 3.19: Runoff capture distribution.

(©2013 Google - DigitalGlobe, GeoEye, U.S. Geological Survey)

These installed drains have efficiency up to $\varphi_c = 0.7$ and can reduce the carryover flow which is assumed to come from 10% of the tributary area of the rainfall. Their intersection capacity is $C = 0.5$. As a result the hydraulic design discharge **Q** at the sag point is sum of the peak runoff discharge and the carryover flow $\mathbf{Q_c}$ as calculated in Appendix A.4:

$$\left.\begin{aligned} Q &= Q_{L,T} + Q_c \\ Q_c &= C\varphi_c A_c I_r \\ A_c &= 0.1 \times A \end{aligned}\right\} Q = Q_{L,T} + Q_c = 20.971 \text{ cfs} \tag{22}$$

This result is based on 10 year recurrence frequency design and 10 minutes time concentration. As a result, the design capacity of the hydraulic system is determined as follows:

$$\begin{cases} Vol_d = T_c Q_c \\ \quad = 60 \times 10 \times 20.971 = 12,583 \text{ ft}^3 \\ \quad = 0.29 \text{ acre-foot} \end{cases} \tag{23}$$

This result will be used in the algorithm to determine the flooding risk, hydroplaning condition, and emergency actions to take. Note that, hydroplaning model is not explicitly function of time. Therefore, constant rainfall conditions are used to evaluate the hydroplaning state; however this model is subject to uncertainty of the variation of the rainfall. The following case study was performed to evaluate the sensitivity of the existing hydraulic system.

3.4.3 Simulation Results and Verification

3.4.3.1 Case Study 1: Under Minimum Hydroplaning Threshold

This is simulation-based verification of the capacity of the hydraulic system at the sag point after some adjustment has been made (i.e. construction of minor drains (helpers)) to the existing design. For sensibility analysis of the initial hydraulic design a worst event scenario is used to simulate the capacity of the hydraulic system given the following input to the algorithm:

$$\begin{cases} T_c = 10 \text{ min} \\ I_r = 6 \text{ } in./hour \end{cases}$$

where T_c is concentration time; I_r is rainfall intensity (constant in time). These data are used for 10 year frequency for the initial design. Results are depicted in Figure 3.20.

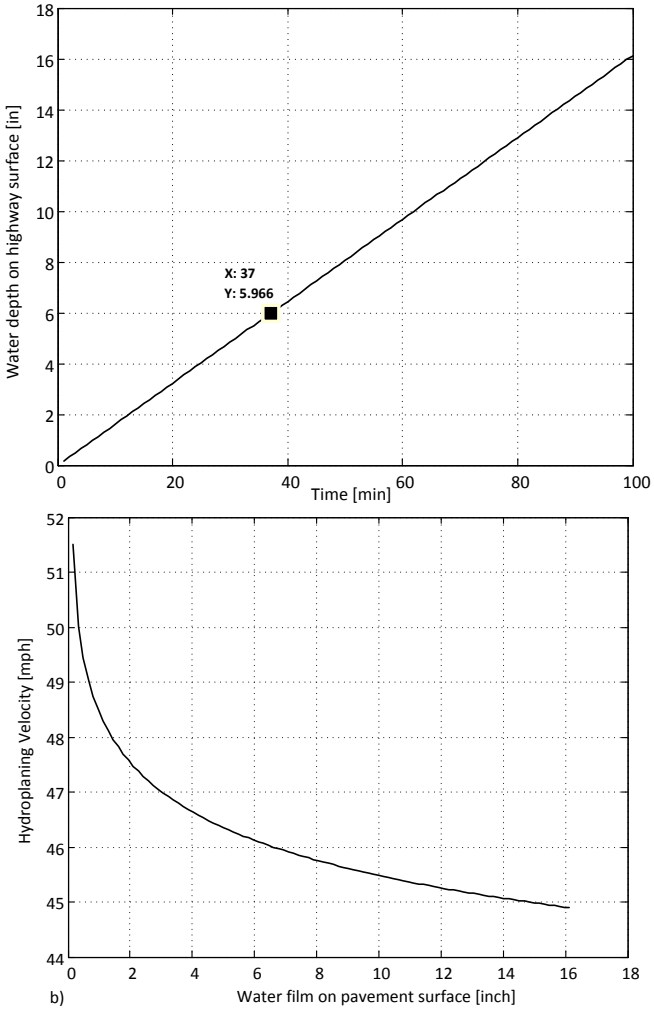

Figure 3.20: Hydroplaning prediction for the initial hydraulic system design.

Figure 3.20a depicts rainfall variation for the given rain sensor data which corresponds to the storm drain design data; Figure 3.20b is the hydroplaning curve.

The algorithm returns the following results:

1) Rain_Duration = (i.e. rainfall duration provided by the operator) which is 10 minutes in this case
2) RainIntensity = (i.e. rainfall intensity provided by the operator and used for the prediction), which in this case is 6in./hour
3) Result of for hydroplaning risks assessment in 15 minutes ahead, which in this case is communicated as follows:
   - *At this intensity and duration the minimum hydroplaning threshold is not reached*
   - *Please repeat the verification process in 10 minutes*

In critical situation which is predicted in 15 minutes ahead a warning message is sent to the operator to take emergency actions (e.g. use of camera to visualize the sag point; reduce the speed limit of the road segment, etc.)

3.4.3.2 Case Study 2: Minimum Hydroplaning Threshold

This is simulation-based verification of the capacity of the hydraulic system used rainfall intensity of 5in./hour and concentration time of 30 minutes. The algorithm returns the following results:

1) Rain_Duration = (i.e. rainfall duration based on the operator's input) which is 30 minutes in this case
2) RainIntensity = (i.e. rainfall intensity provided by the operator and used for hydroplaning risks prediction), which in this case is 5in./hour
3) Water film = (i.e. water film depth prediction on the road surface in 15 minutes ahead), which in this case is: ***0.107 inches***. The operator will use this value to immediately set the speed limits, Figure 3.21
4) Result of for hydroplaning risks assessment in 15 minutes ahead, which in this case is communicated as follows:
   - *Basin overflow, please consider required safety actions now!!*
   - *Use Water film value and Hydroplaning curve to monitor traffic speed*

As we can see on the hydroplaning curve, Figure 3.21, ***0.107 inches*** is slimly equals to the minimum hydroplaning threshold of ***0.095 inches***. Therefore the maximum highway design speed limit can be used to monitor the road segment within the prediction time limit.

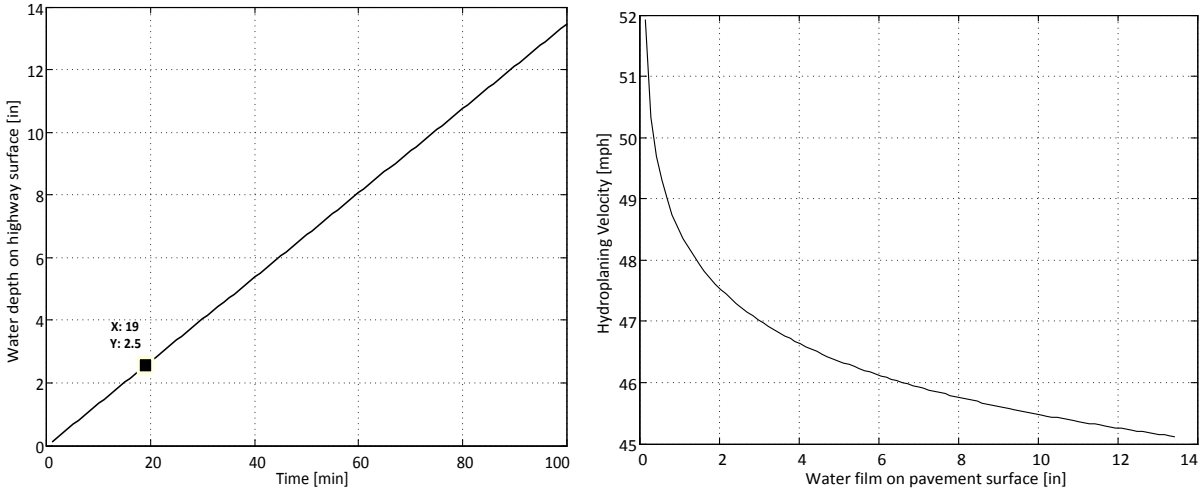

Figure 3.21: Hydroplaning minimum threshold.

3.4.3.3 Case Study 3: Maximum Hydroplaning Threshold

This case evaluates whether or not the maximum hydroplaning limit is reached and communicate the risk level. The illustrative examplpe uses the initial design rainfall intensity of 6in./hour and longer concentration time of 40 minutes. The algorithm returns the following results:

1) Rain_Duration = (i.e. rainfall duration based on the operator's input) which is 40 minutes in this case

2) RainIntensity = (i.e. rainfall intensity provided by the operator and used for hydroplaning risks prediction), which in this case is 6in./hour
3) Water film = (i.e. water film depth prediction on the road surface in 15 minutes ahead), which in this case is: ***1.39 inches***. The operator will use this value to immediately set the speed limits, Figure 3.22
4) Result of for hydroplaning risks assessment in 15 minutes ahead, which in this case is communicated as follows:
   - *Basin overflow, please consider required safety actions now!!*
   - *Use Water film value and Hydroplaning curve to monitor traffic speed*

As depicted in Figure 3.22a, the tributary area received ***4.0 inches*** of rainfall within this period of time. For the prediction time the overflow (Water film) will be is: ***1.39 inches***. The maximum threshold of ***2.0 inches*** for emergency is not reached. The operator should use the hydroplaning curve to set the speed limit to 48mph as shown in in Figure 3.22b.

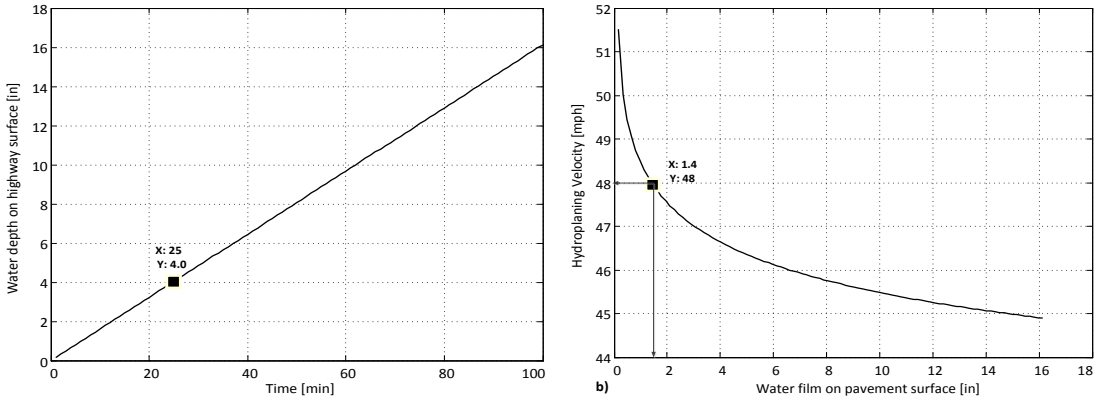

Figure 3.22: Hydroplaning monitoring.

3.4.4 Discussion and Recommendations

Computation of the hydroplaning speed for a given set of wet pavement conditions is an iterative process. To better understand hydroplaning phenomena, an approximate theory is developed for this study by considering a dynamic hydroplaning tire as a planning surface of a small aspect ratio in extremely shallow water. Moreover, we assume that the locked-wheel sliding speed is not the hydroplaning speed.

Based on these considerations, we foresee that this approximation would exhibit hydrodynamic behavior similar to that of hydroplaning pneumatic tires and thus would indicate that the tire hydroplaning phenomenon can be described from the standpoint of in viscid hydrodynamics. This analysis provides a variety of curves which represent, quantitatively, the complexity of the starting point of hydroplaning and thus give qualitative guidance for making evidence-based decisions to avoid the undesirable hydroplaning conditions on flooded roads or to close the flooded segment of the sag point.

From the literature (Office of the Federal Coordinator for Meteorology), it is apparent that there are many weather parameters that affect highway safety and operations. It is important to distinguish hydrologic system analyses from designs. The analyses rely on risk-based approach.

Therefore, the evaluation goes beyond the application of models to calculate runoff peak flow rates and volumes. As a part of this study, reasonableness checks were conducted on computed peak flow rates and runoff volumes. These include methods of calculation such as the Rational Method, and fluid dynamics in order to estimate the runoff with a reasonable margin of safety to ensure protection of public safety.

The logical conclusion drawn on risk-based knowledge and available evidence in this study is that, at the sag point, there are two-year downstream flooding problems. Volumes are set too low, because the actual runoff hydrograph is not truncated like a simple triangle. As a result, the existing 10-year design control does nothing for two-year downstream flooding problems.

As a result the initial design was up-grated to catch as much as possible carryover flow using minor drains. This analysis considers the flooding problem as a runoff volume problem not a peak problem. Although, corrective actions have been taken to improve flooding risks at the sag point around 42nd Street, risk management plan is strongly recommended to proactively monitor road safety of this segment of the UPA corridor. This proactive approach should complement the more traditional, reactive methods and emergency actions in use.

At this time there is only one rain sensor site. Data collected from a single point is not enough to describe the situation of the entire zone under consideration. The lack of large gage network around sag points did not help providing adequately design information used by contractors for the entire drainage area. Therefore, the next step toward validation and improvement of the algorithm is to develop a procedure that requires a large amount of data and extensive effort of calibrations. Then using multiple regression analyses where watershed and rainfall tributary area characteristics are set as independent variables, the carryover flow discharges at ungagged sites can be related to the observations at gaged sites.

3.5 Conclusion

This research study used a combination of fluid dynamics principles and modified discharge rational methods. Specific forms of these methods are explicitly derived from the underlying simple analytical approximations of common distribution functions and allow mathematically convenient expressions of IDF (Intensity-Duration-Frequency) relationships. Yet, the resulting flooding and hydroplaning risks monitoring tools have not been tested by worst-case storms. Collection of these data with which to test the validity of the method would has been an asset for the model sensibility in a variety of situations.

Although the method still quantitative in nature, due to the lack of design safety data from multiple sag points and qualitative criteria for comparison at that stage, the similarity of the pattern of the alertness guideline generated for informed decision-making by the algorithm to that produced by an objective operator’s judgment method indicated the validity of the principles that govern the risk management incentive derived by the proposed algorithm.

The most important conclusion of this research is that weather matters—weather conditions have an important impact on traffic safety, traffic demand, and traffic flow. Such a systematic framework of quantitative risk analysis procedure can facilitate efficient risk management. Moreover, the proposed risk assessment tool can be combined with ITS, and risk communication

and operation control in order to predict relative crash susceptibility in various segments of the corridor based on knowledge of local geography, topography, storm rain intensity, and other risk factors.

Although the hydrologic analysis developed in this study is relevant in establishing the quantity of the standing water that must be considered for the design of the drainage systems, the extent of such studies are commensurate with the importance of the highway flow density, the estimate of the potential for damage to the highway, material loss, and the potential risk to traveling public life, but cannot be considered as an absolute approach for redesigning the hydrologic and hydraulic systems. Much more research is needed to measure, understand, implement, and validate management strategies receptive to mitigate inclement weather impacts at both sag points.

4. Evaluation of Bus Operations on the MnPASS PDSL

4.1 Introduction

One of the biggest advantages of the 35W BRT corridor is the fact that the busses are traveling on the MnPASS lane therefore guaranteeing travel under uncongested traffic conditions. To facilitate quick boardings and alightings of transit passengers as well as to reduce the delay involved in entering and exiting the freeway, the 46th St. BRT station is located in the median of I-35W. Although such design is common in freeway BRT corridors, its interaction with the existing right hand side station on Lake St. could be an issue.

According to Metro Transit plans, routes 152,535, and 578 utilize the 46th St. station with a peak frequency between 5 and 7.5 minutes. Additional routes may exist like the 467 and 477V of MVTA. Not all of these routes utilize the Lake St. station. This research focuses on route 535 which has both high frequency and utilizes both stations. These busses have to traverse four lanes between the MnPASS lane on the left and the Lake St. station on the far right. There is a proposal and discussion of constructing a new median placed Lake St. station, a multi-million dollar project. This research may assist policy makers in their deliberations.

The 46th St. Transit station as planned came online in late fall 2010. After this period, the research focused on two perspectives of the bus lane changes, the impact these lane changes have on the freeway mainline flow and the safety implications for the busses making these lane changes. The latter also includes a performance evaluation of the BRT corridor operations. Two types of information were involved in this analysis.

a) Busses require larger gaps and have reduced acceleration capabilities. Depending on the state of the traffic flow, during such lane changes the bus may cause shockwaves and possibly initiate a traffic flow breakdown. Based on the identified location of lane changes, speed data from MnDOT loop detectors was correlated and examined for shockwave activity.
b) The amount of difficulty in performing the required lane changes will determine the location where the drivers will select to enter/exit the MnPASS lane. Metro transit drivers will adapt to road reality as they did with driving on the shoulder. We assume that the drivers will select the safest location for the lane changes which may not be the desired in order to take the benefit from the fast moving MNPASS lane.

The rest of this chapter first describes the method followed for data collection as well as the time periods collection took place. Second, the methodology for data tabulation, cleanup and visualization of information is described. Of specific interest is the methods data from different sources were combined and visualized in order to efficiently facilitate answering the aforementioned questions. Finally, the analysis results are presented along with a discussion and recommendations.

4.2 Data Collection

The data collection strategy involved monitoring bus trajectories along I-35W by carrying handheld GPS units on buses traveling between the 46th Street Station and Lake Street. Research was conducted to determine which bus routes serviced both bus stops of concern. Route 535 was chosen as the sole route to monitor due primarily to its frequent rush hour trips.

Three student researchers from the Minnesota Traffic Observatory rode route 535 buses during morning and evening rush hours, or approximately 06:00-09:00 and 14:30-19:00, from Tuesday 7/5/2011 through Friday 7/8/2011. The northbound and southbound trips between the bus stops of interest were recreated into schedules for each of the researchers, denoted in the table below.

Certain practices were followed during the bus trips to ensure more useful and accurate data. After either paying for fare or using a transfer, in order to maintain relative consistency among data points, the device was placed nearest the seat immediately behind the driver. The researchers focused their attention on the bus driver's behavior and external traffic conditions. The GPS device, QSTARZ BT-Q1000p GPS Travel Recorder, was used as it has a push button that instantaneously records time and location data. The button was pressed during each lane change to provide additional clarification for lane change events during data processing. The device also monitored the travel trajectories of each bus at a frequency of one point per second when the bus speed exceeded 10 kilometers per hour.

The transition between northbound and southbound bus trips had to be taken into account while creating the schedules, as the northbound and southbound bus bays on Lake Street are on opposite sides of the interstate. Walking from one bus bay to the other could take up to five minutes, depending on traffic conditions along Lake Street. Alternatively, transferring buses at the 46th Street Station was considerably easier as the northbound and southbound bus stops shared the same transit platform.

Table 4.1: Bus trip schedules for student researchers.

Schedule #1

Northbound		**Southbound**	
46th Street Station	*Lake Street*	*Lake Street*	*46th Street Station*
5:58	6:01	6:10	6:13
6:27	6:30	6:40	6:43
6:57	7:00	7:10	7:13
7:42	7:45	8:10	8:13
8:28	8:31	9:20	9:23
2:40	2:43	2:55	2:58
3:10	3:13	3:25	3:28
3:40	3:43	4:00	4:04
4:20	4:23	4:35	4:39
5:00	5:03	5:20	5:24
5:48	5:51	6:06	6:09
6:40	6:43	6:51	6:54

Schedule #2

Northbound		**Southbound**	
46th Street Station	*Lake Street*	*Lake Street*	*46th Street Station*
6:42	6:45	7:10	7:13
7:27	7:30	7:40	7:43
8:12	8:15	8:40	8:43
9:03	9:06	9:20	9:23
3:10	3:13	3:40	3:44
4:05	4:08	4:15	4:19
4:32	4:35	4:50	4:54
5:10	5:13	5:35	5:39
6:10	6:13	6:21	6:24

Schedule #3

Northbound		**Southbound**	
46th Street Station	*Lake Street*	*Lake Street*	*46th Street Station*
7:12	7:15	7:25	7:28
7:57	8:00	8:10	8:13
8:43	8:46	9:20	9:23
4:40	4:43	5:05	5:09
5:30	5:33	5:50	5:53

4.3 Processing and Tabulation of GPS Bus Trajectories

Once the actual data collection was completed, the processing phase begun. First, the data was downloaded from each of the GPS units and collected in a database. They were then imported into ArcGIS, placed in a layer, and superimposed over an image of the roadway from MnDOT aerial surveys. Using the I-35W corridor between Lake Street and 46th Street as a guideline, points were removed that fell into one of the three following categories:

- erroneous points from GPS drift or lack of signal,
- points referring to trips to or from the area, or
- points referring to time spent waiting for and/or transferring between buses.

A side effect of this initial processing was that, upon exporting the data from GIS, timestamps for all points were reset to 12:00 midnight. Because these timestamps were critical for subsequent data processing and analysis, it was necessary to recover them from the original database that had been created from the raw GPS data. A MATLAB script was used to lookup points in the database based on their index number, cross-check the latitude and longitude values for accuracy, extract the timestamp, and copy it into the processed data.

In addition to the problem of the missing timestamps, there was also an issue with missing points. The software packaged with the GPS receivers was able to export the tracks for all three units but only the button waypoints for one of the units. As a result of this, two sets of data contained no points corresponding to rider button-presses, meaning that for much of the data there was no clear indication of where and when a lane change occurred. To remedy this, a third-party utility was used to download the remaining data from the receivers. The program used, called GPSBabel, allows for data from various GPS receivers produced by multiple manufacturers to be accessed with relative ease.

The program was used to dump the waypoints from the receivers into a CSV file, a format compatible with the rest of the data. These points were then inserted into the existing data using their date and timestamps, and a few were randomly checked manually to ensure that their placement within the data was accurate.

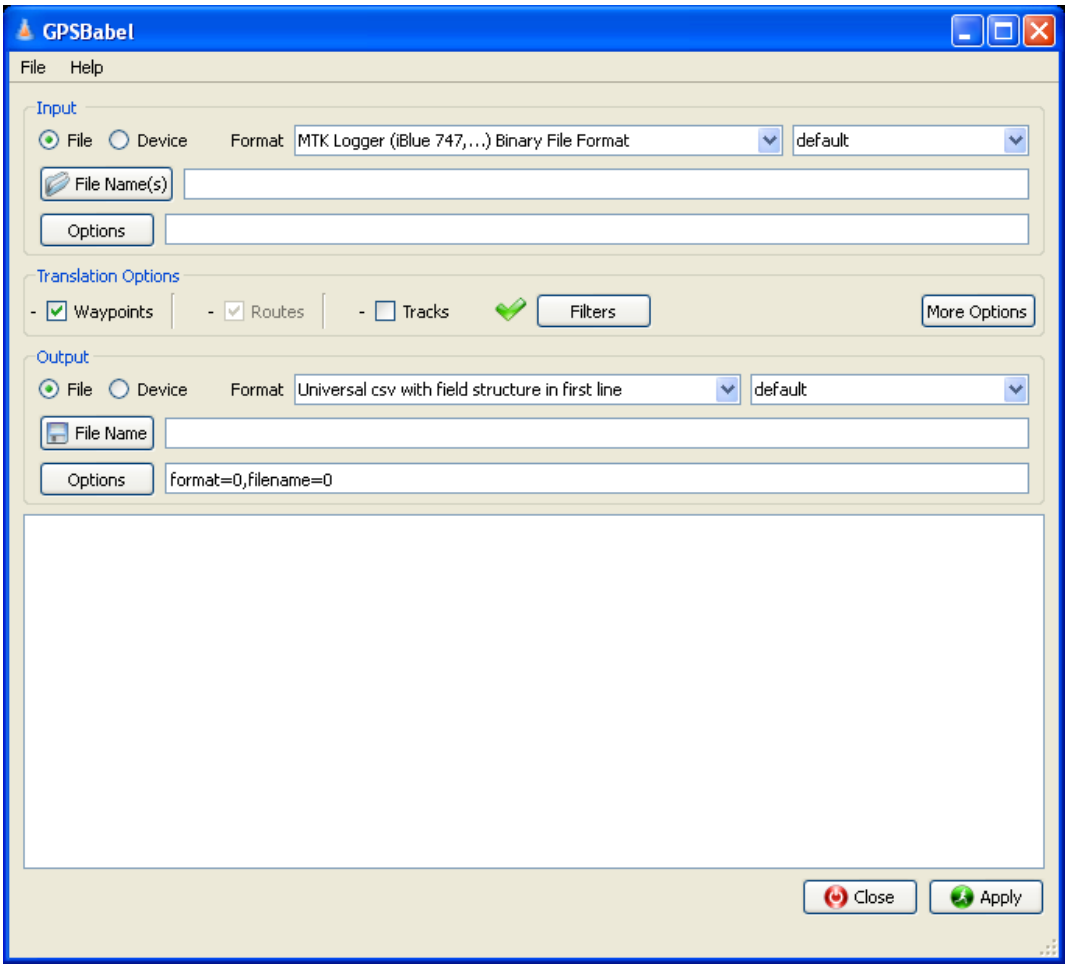

Figure 4.1: Screenshot of GPSBabel, used for extracting missing data from GPS receivers.

4.3.1 Data Processing

The ultimate goal for this project, to discern a relationship between traffic conditions, primarily road speed, and bus lane change behavior over the extent of the route segment being observed, required processing beyond initial tabulation and filtering. Since all of the data was still collected in a large database, with one large table of points for each rider, it was necessary to parse this data into individual runs each corresponding to one trip made by a rider on the bus between the Lake and 46th St. Stations, either northbound or southbound. This was done, again using MATLAB, by checking timestamps for gaps between subsequent points larger than 30 seconds, and declaring the resulting data segments as trips. In all examined cases, gaps were considerably larger than the 30-second threshold, on the order of minutes, as the receivers were set to record points every second, and points referring to bus transfers had been removed by earlier processing.

Once the data for each rider had been split into runs, they were sorted by date. From this point, the project goals required two further steps: the runs needed to be checked to ensure that the GPS data was accurate, and the loop detector IDs corresponding to each lane-change event needed to be collected so that additional traffic information could be associated with the runs. Because this

data was already heavily associated with the geometry of the roadway, it was decided that visual inspection of the geographical data would be the easiest and least error-prone method of carrying this out. Since Google Earth is free to use, has a simple and easily-learned user interface, and contained all of the features necessary for analyzing the data, it was chosen as the means for performing this analysis.

Google Earth allows GPS data to be imported and viewed through the use of Keyhole Markup Language (KML) files. The data is plotted in the program using latitude and longitude coordinates, with any additional attributes accessible by clicking on the point, displaying a bubble with the text descriptions. Since the KML file type is based on Extensible Markup Language (XML) notation, it was possible to create custom KML files from the data using MATLAB. In its Mapping Toolbox, MATLAB natively supports writing these files using a function that takes latitude and longitude coordinates, along with a string of descriptions for each point. Since the KML files written by this function are simply a string of points, an additional function was modified from one on the MATLAB File Exchange capable of creating a single-line KML file to complement the file containing the individual data point markers. Additionally, a separate KML file with button waypoints highlighted was created to make clear where lane changes occurred. These files were all directly associated to the run in question by unique file names corresponding to the run's index number.

In addition to having the collected GPS data formatted for geographic analysis, layers were added containing the ID numbers of all detectors within the segment of the roadway of interest. This information was extracted from XML documents describing the freeway, obtained from MnDOT, and written to a KML file to be loaded at the start of each processing session to assist in the data reduction. Figure 4.2 to Figure 4.4 contain screenshots of examples of these files once imported into Google Earth.

Figure 4.2: A northbound run in Google Earth with line, button, and detector files displayed.

(©2013 Google - DigitalGlobe, GeoEye, U.S. Geological Survey)

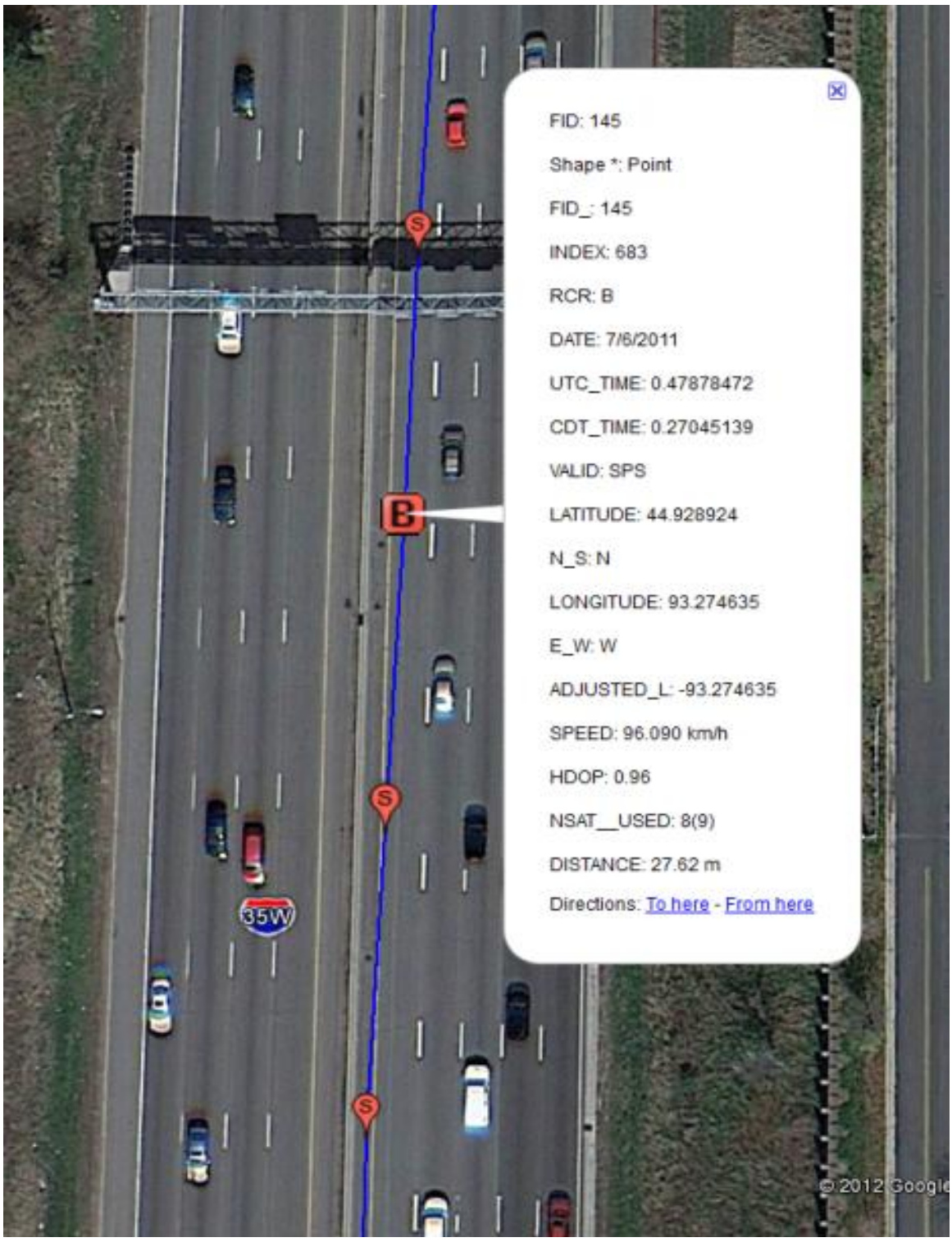

Figure 4.3: A lane change visible on the roadway. The "B" indicates a rider button press.
(©2013 Google - DigitalGlobe, GeoEye, U.S. Geological Survey)

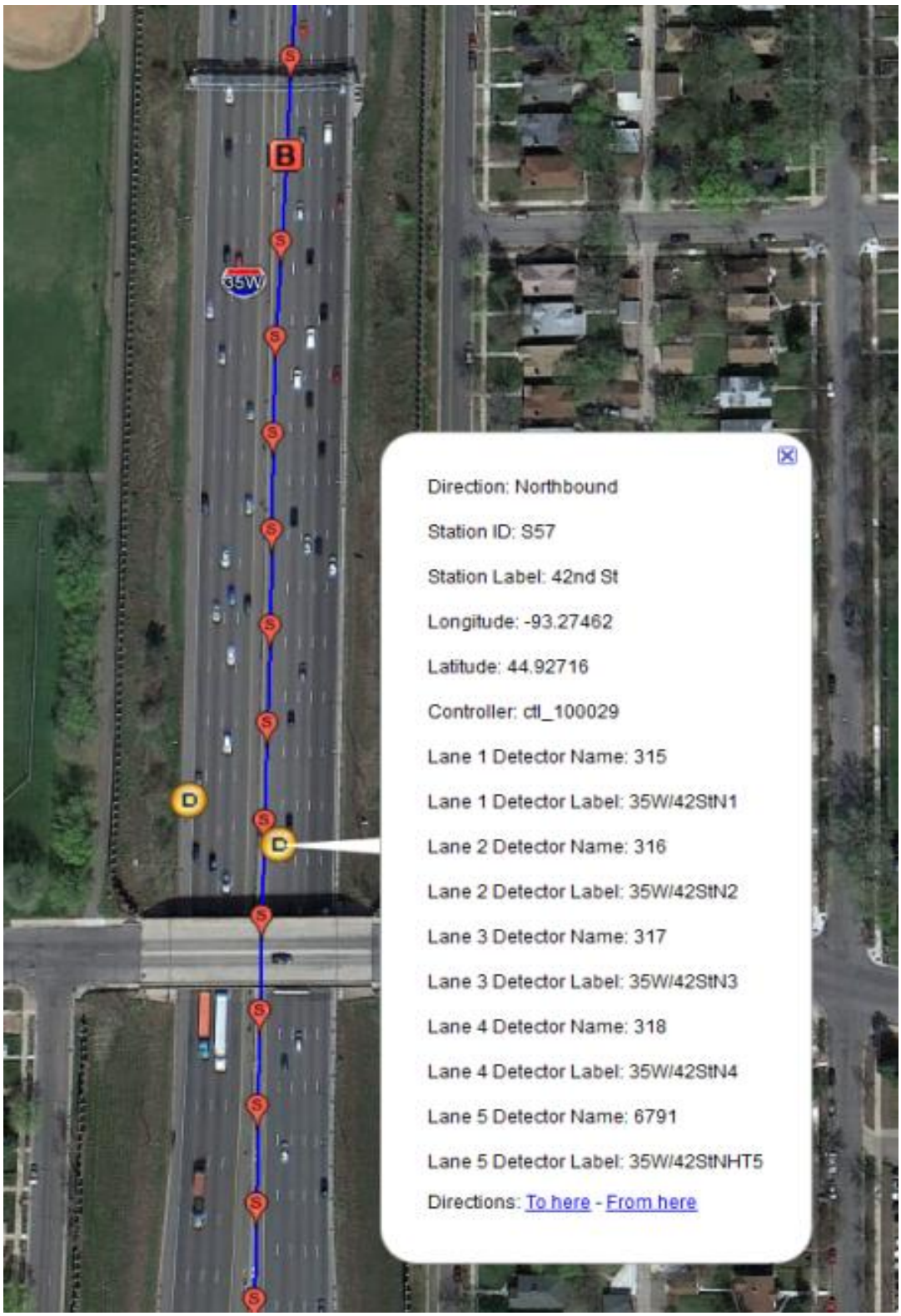

Figure 4.4: Detector information, by lane.

(©2013 Google - DigitalGeoEye, U.S. Geological Survey)

Table 4.2: Breakdown of runs.

		Northbound		Southbound	
		AM	PM	AM	PM
7/5/2011 (Tuesday)	Total Runs	12	8	9	8
	Used Runs	5	5	9	6
7/6/2011 (Wednesday)	Total Runs	10	15	11	15
	Used Runs	8	11	11	10
7/7/2011 (Thursday)	Total Runs	10	17	10	18
	Used Runs	9	13	7	17
7/8/2011 (Friday)	Total Runs	11	14	10	11
	Used Runs	7	11	10	10
Total (4 Days)	Total Runs	43	54	40	52
	Used Runs	29	40	37	43

4.3.2 Data Visualization

After cleaning the raw GPS data and extracting each useable lane change, visualizations of the data were created to look for trends in bus behavior. This phase produced two sets of visual representations of the data, both generated using MATLAB: a set using only GPS data that plotted the position of each lane change against the speed of the bus, and a set using speed and occupancy data from the detectors on the road showing the road conditions before and after each lane change.

4.3.2.1 Lane Change Position Plots

Since the first set of plots used the speed of the bus immediately after the lane change as recorded by the GPS receivers, it was assumed that the bus did not influence the speed of the traffic in the receiving lane, and instead modified its speed to match that of the vehicles already present in the receiving lane. This assumption was supported by the data; in instances where the bus was required to leave the high-occupancy vehicle (HOV) lane during heavy traffic, the bus slowed noticeably to match the speed of the receiving stream of traffic. When little to no traffic was present in the receiving lane, the bus would change lane into a sufficiently large gap so as to maintain preferred speed.

This type of visualization contained two sets of plots: one displaying the position of a lane change relative to the start of the run, and the other displaying the position of the lane change relative to the previous event (i.e. the start of the run or the previous lane change). These two sets were termed as using “absolute” and “relative” position, respectively. Both sets plotted lane change position in kilometers along the y-axis, and GPS speed (in kilometers per hour) along the x-axis, with the individual points plotted as integers corresponding to the particular run number for that data set.

For these plots, only the first three out of four lane changes were shown for northbound runs, so that plots could be made including both north- and southbound runs (where there are only three lane changes). Since the first lane change, that from the HOV lane was the most concerning one, this was adequate for this set of plots. In addition to this, the speed used to plot the data was smoothed by averaging the speed over the first three seconds of travel in the new lane, in order to prevent cases of instantaneous speed change from skewing the data.

An example analysis of one day is presented here. When comparing Figure 4.5 and Figure 4.6, “absolute” and “relative” plots of the same data, one can see the variation in the rate of lane change in different ways. The numbers indicate run ID. Notice how in the “absolute” plots the numbers corresponding to the lane changes climb the y-axis, following the trajectory of the bus, whereas in the “relative plots” the points stay near the x-axis, suggesting that the buses tended towards a rapid progression of lane changes when required to make this trip. More detailed interpretation of the plots is presented in the analysis section.

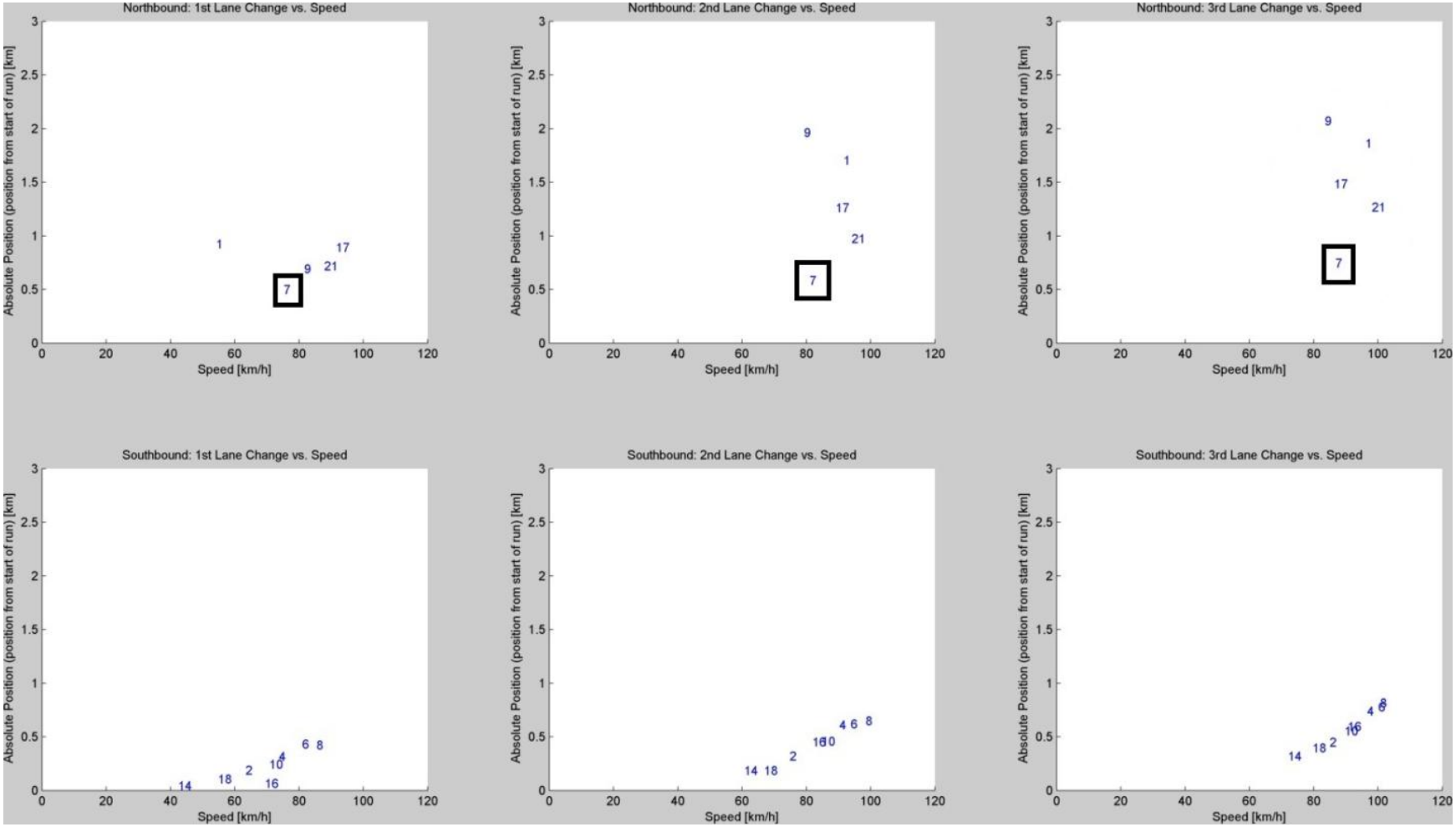

Figure 4.5: A plot of the runs during the morning of July 5, 2011, with "absolute" positioning of lane changes shown.

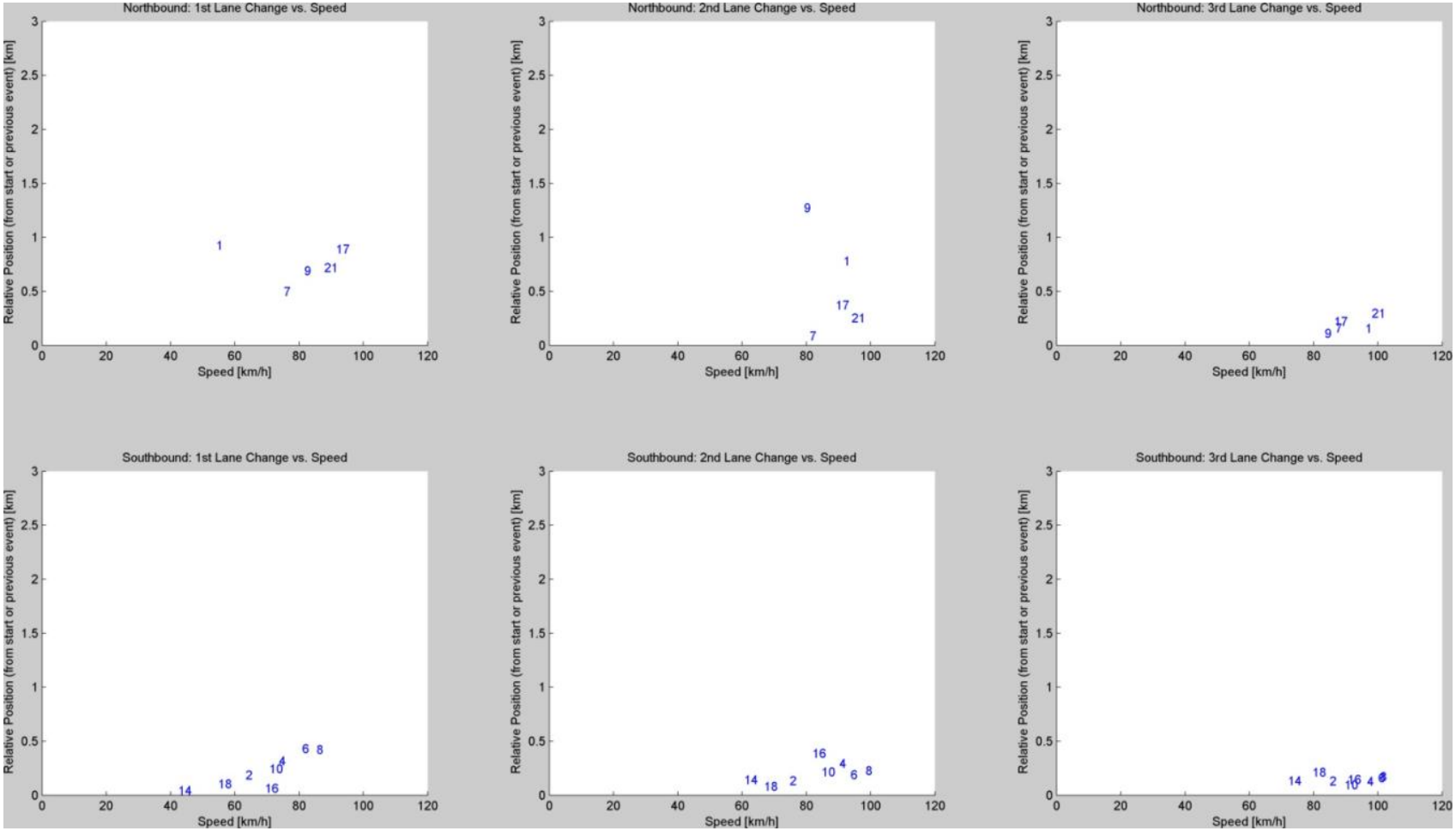

Figure 4.6: A plot of the runs during the morning of July 5, 2011, with "relative" positioning of lane changes shown.

4.3.2.2 Detector Speed and Occupancy Plots

The second set of plots made use of 30-second detector data from MnDOT. With each lane change tied to a specific set of detectors (i.e. upstream and downstream for the lanes before and after each change), these plots could be generated. For each run, speed and occupancy contours for several minutes before and after each lane change were plotted. Speed is not directly captured by the single-loop detectors found along the I-35W freeway so speed was estimated using calibrated detector field lengths along with 30-second volume and occupancy data. The field lengths for each detector were taken from the configuration file describing the freeway network as maintained by MnDOT. The values used were roughly six months older at the time of the experiment, but it was assumed that the field lengths were still sufficiently calibrated to give accurate estimates of speed. In cases where the field length was not listed in the configuration file, the value was assumed to be 24.0. Only northbound runs were visualized using this method.

With the field lengths for each detector, a function was written that would assemble the data for each lane change, query the detector volume and occupancy from MnDOT, estimate the speed at each 30-second interval for each detector from the volume, occupancy, and field length, and plot the resulting information. Before it was used in the speed calculations, occupancy data was smoothed using a five-point moving average in order to reduce noise in the data. A sample plot is shown in Figure 4.7.

The x-axis of each subplot outlines a 10-minute interval surrounding each lane change, 5 minutes before and after the event. In each of these subplots, the lane change in question is designated by a dashed black line in the middle of each plot. The exact time of the lane change is displayed in the x-axis label of each plot (the lane changes frequently occurred within seconds of one another).

These plots use a color map to show the speed and occupancy as measured by each detector. The detectors are identified relative to the lane change, where “Pre” indicates the detector for the generating lane, “Post” indicates the detector for the receiving lane, “Up” indicates the upstream detector for each lane, and “Down” the downstream detector. This designation is outlined on the y-axis label for the leftmost plots. The color map chosen for each value shown correspond to “desired” conditions on the roadway, with red indicating areas of the most concern, i.e. low speed or high occupancy. For instance in Figure 4.8, one can see the speed drop slightly in the receiving lane shortly following the bus’ lane change.

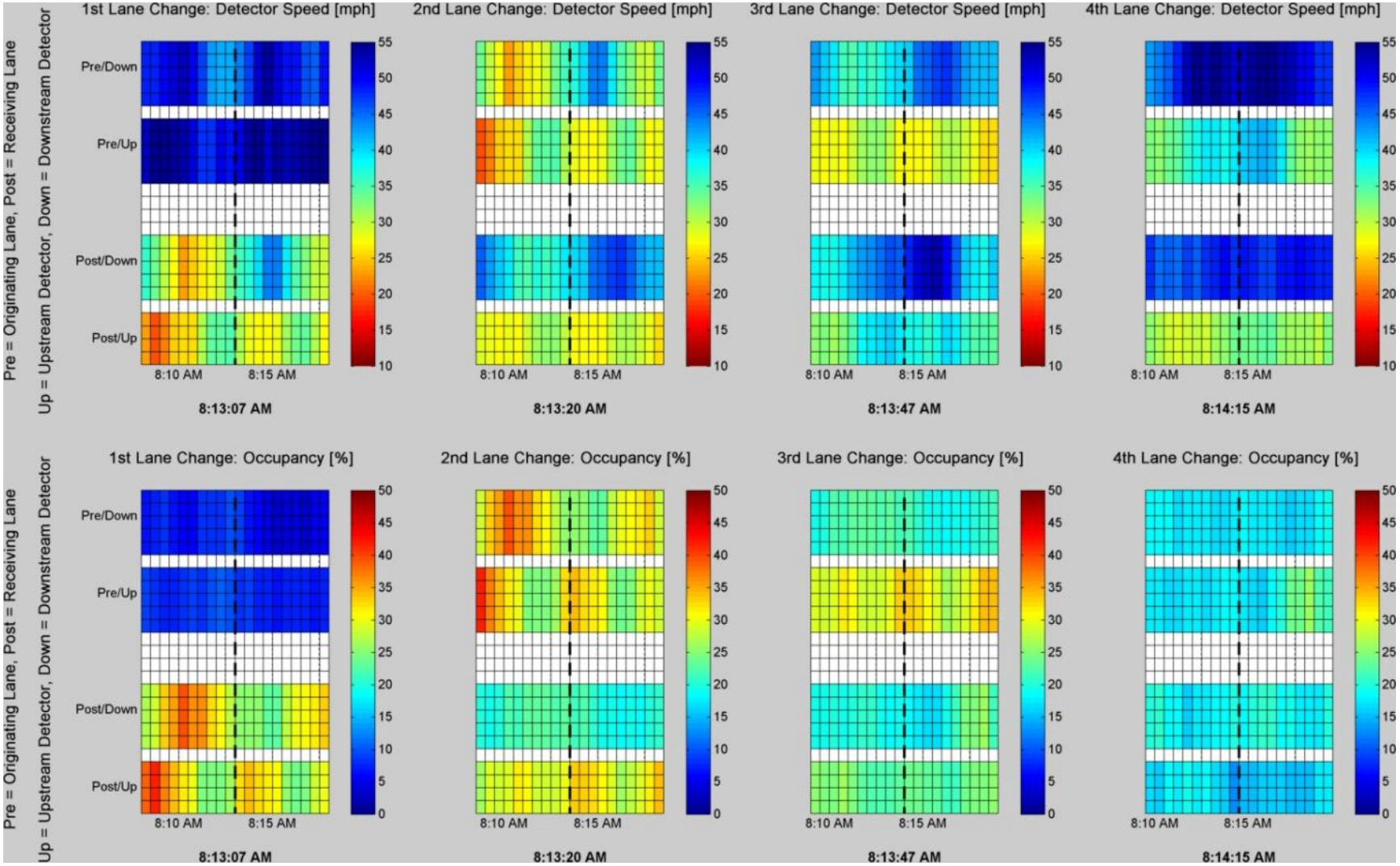

Figure 4.7: Plots of detector speed and occupancy for each of the four lane changes occurring during a northbound run in the afternoon of July 6, 2011.

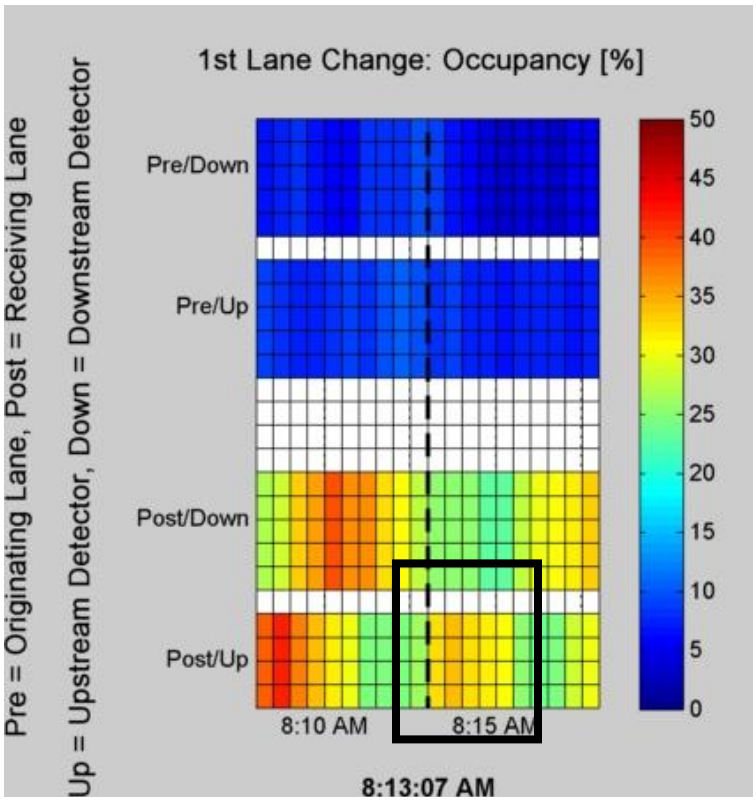

Figure 4.8: A closer view of one of the subplots in Figure 4-7.

The limits of the color maps in the plots produced are different for the speed and occupancy data. For the speed plots, all speeds below 10 mph are mapped to deep red and above 55 mph are mapped to deep blue, the rationale behind this being that any traffic travelling 10 mph or slower indicates heavily congested conditions, and any traffic travelling 55 mph or higher indicates that traffic is moving at approximately free flow speeds. An important note here is that in cases where there were no cars present during the 30-second measurement interval of the detector, the speed estimation function assumed the speed limit of 55 mph.

4.4 Data Analysis

4.4.1 MNPASS Lane Utilization and Locations of Lane Changes

All the results described in section are based on close scrutiny of the aforementioned visualizations produced for every bus run in the collected data set. First the Morning Northbound trips are explored in respect to the Relative distance traveled between lane changes. The leftmost graph given that is the first lane change it is also the distance from the exit ramp of the station.

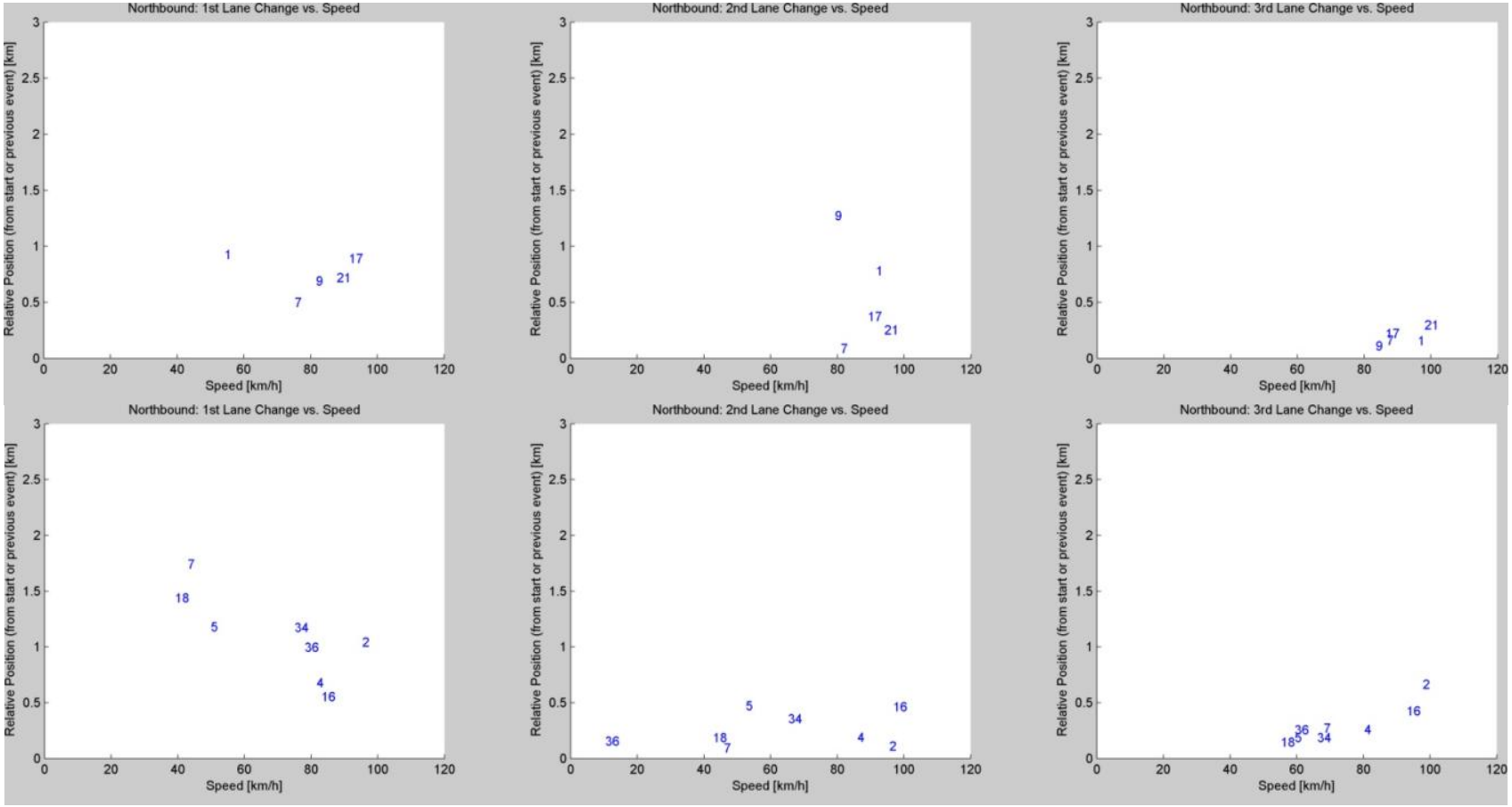

Figure 4.9: Morning Northbound Trips: Speed vs Relative distance between lane changes. July 5th and 6th, 2011.

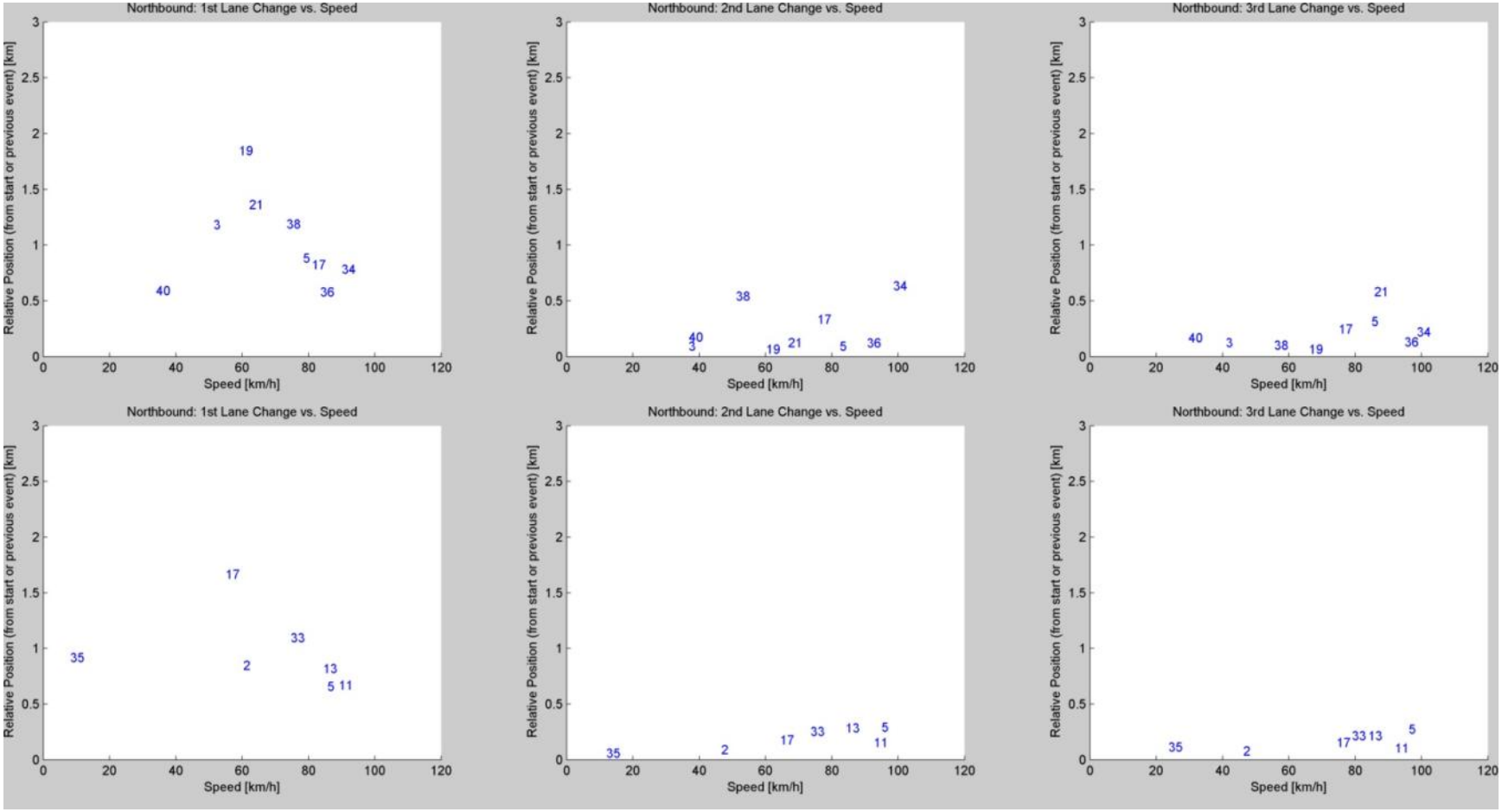

Figure 4.10: Morning Northbound Trips: Speed vs. Relative distance between lane changes. July 7th and 8th, 2011.

As observed from Figure 4.9 and Figure 4.10 the bus drivers in the majority of cases choose to change lanes as soon as possible. Consistently the first lane change that takes them from the MNPASS lane to the General Purpose Lane (GPL) is performed upstream of the middle point between the two stations, even when there is no much traffic. Naturally, one could argue that when the GPL are flowing freely there is no real purpose to be on the MNPASS but even at lower speeds it seems that they change as soon as allowed. Interestingly one can observe that the lower the speed the farther they travel on the HOT presumably only because their speed there is higher than 80 km/h so they cover a longer distance till they find an appropriate gap to perform the lane change. All subsequent lane changes are performed also as fast as possible. This tendency observation is reinforced by the fact that the slower the speeds the smaller the distance between subsequent lane changes. Similar observations can be drawn from the Morning Northbound Absolute distance figures; only two days are presented for simplicity. Figure 4.11 additionally shows that the last lane change to the rightmost lane is performed at least a kilometer upstream of the Lake street station. This observation is consistent over all four days of the experiment. The same observations were made in regards to the Afternoon Peak Northbound trips.

Although not pertinent to this work since the MNPASS lane in the southbound direction does not start till after the 46th St. Station, present the same patterns as in the case of the northbound. In this case bus drivers change lanes immediately after the depart from the Lake St station. In the majority of cases all lane changes from right to left were concluded in a space less than a kilometer from the Lake St station.

One can only hypothesize why the bus drivers do not use the MNPASS lane longer. When they were asked by the experiments participants they simply stated that they perform the changes in the manner that is the safest for the bus and the surrounding vehicles.

4.4.2 Effect of Bus Lane Changes on Traffic Flow

This next section discusses the effect the busses have on the traffic flow of the GPL while they perform the lane changes from one side of the freeway to the other. In difference to the earlier visualization the Speed & Occupancy plots are produced separately for each of the trips in the experiment. For this reason it is not possible to present all of them in this report. A few selected visualizations are presented in order to illustrate the observations made by the project team

One can separate the flow conditions on the freeway lanes between the two stations into three categories, free flowing, moderate congestion and heavy congestion. In the case of free flowing traffic, speed of 45mph and higher the busses do not seem to have any effect on the traffic flow. This is reasonable since there are plenty of large gaps to select and cause minimum disturbance. In trips performed while the flow conditions were moderate or heavy congestion the busses have an observable effect. We will explore these cases separately starting from the simpler case of heavy congestion.

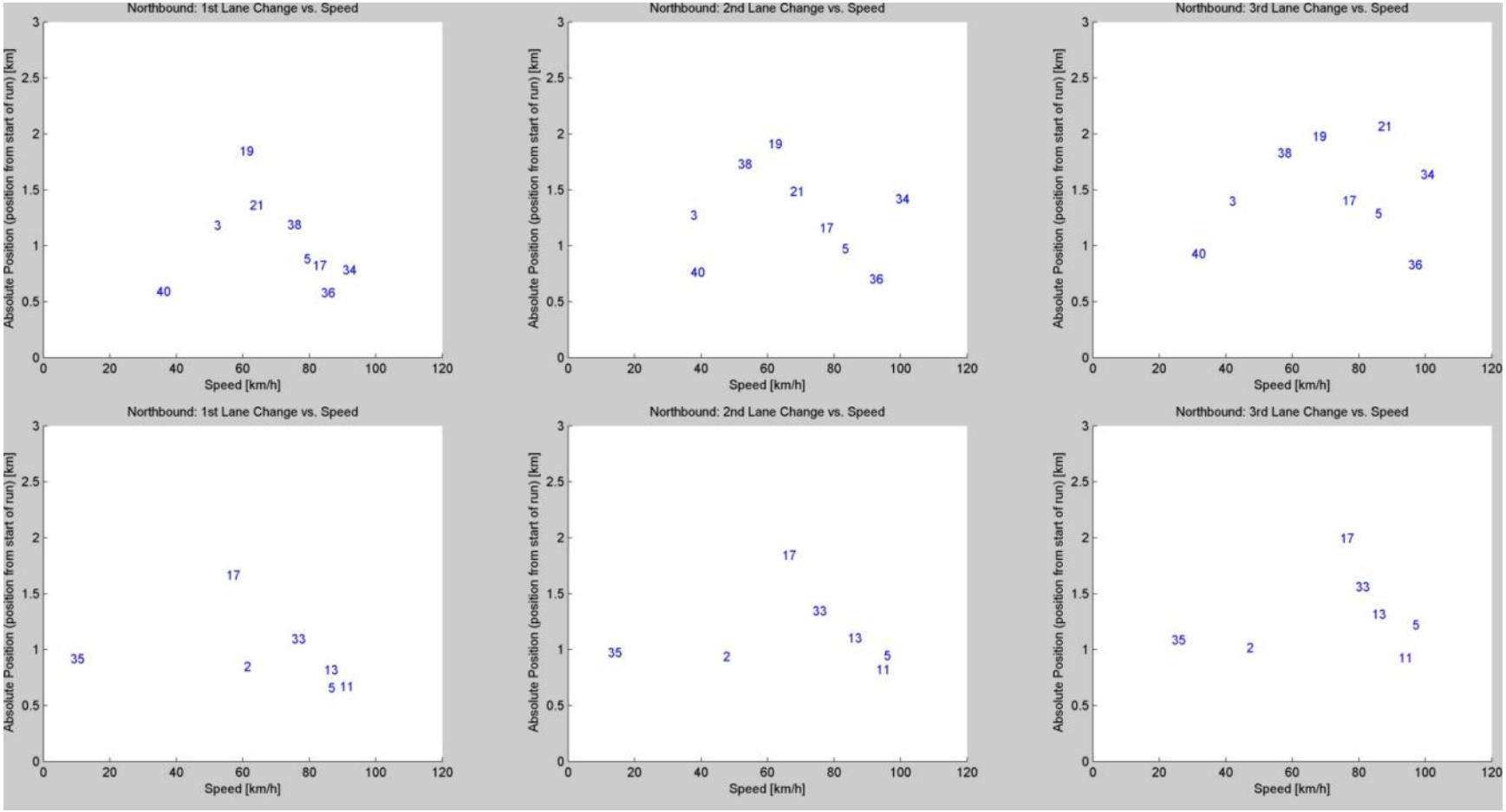

Figure 4.11: Morning Northbound Trips: Speed vs. Absolute distance from station. July 7th and 8th, 2011.

From Figure 4.12 we observe that the bus has an observable effect on the MNPASS lane as recorded on the upstream loop detector (leftmost graph). The data suggest that given the receiving lane had very low speed due to congestion the bus had to slow down in order to accept a safe gap. From Figure 4.11 we can see that the bus of trip 35 exited the MNPASS lane less than a kilometer from the median station. The disturbance caused by the bus lasted around a minute and then dissipated. There is no evidence that it generated a lasting problem on the HOT. Similar patterns of influence can be seeing on subsequent lane changes although flows seem to be improving towards the right lanes. The rightmost graph on Figure 4.12 also presents a small disturbance to the flow of the right lane, this disturbance also did not last more than a minute.

Figure 4.13 is a good example of a trip performed during moderate congestion conditions. Again there are observable patterns of disturbance to the receiving lane flows. Given that during cases of moderate congestion suitable gaps are more available, there is no indication of disturbance on the originating lane during lane changes. Again, as in the case of heavy congested conditions, the disturbance caused by the bus lane change is short lived. Under moderate congestion levels flow has not yet broken down and there is no evidence that the disturbance caused by the bus is the instigator of a flow breakdown.

There were no Speed & occupancy visualizations produced for the southbound trips since in the morning conditions are always free flowing while in the afternoon it is the opposite with heavy congestion caused well downstream the location where the last bus lane change is performed (absolving the bus from any fault). The conclusion from this investigation is that the bus although it does generate a shockwave on the receiving lane, the disturbance is not strong enough to cause a flow breakdown. It is logical to expect that in some special cases where the conditions of the receiving lane are already nearing capacity and therefore unstable, the bus lane change may instigate a flow breakdown. We did not observe any such cases nor is it logical to take action given the possibility since it is suggested by the data that unless flow is nearing capacity the bus lane change will not affect flow. At near capacity the action of any vehicle can tip over the scale anyway.

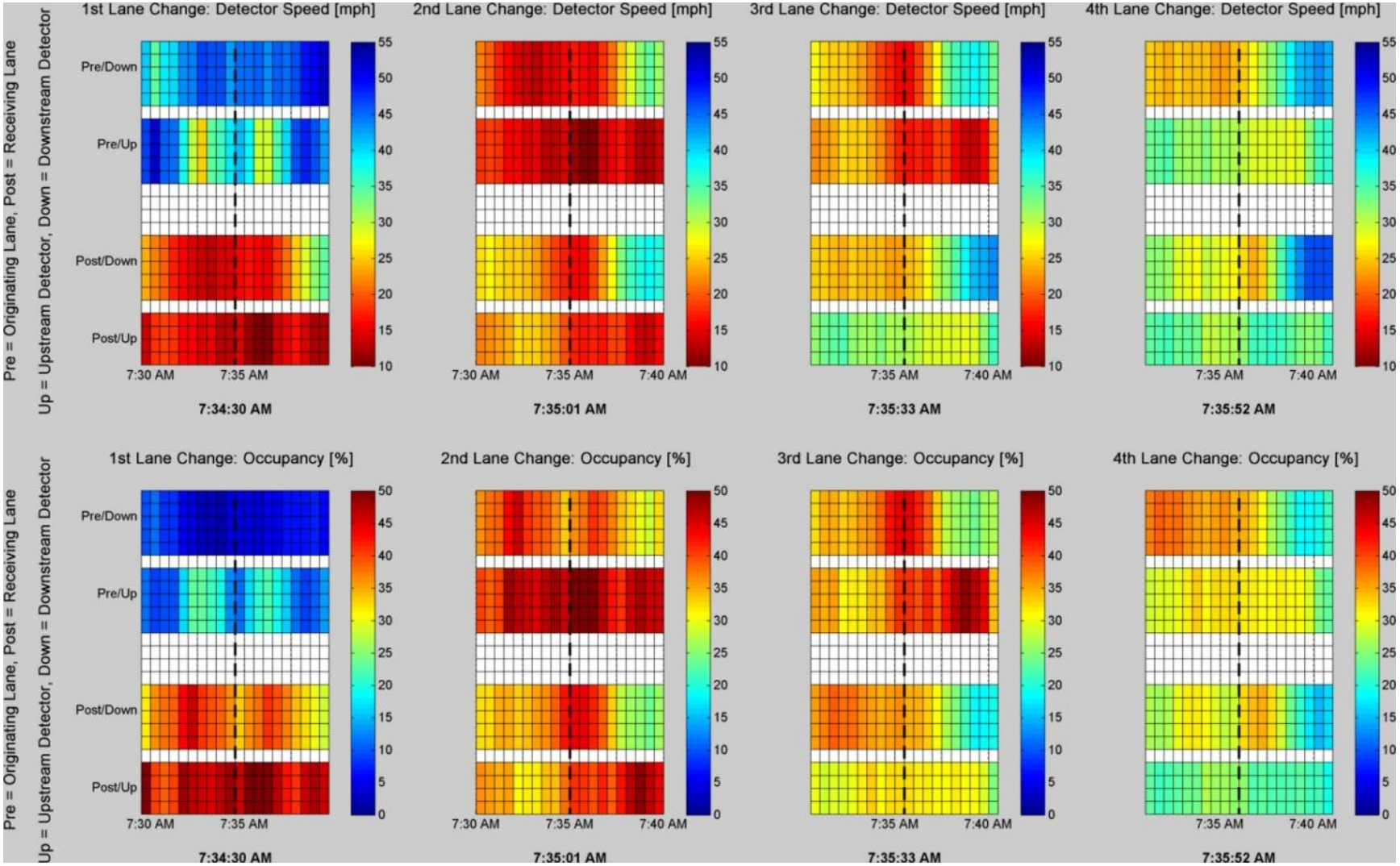

Figure 4.12: Speed & Occupancy plot of Trip 35 on July 8th, 2011.

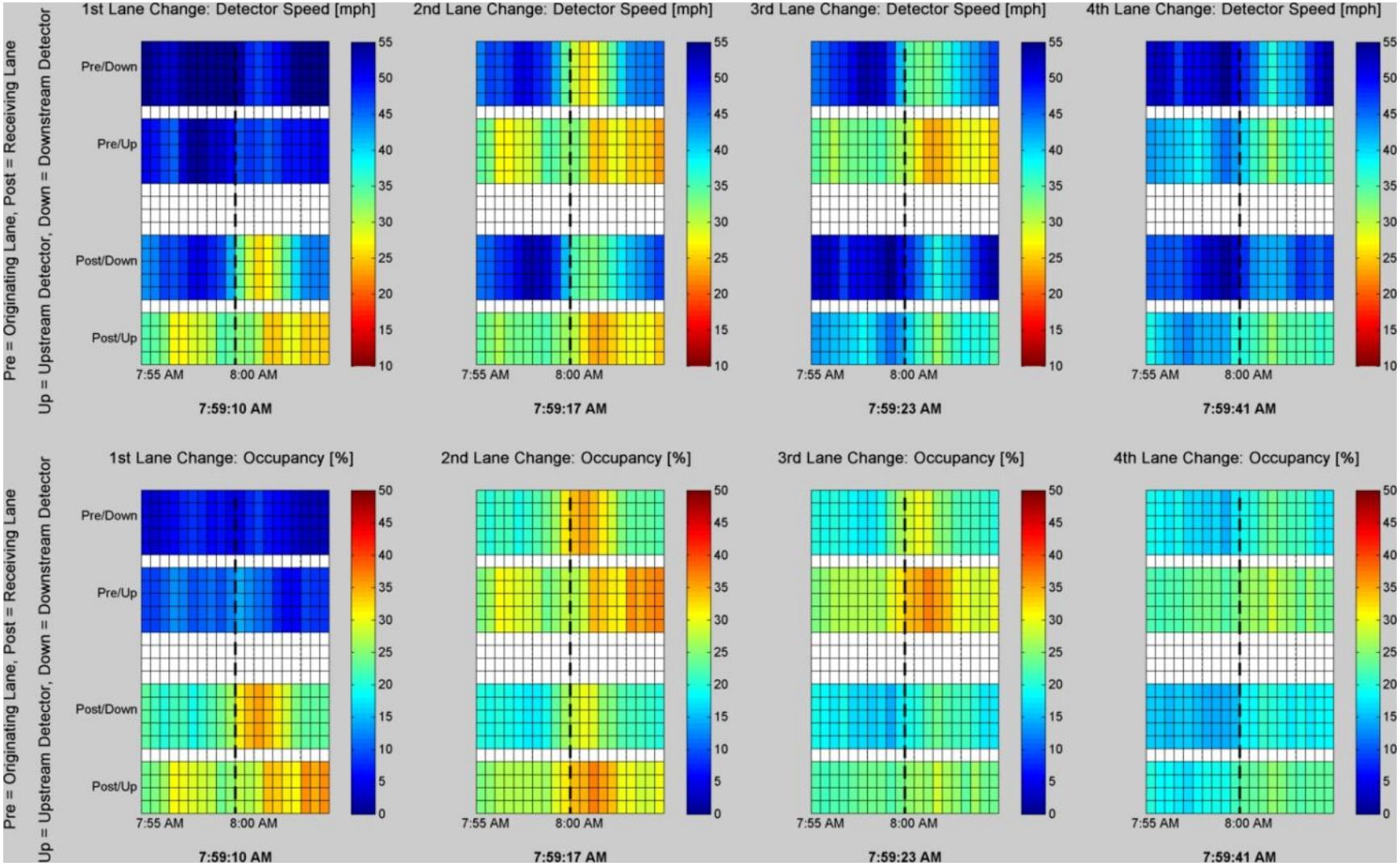

Figure 4.13: Speed & Occupancy plot of Trip 2 on July 8th, 2011.

4.5 Hypothetical Scenario of a Lake Street Median Station

One active discussion currently is the construction of a Lake St median station. Given the observed behavior of the drivers such a station will eliminate the need for lane changes and therefore offer a better service for the bus users. A natural question is what is the benefit/cost ratio of such a project? This project does not have all the facts required to give a complete answer to this question. In order to assist MnDOT engineers who may be called to estimate such a ratio in this section we try to estimate the time lost from each trip from not using the full length of the MNPASS lane as the busses not stopping on Lake St do. In extend we try to determine the associated temporal delay difference between the hypothetical scenario of a Lake St median station versus the current conditions. The following analysis was performed using GPS data for northbound bus trips between the 46th Street Station and the bus bay at Lake Street during the peak traffic periods of approximately 06:00-09:00 and 14:30-18:30 from 7/5/2011-7/8/2011.

In order to analyze the collected data, a portion of I-35W between the 46th Street Station and the bus bay at Lake Street was selected. The initial and terminal points for this distance were selected to isolate relevant bus behavior among the recorded runs, as demonstrated in Figure 4.14. This stretch of highway provided the basis for calculating the delay time. The initial latitude was selected to correspond to the location at which the bus lane begins to merge with the HOV lane. The terminal latitude was set to correspond with a location immediately before the entrance to the bus bay at the Lake Street. These points were selected to neglect the time required to reach highway speeds after leaving the 46th Street Station, as well as the time spent decelerating before reaching the Lake Street bus bay.

78 northbound runs were collected during the analysis period. For each run, both the time and GPS coordinates of the data points nearest the specified initial and terminal locations, respectively, were recorded. The latitudinal trip distance averaged 8801.2 feet (1.67 miles) with a standard deviation of 48.3 feet (or 0.6 seconds at 55 mph). The total trip duration was calculated for each run by subtracting the time at the initial point from the time at the terminal point.

To determine the temporal delay for each trip, the ‘no-delay’ run is required. This run time, 109.3 seconds, was determined by calculating the time for a bus to traverse the average run distance of 1.67 mile at the speed limit of 55 miles per hour. A supplementary ‘no-delay’ run time corresponding to a speed of 65 miles per hour was determined to be 92.5 seconds. The GPS data revealed that a significant portion of trips under free flow traffic conditions exhibited speeds exceeding the speed limit. These run times assume that there is no delay both before the bus can begin merging with the HOV lane after the 46th Street Station, as well as after it begins its exit into the bus bay at Lake Street, and that there is no delay from traffic congestion. Figure 4.15 and Figure 4.16 exhibit this estimated run time for the proposed Lake Street configuration, as well as the run times demonstrated by the collected data.

Figure 4.14: Boundaries of the Northbound I-35W section for delay estimation.

(©2013 Google - DigitalGlobe, GeoEye, U.S. Geological Survey)

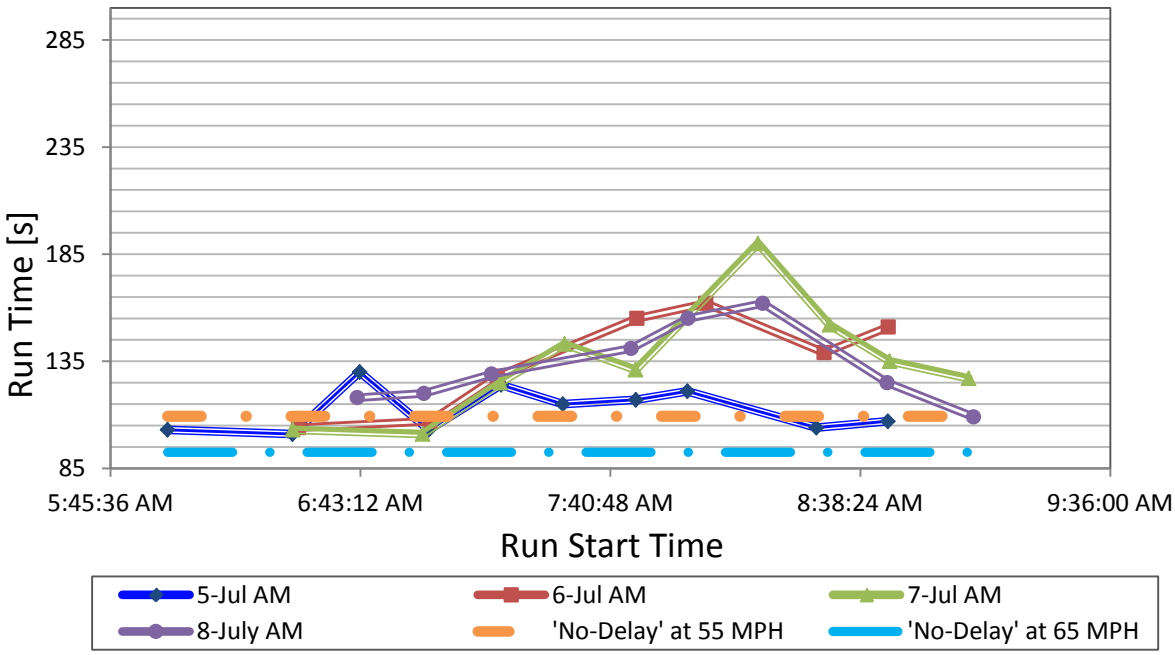

Figure 4.15: Morning run time as a function of run start time.

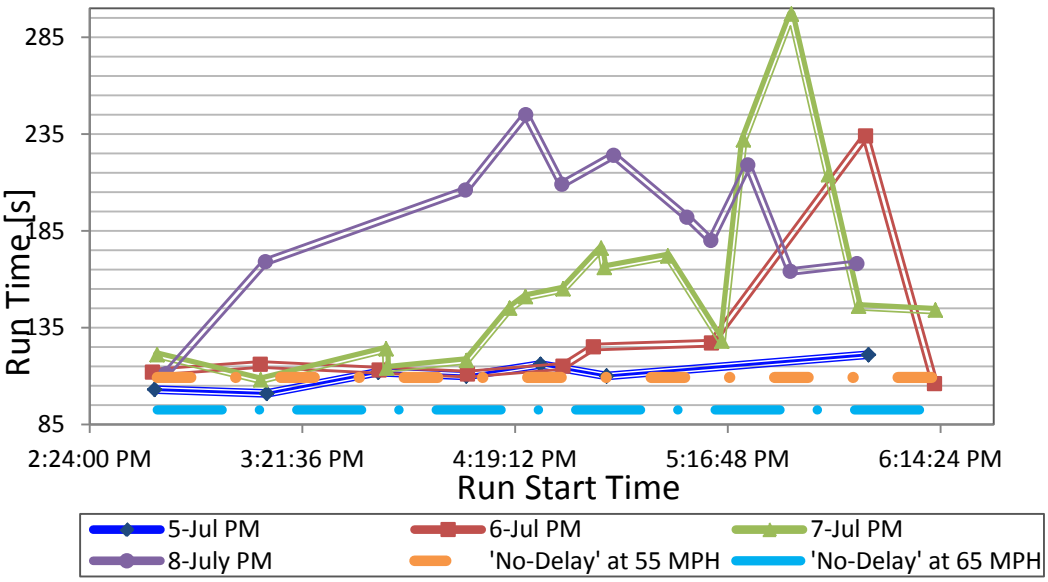

Figure 4.16: Afternoon run time as a function of run start time.

To quantify trends, the more consistent data was used to produce an empirical model to estimate delay as a function of a run's time of day. For morning peak trends, data from 7/6/11, 7/7/11, and 7/8/11 were implemented into the model, while only 7/6/11 and 7/7/11 were incorporated for the afternoon peak. To create the empirical model, the aforementioned data was segmented into portions that visually demonstrated linear trends, as shown in Figure 4.17 and Figure 4.18.

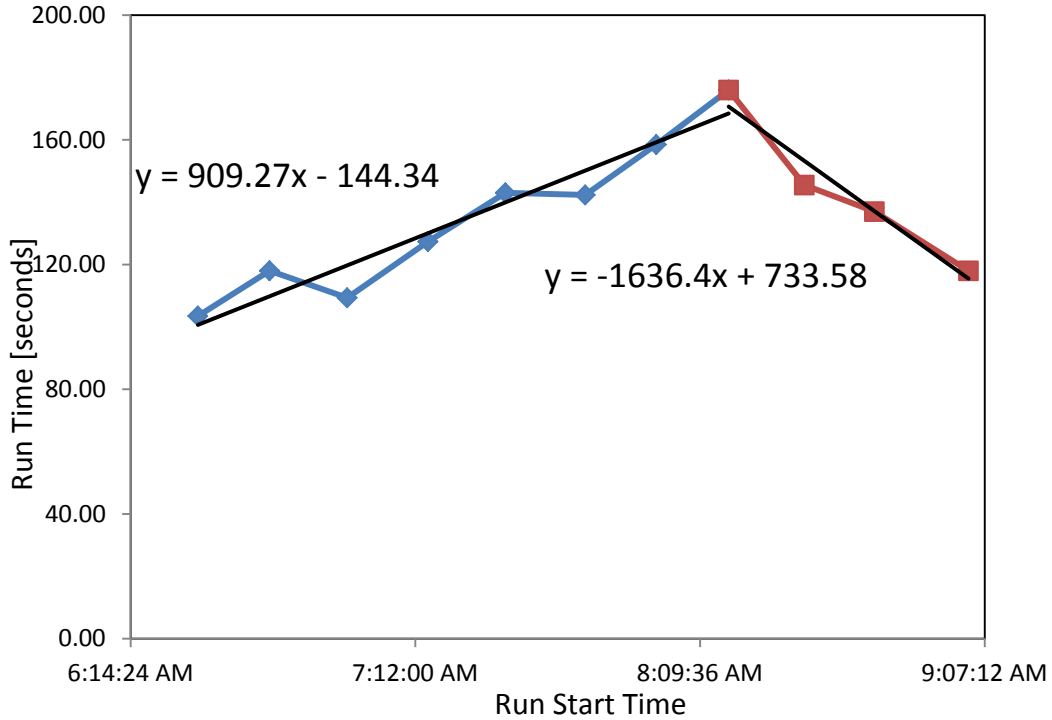

Figure 4.17: Linear trends for morning run delays.

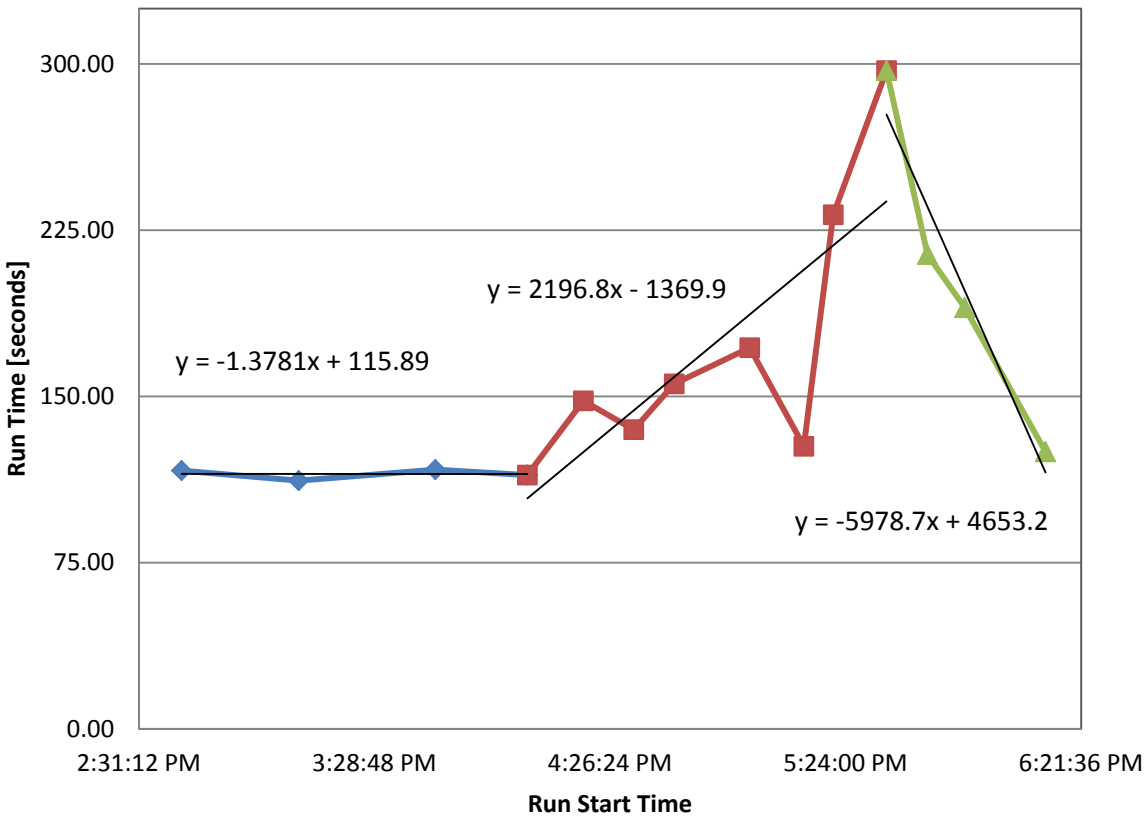

Figure 4.18: Linear trends for afternoon run delays.

From these segments linear trend lines were fitted and the associated equations were compiled to produce an empirical model that estimates the relationship between run time and delay, as demonstrated by Figure 4.19. The model was then applied to Metro Transit route 535's schedule to estimate the temporal delay associated with the scheduled runs during the morning and evening peak periods. The route arrival times at the 46th Street Station and the corresponding delay estimated from the empirical model are in Table 4.3.

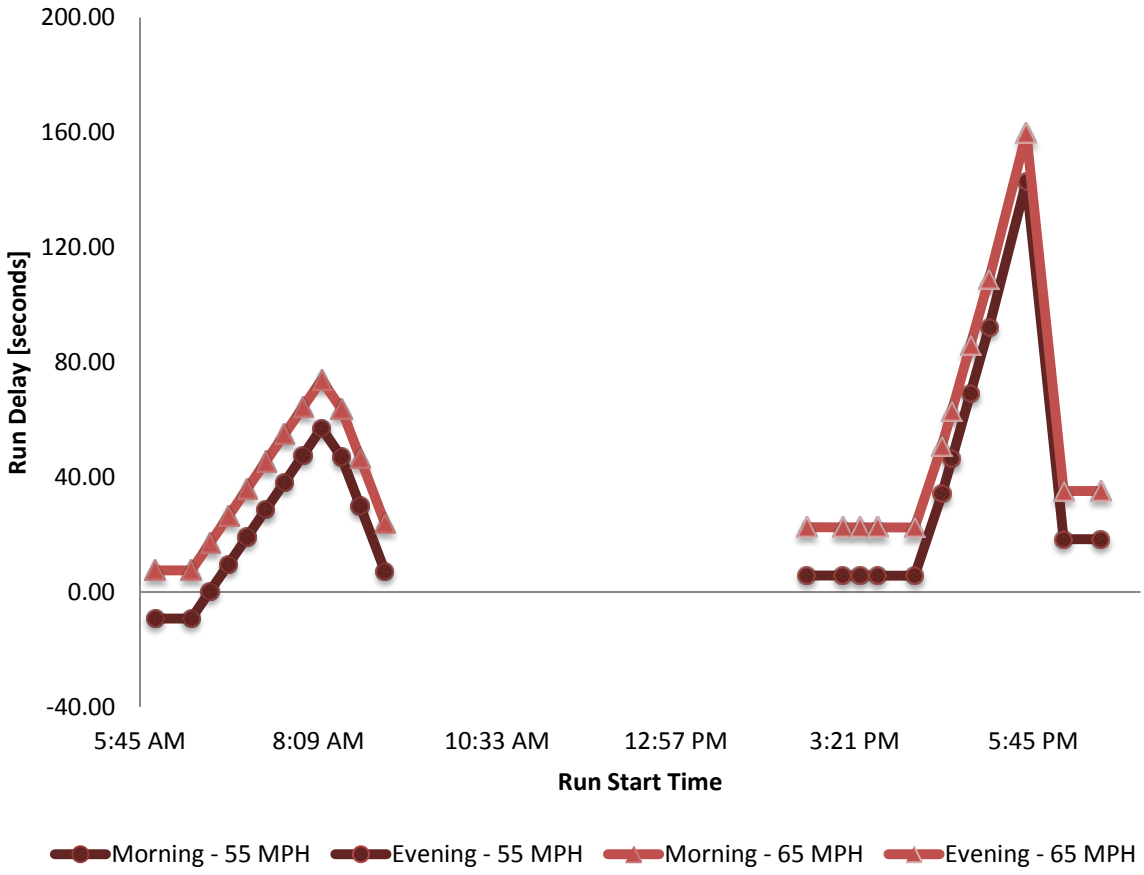

Figure 4.19: Run delay vs. run start time estimates.

Table 4.3 Route 535 Run Times and Associated Estimated Delays

Route 535 at 55 MPH			
Morning Peak		**Afternoon Peak**	
Start Time	Delay [s]	Start Time	Delay [s]
5:58 AM	-9.27	2:43 PM	5.74
6:27 AM	-9.27	3:12 PM	5.72
6:42 AM	0.20	3:26 PM	5.70
6:57 AM	9.67	3:40 PM	5.69
7:12 AM	19.14	4:10 PM	5.66
7:27 AM	28.61	4:32 PM	34.15
7:42 AM	38.08	4:40 PM	46.36
7:57 AM	47.56	4:55 PM	69.24
8:12 AM	57.03	5:10 PM	92.12
8:28 AM	46.99	5:40 PM	142.91
8:43 AM	29.95	6:10 PM	18.36
9:03 AM	7.22	6:40 PM	18.36
Total Delay		715.9	

Route 535 at 65 MPH			
Morning Peak		**Afternoon Peak**	
Start Time	Delay [s]	Start Time	Delay [s]
5:58 AM	7.53	2:43 PM	22.54
6:27 AM	7.53	3:12 PM	22.52
6:42 AM	17.00	3:26 PM	22.50
6:57 AM	26.47	3:40 PM	22.49
7:12 AM	35.94	4:10 PM	22.46
7:27 AM	45.41	4:32 PM	50.95
7:42 AM	54.88	4:40 PM	63.16
7:57 AM	64.36	4:55 PM	86.04
8:12 AM	73.83	5:10 PM	108.92
8:28 AM	63.79	5:40 PM	159.71
8:43 AM	46.75	6:10 PM	35.16
9:03 AM	24.02	6:40 PM	35.16
Total Delay		1119.1	

To estimate the total delay per day, the sum of the estimated delay for each trip was computed, resulting in daily delays of 715.9 seconds (12 minutes) for average speeds of 55 miles per hour, and 1119.1 seconds (19 minutes) for average speeds of 65 miles per hour. This estimate applies only on the northbound direction. Delays, if any, generated from the southbound trip are not easy to estimate since there is no MNPASS lane and the left lane is frequently congested. These

numbers can be multiplied by the average number of passengers that use route 535 daily and extrapolate a total cost due to delay for a longer time period than a day.

4.6 Conclusions

Chapter 4 offered an investigation of the interactions of bus operations between the 46th St median station and the Lake St right side station with the MNPASS operation and explored the effect bus lane changes have on freeway traffic flow. The summary of the observations and analysis resulted in the following:

- The bus drivers seem to underutilize the MNPASS lane. They tend to perform the left to right lane changes as soon as possible after leaving the 46th St median station.
- The bus lane changes as it traverses the freeway do generate a visible disturbance under moderate and heavy congestion but such disturbances do not amplify and therefore do not seem to be the cause of flow breakdown in this freeway section.
- There is an accumulated delay of 12 to 19 minutes daily due to the present bus driver behavior and the fact that several lane changes are need to move from the median station to the right side on Lake street.

5. Conclusions and Further Research

5.1 Summary of Findings

5.1.1 Evaluation of Speed Harmonization System

The evaluation of the Speed Harmonization system of I-35W utilized loop detector measurements combined with speed sign activation records. The goal was to explore the impact the VSLs have on traffic flow on a macroscopic sense. Three approaches were followed in order to visualize the available data and draw conclusions.

First, multiple speed contour plots were generated that included the time and value of the posted VSL. These plats allowed the research team to visualize the congestion patterns and compare them with individual sign activation. In general, the signs respond individually or with one immediate neighbor, and only rarely in groups of three. Since they only activate along short lengths of the network as congestion begins, the congestion wave travels back past the influence of the activated signs. The next set of signs then catch the wave, but again only activate along a short region of the roadway. For the days were data were collected it seems that the speed of the congestion wave is too fast for the VSL signs to give significant warning to oncoming traffic. Regardless, looking at the general congestion patterns, the VSL system does appear to positively impact the most severe congestion (speeds below 10-15 mph). Specifically, the instances and spread of extreme congestion waves (speeds bellow 10 mph) has been reduced after the VSL system activation. Severe shockwaves propagating upstream are a serious danger of rear-end collisions therefore their reduction is a valuable effect of the VSL.

The research team investigated deeper the effect of the VSL on traffic flow with the help of flow-occupancy plots and the statistical evaluation of the flow-occupancy relationships before and after the VSL activation. This analysis seems to corroborate the observations described earlier since although the fundamental diagram seems generally unchanged, a region of congested conditions (occupancy levels between 29% and 45%) has evidence of a change in the behavior of drivers. Although it is not possible to make definitive observations of this effect through loop detector data, it looks like that although drivers do not comply with the advisory speed limit, they do take it into consideration. One can hypothesize that the drivers use the advisory speed limit as a gage of downstream congestion and prepare themselves for encountering the upcoming shockwaves. The effect, is observable albeit weak since the signs, as pointed out earlier, activate later than what would be the optimal.

Finally, in order to evaluate the system-wide effect the VSL system has on speeds and in extend congestion, a statistical analysis of all before and after speeds was conducted. This analysis, allowed for the estimation of the change in congestion levels overall for the periods this project investigated. The results are presented for selected regions of the roadway.

For the Cliff Road bottleneck, after VSL implementation, overall congestion (speeds under 45 mph) were decreased by nearly 7% for well correlated days. Speeds below 40 mph were cut by slightly more than 8% and extremely low speeds were reduced by about 15%. For well

correlated days, the average AM peak between 4 and 5 minutes less congestion along the entire segment than before the VSL system was implemented.

The amount of time spent under 45 mph for the I-494 bottleneck region fell by nearly 13 minutes per morning among the well correlated days. The contribution of the slowest speeds (under 10 mph), while relatively small even before the VSL implementation, were reduced by approximately 40%.

On average, the morning peak experienced over 17% less congestion with the VSL system in place, although for those same days the lower speeds were largely unchanged (25 mph or less). The entire VSL active region had 7.6 minutes less congestion during AM peak.

5.1.2 Evaluation of UPA Corridor Operations during Inclement Weather Conditions

The objective of this part of the project is to evaluate to what extent inclement weather conditions may affect road safety and formulate recommendations that can help improve traffic operations and the safety of the traveling public. The method used in this analysis considered visual and technical design data of the highway, rainfall frequency and duration relationships throughout Minnesota areas, and a modified Gallaway's hydroplaning equation, [22], [10], [8], [9]. Continuity equation and control volume principle [7], is used to develop storm rain accumulation model and predict the depth of standing water on the roadway.

Both the rainfall water accumulation rate and the hydroplaning models describe the ways that aggregate inherent risk factors which are calculated can be used to implement a weather-responsive algorithm that can help make informed decisions: (1) Determine under what rainy conditions the PDSL should be closed; and (2) Provide a set of performance measures for the monitoring of the operation of the speed harmonization system on the highway section between Blackdog Road and 90th Street based on the prediction of rainfall accumulation.

This study used a combination of fluid dynamics principles and modified discharge rational methods. Specific forms of these methods are explicitly derived from the underlying simple analytical approximations of common distribution functions and allow mathematically convenient expressions of IDF (Intensity-Duration-Frequency) relationships. Yet, the resulting flooding and hydroplaning risks monitoring tools have not been tested by worst-case storms. Collection of these data with which to test the validity of the method would has been an asset for the model sensibility in a variety of situations.

Although the method still quantitative in nature, due to the lack of design safety data from multiple sag points and qualitative criteria for comparison at that stage, the similarity of the pattern of the alertness guideline generated for informed decision-making by the algorithm to that produced by an objective operator's judgment method indicated the validity of the principles that govern the risk management incentive derived by the proposed algorithm.

The most important conclusion of this research is that weather matters—weather conditions have an important impact on traffic safety, traffic demand, and traffic flow. Such a systematic framework of quantitative risk analysis procedure can facilitate efficient risk management.

Moreover, the proposed risk assessment tool can be combined with ITS, and risk communication and operation control in order to predict relative crash susceptibility in various segments of the corridor based on knowledge of local geography, topography, storm rain intensity, and other risk factors.

5.1.3 Evaluation of Bus Operations on the MnPASS PDSL

One of the biggest advantages of the 35W BRT corridor is the fact that the busses are traveling on the MnPASS lane therefore guaranteeing travel under uncongested traffic conditions. To facilitate quick boardings and alightings of transit passengers as well as to reduce the delay involved in entering and exiting the freeway, the 46th St. BRT station is located in the median of I-35W. The BRT operation would have been straightforward if the old right side station on Lake St. was not there or was transferred in the median. Since this is not the case today, some of the MTA transit lines are required to traverse several freeway lanes to in order to reach both stations. This part of the project was tasked in evaluating the effect of these lane changes on the traffic flow, the behavior of the drivers in terms of utilizing the MNPASS lane, and estimated the delay accumulated as compared to having a Lake St. median station.

From the observations and data collected it is suggested that the bus drivers underutilize the MNPASS lane. They tend to perform the left to right lane changes as soon as possible after leaving the 46th St median station. In addition, the bus lane changes as it traverses the freeway do generate a visible disturbance under moderate and heavy congestion but such disturbances do not amplify and therefore do not seem to be the cause of flow breakdown in this freeway section. Finally, there is an accumulated delay of 12 to 19 minutes daily due to the present bus driver behavior and the fact that several lane changes are need to move from the median station to the right side on Lake street. This eliminating this delay would be a benefit if the Lake St station is transferred to the median.

5.2 Conclusions

The project described in this report had three separate objectives. First, to evaluate the operations of the I-35W Speed Harmonization system that came online on July 2010. Second, given that the new road design of I-35W uses the shoulder as a driving lane, the project evaluated the safety effect of accumulated water due to rainfall and the danger of hydroplaning. Third, the new I-35W design includes a median transit station at 46th St so the busses can take advantage of the fast moving MNPASS lane although busses still need to change lanes to the other side of the road to reach the Lake St. station which is on the right side. This project evaluated the effect of these lane changes on the traffic flow, the behavior of the drivers in terms of utilizing the MNPASS lane, and estimated the delay accumulated as compared to having a Lake St. median station.

Although the project objectives are independent, there are linkages. For example, the methodology developed in chapter 3 estimates the safe speed given current rainfall conditions. The speed harmonization system can be used to advise or enforce a new speed limit on that lane to reduce the danger and produce a more efficient operation as compared to closing the lane. Busses have different behaviors as regards to hydroplaning given their size and tire size. The

information on chapter 3 can be used to evaluate the safety of operating the BRT lane during heavy rainfall.

5.3 Study Limitations

This research did not investigate the behavior of individual drivers in respect of the VSLs. Although this effort dug deep into the loop detector data, the presented results are an aggregation of the particular driver's behavior. It would be of benefit to investigate exactly how the driving behaviors of drivers change by collecting individual vehicle data.

Furthermore, although the hydrologic analysis developed in this study is relevant in establishing the quantity of the standing water that must be considered for the design of the drainage systems, the extent of such studies are commensurate with the importance of the highway flow density, the estimate of the potential for damage to the highway, material loss, and the potential risk to traveling public life, but cannot be considered as an absolute approach for redesigning the hydrologic and hydraulic systems. Much more research is needed to measure, understand, implement, and validate management strategies receptive to mitigate inclement weather impacts at both sag points.

Finally, this study originally intended on evaluating the safety of the lane changing maneuvers of the busses. This could only be possible is we had detailed high-resolution vehicle data. The project team attempted to use the data collected by the MVTA instrumented busses for this purpose but given the then organization of these data and effort required by the researchers of the Intelligent Vehicle Lab this aspect of the project was not possible. The MVTA instrumented busses collect a wealth of information that can support a variety of research efforts looking into the subject of large vehicle maneuvers in congested traffic.

References

American Association of State Highway and Transportation Officials, *A Policy on Geometric Design of Highways and Streets*, Washington, D.C. 1990.

Anderson, D. A., R. S. Huebner, J. R. Reed, J. C. Warner, and J. J. Henry; *Improved Surface Drainage of Pavements: Final Report.* NCHRP Web Document 16; Pennsylvania Transportation Institute, Pennsylvania State University, State College, PA. 1998.

Clark, S. K., editor, Mechanics of Pneumatic Tires, U.S. Dept. of Transportation, NHTSA, 1981.

Debo, Thomas N., and Andrew J. Reese; *Municipal Storm Water Management*. Lewis Publishers: CRC Press, Inc., Boca Raton, FL, 1995.

Huff, Floyd A. and James R. Angel. "Rainfall frequency atlas of the Midwest," *Midwestern climate center*, Illinois state water survey, 1992.

Frank M. White, *Fluid mechanics*, McGraw-Hill, 7th edition, 2009.

Franzini, Joseph B.; Finnemore, E. John; *Fluid Mechanics with Engineering Applications*; McGraw-Hill, 9th edition, 1997.

Gallaway B. M., et. al., "Pavement and Geometric Design Criteria for Minimizing Hydroplaning," *Federal Highway Administration*, Report No FHWARD-79-31, 1979.

Gallaway, B. M., and Jerry G. Rose, "The Effects of Rainfall Intensity, Pavement Cross Slope, Surface Texture, and Drainage Length on Pavement Water Depths," *Texas Transportation Institute*, Research Report No. 138-5, 1971.

Hays, G. G., D. L Ivey,., and B. M Gallaway., "Hydroplaning, Hydrodynamic Drag, and Vehicle Stability," *Frictional Interaction of Tire and Pavement* ASTM STP793, W. E. M. Meyer and J. D. Walter, Eds., *American Society for Testing and Materials*, pp. 151-166, 1983.

Hight, P.V., J.B. Wheeler, T.J. Reust, *The Effects of Right Side Water Drag on Vehicle Dynamics and Accident Causation*, SAE Paper No. 900105.

Holdener, D.J., "The effects of rainfall on freeway speeds," *ITE Journal*, Vol. 68, No. 11.

Horne, W. B. and R. C. Dreher. *Phenomena of Pneumatic Tire Hydroplaning*. NASA TN D-2056, 1963.

http://images.mitrasites.com/aquaplaning.html.

http://www.climate.umn.edu/doc/online_resources.htm#heavy_rain.

Huebner, R.S., J.R. Reed, J.J. Henry, "Criteria for Predicting Hydroplaning Potential", *Journal of Transportation Engineering*, Volume 112, No. 5, Sept. 1986.

Huff, F. A., and J. R Angel.; “Rainfall Frequency Atlas of the Midwest,” *Illinois State Water Survey*, Champaign, Bulletin 71, 1992.

Ivey, D.L., J.M. Mounce, “Water Accumulations”, *The Influence of Roadway Surface Discontinuities on Safety, Transportation Research Board*, National Research Council, Washington, D.C., 1984.

Kyte M., Z. Khatib, P. Shannon, and F. Kitchener, “Effect of weather on free-flow speed,” *Transportation Research Record: Journal of the Transportation Research Board*, No. 1776, National Research Council, Washington D.C., pp. 60-68, 2001.

Navin, F., *Hydroplaning and Accident Reconstruction*, SAE Paper No. 950138.

NCHRP Research Results Digest, Number 243, *Proposed Design Guidelines for Reducing Hydroplaning on New and Rehabilitated Pavements*, September, 1999.

Ong, G. P., and T. F. Fwa; “Prediction of Wet-Pavement Skid Resistance and Hydroplaning Potential,” *Transportation Research Record: Journal of the Transportation Research Board, No. 2005*, Transportation Research Board of the National Academies, Washington, D.C., pp. 160–171, 2007.

Rakha, H., M. Farzaneh, M. Arafeh, and E. Sterzin, “Inclement Weather Impacts on Freeway Traffic Stream Behavior,” *Transportation Research Record: Journal of the Transportation Research Board*, No. 2071, National Research Council, Washington D.C., 2008, pp. 8-18.

U.S. National Research Council, Transportation Research Board; *Highway Capacity Manual*; 2000.

Appendix A.

A.1: Analysis of Partial Spread on the Roadway

Consider the worst-case scenario where the gutter-full depth is set to be the curb height $D_m = h_c = 6\text{in}$. Water spread into traffic lane is limited to 14ft (see Figure 3.8); the gutter width and depression is respectively W=3ft and $D_s = 2in$. The driving lane width is $L = 11\text{ft}$. In these circumstances, the lower threshold hydraulic capacity is determined as follows for only one unit (see Figure 3.8):

$$\begin{cases} T_m = L + 3 = 14\,\text{ft} \\ T = \min\left(T_m, \dfrac{D_m - D_s}{S_x}\right) \\ \quad = \min\left(14, \dfrac{6-2}{0.02\times 12}\right) \\ \quad = \min\left(14, 16.7\right) = 14\,\text{ft} \end{cases} \tag{A.1.1}$$

The water depth (curb height) is:

$$\begin{cases} D = T \times S_x + \dfrac{D_s}{12} \\ \quad = 14 \times 0.02 + \dfrac{2}{12} = 0.45\,\text{ft} \end{cases} \tag{A.1.2}$$

The minimum spread

$$\begin{cases} T_x = T - W \\ \quad = 14 - 3 = 11\text{ft} \end{cases} \tag{A.1.3}$$

$$S_w = S_x + \frac{D_s}{12W} = 0.02 + \frac{2}{12\times 3} = 0.076$$
$$T_s = \frac{D}{S_w} = \frac{0.45}{0.076} = 5.92\text{ ft} \tag{A.1.4}$$

The hydraulic capacity for one unit is:

$$\begin{cases} Q_o = \dfrac{0.56}{n} S_x^{1.67} S^{0.5} T^{2.67} \\ Q_L = Q_x + Q_w \\ Q_x = \dfrac{0.56}{n} S_x^{1.67} S^{0.5} T_x^{2.67} = \dfrac{0.56}{0.016} 0.02^{1.67} \times 0.03^{0.5} \times 11^{2.67} = 5.32 \\ Q_w = \dfrac{0.56}{0.016} S_w^{1.67} \times S^{0.5} \left(T_s^{2.67} - (T_s - W)^{2.67} \right) \\ \quad = \dfrac{0.56}{0.016} 0.076^{1.67} \times 0.03^{0.5} \times \left(5.92^{2.67} - (5.92 - 3)^{2.67} \right) = 7.92 \\ Q_L = 5.32 + 7.92 = 13.24 \text{ cfs} \end{cases} \quad \text{(A.1.5)}$$

There are three major drains along the length of the sag area. Assuming efficiency $\varphi_d = 0.85$ and clogging factor $C_g = 0.55$, the total hydraulic capacity without minor drains (helpers) becomes:

$$\begin{cases} Q_{L,T} = 3C_g \left(\varphi_d Q_x + Q_w \right) \\ \quad = 3 \times 0.55 \left(0.85 \times 5.32 + 7.92 \right) = 20.53 \text{ cfs} \end{cases} \quad \text{(A.1.6)}$$

A.2: Runoff Analysis

Using a concept similar to hydroplaning analysis, one may adopt the hyperbolic relationship between water velocity and depth in a gutter as a control of the maximum runoff discharge on the street. Using a selected risk level applied to the entire area of the sag point, Figure 3.13 shows that for maximum safety at the sag point, the allowable water spread $T_{\max,s} = 0.33L$ and $T_{\max,s} = 0.5L$ respectively for minor storm events and major storm events.

$$\begin{cases} \mathrm{R}_{ed} = \dfrac{Q_{red}}{Q_{full}}; \quad 0 < \mathrm{R}_{ed} \le 1 \\ \quad = \dfrac{1}{(T_{\max,s} S_x)^{2.67}} \left(\dfrac{n p_{vd}}{2k S^{0.5}} \right)^{1.60} \end{cases} \quad \text{(A.2.1)}$$

where Q_{full} is the gutter-full capacity; $p_{vd} = VD$ is the permissible product (i.e. the product of the runoff velocity V, and the depth of the curb D) as set in the hypothesis section. Maintaining $T_{\max,s} = 0.5L$ we have:

$$\mathrm{R}_{ed} = \frac{1}{(0.5 \times 11 \times 0.02)^{2.67}} \left(\frac{0.016 \times 1}{2 \times 0.56 \times 0.03^{0.5}} \right)^{1.60} = 6.7 > 1 \quad \text{(A.2.2)}$$

$R_{ed} > 1$ indicates that the gutter can carry the discharge if a maximum spread is maintained to $T_{\max,s} = 0.5L$

Optimum time duration

Using modified rational method we can determine the storm detention volume $\not{V}_d$. Extrapolation of the rainfall intensity I_r from IDF curve for 10 year event frequency is determined as follows:

$$\begin{cases} I_r = 8.4 - 295\times10^{-3} t_m^{0.982} + 53\times10^{-4} t_m^{2.01} - 28\times10^{-5} t_m^{2.54} \\ \not{V}_{in} = 60 k_r I_r A t_m \\ \not{V}_{out} = 60 Q_s t_m \end{cases} \qquad \text{(A.3.1)}$$

where $\not{V}_{in}$ is the inflow runoff volume; $\not{V}_{out}$ is the outflow volume; Q_s is the existing sump inlet capacity designed for 10 year frequency (see equation (15)). Using equation (A.3.1), the storm water detention volume $\not{V}_d$ is determined as follows:

$$\begin{cases} \not{V}_d = \not{V}_{in} - \not{V}_{out} \\ \quad = 60 t_m \left(k_r A I_r - Q_s \right) \end{cases} \qquad \text{(A.3.2)}$$

Using equation (A.3.2) the optimum detention time T_{opt} is determined:

$$\left. \frac{d\not{V}_d}{dt_m} \right|_{t_m = T_{opt}} = 0 \Leftrightarrow 60\left(k_r A I_r - Q_s \right) + 60 t_m \left(k_r A I_r - Q_s \right)' = 0 \qquad \text{(A.3.3)}$$

Solving equation (A.3.3) for T_{opt} using the capacity of the sump discharge $Q_s = 1.08\text{cfs}$ gives the optimum detention time $T_{opt} = 28$ minutes and the storm water detention volume $\not{V}_d = 3586\ \text{ft}^3$ from equation (A.3.2).

A.4: The design discharge

$$\begin{cases} Q = Q_{L,T} + Q_c \\ Q_c = C\varphi_c A_c I_r \\ A_c = 0.1\times A \end{cases} \qquad \text{(A.4.1)}$$

$$\begin{cases} Q_{L,T} = 20.53 \\ A_c = 0.1\times A \\ Q_c = 0.7\times0.5\times0.1\times2.1\times6 = 0.441\,\text{cfs} \\ Q = Q_{L,T} + Q_c = 20.971\,\text{cfs} \end{cases} \qquad \text{(A.4.2)}$$